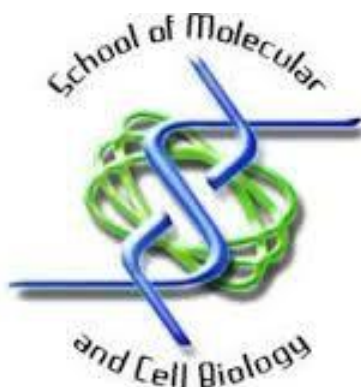# Further elucidating the steroid isomerisation reaction mechanism of GSTA3-3

Gary Jay Robertson (0511981A)

Johannesburg, 2017

A thesis submitted to the Faculty of Science, University of the Witwatersrand, Johannesburg, in fulfilment of the requirements for the degree of Doctor of Philosophy.
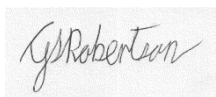
Declaration

I, Gary Jay Robertson (0511981A), am a student registered for the degree of Doctor of Philosophy (PhD) in the academic year 2017.

I hereby declare the following:

- I am aware that plagiarism (the use of someone else's work without their permission and/or without acknowledging the original source) is wrong.
- I confirm that the work submitted for assessment for the above degree is my own unaided work except where explicitly indicated otherwise.
- I have followed the required conventions in referencing the thoughts and ideas of others.
- I understand that the University of the Witwatersrand may take disciplinary action against me if there is a belief that this is not my own unaided work or that I have failed to acknowledge the source of the ideas or words in my writing.

Signature: Date: 14/07/2017

Gary Jay Robertson

Supervisor: Dr Ikechukwu A. Achilonu
Co-supervisor: Prof. Yasien Sayed

Abstract

Glutathione *S*-transferase A3-3 is the most catalytically efficient steroid isomerase enzyme known in humans, transforming Δ^5-androstene-3-17-dione into Δ^4-androstene-3-17-dione. Though its mechanism of action remains unsolved. GSTA3-3 catalyses this reaction with at least ten-fold greater efficiency than GSTA1-1, its closest competitor in the Alpha class of GSTs. In order to examine the differences between Alpha class GSTs and to better elucidate the mechanism of GSTA3-3 the roles of Tyr9 and Arg15 were examined. Tyr9 is the major catalytic residue of Alpha class GSTs and Arg15 is proposed to be catalytically important to GSTA3-3 but never before experimentally examined. While the structure and stability of the Alpha class enzymes are highly comparable, subtle differences at the G-site of the enzymes account for GSTA3-3 having a ten-fold greater affinity for the substrate GSH. Y9F and R15L mutations, singly or together, have no effect on the structure and stability of GSTA3-3 (the same effect they have on GSTA1-1) despite the R15L mutation removing an interdomain salt-bridge at the active site. Hydrogen-deuterium exchange mass spectrometry also revealed that neither mutation had a significant effect on the conformational dynamics of GSTA3-3. The R15L and Y9F mutations are equally important to the specific activity of the steroid isomerase reaction; however, Arg15 is more important for lowering the pK_a of GSH. Lowering the pK_a of GSH being how GSTs catalyse their reactions. This suggests an additional role for Tyr9, with an important mechanistic implication. Factoring in the inability to detect an intermediate during the reaction, all data are in agreement with the mechanism being concerted and that Tyr9 acts as a proton shuttle. Additionally, there is evidence to suggest that Arg15 is integral to allowing GSTA3-3 to differentiate between Δ^5-androstene-3-17-dione and Δ^4-androstene-3-17-dione, indicating that Arg15 is a more important active-site residue than previously recognized.

Research Outputs

Original Publications:

Robertson, G. J., Stoychev, S. H., Sayed, Y., Achilonu, I., and Dirr, H. W. (2017) The effects of mutating Tyr9 and Arg15 on the structure, stability, conformational dynamics and mechanism of GSTA3-3, *Biophys. Chem.* **224**, 40-48.

Conference Outputs:

25th South African Society for Biochemistry and Molecular Biology conference 2016
Oral Presentation

Title: The effects of mutating the highly conserved Tyr9 and Arg15 on the structure, stability and the conformational dynamics of GSTA3-3 and the ensuing mechanistic implications

Authors: Gary Robertson, Yasien Sayed and Ikechukwu Achilonu

7th Molecular Biosciences Research Thrust research day 2016
Oral Presentation

Title: The effects of mutating the highly conserved Tyr9 and Arg15 on the structure, stability and the conformational dynamics of GSTA3-3 and the ensuing mechanistic implications

Authors: Gary Robertson, Yasien Sayed and Ikechukwu Achilonu

Prize: Best Presentation

Acknowledgements

I would like to thank the following people:

Dr Ikechukwu Achilonu and Professor Yasien Sayed for their supervision. I owe each of you a debt of gratitude for your unwavering support and trust. Your passion, dedication and expertise are a credit to yourselves, your students and the PSFRU.

Professor Heini Dirr for the amazing opportunity to work with him in his laboratory and with the members of the PSFRU; the PSFRU has given me the training I need to enter the wider world.

Dr Stoyan Stoychev for his invaluable technical and intellectual contribution to the hydrogen-deuterium exchange mass-spectrometry experiments.

All my current and past colleagues of the Protein Structure-Function Research Unit. In particular, I would like to thank Allison Williams, Ashleigh Blane, Derryn Legg, Gavin Owen, Nish Parbhoo and Samantha Gildenhuys. Each of you has provided me with guidance, support, friendship and laughter over the years.

My family, your support and understanding has been invaluable over the years.

-Thank You
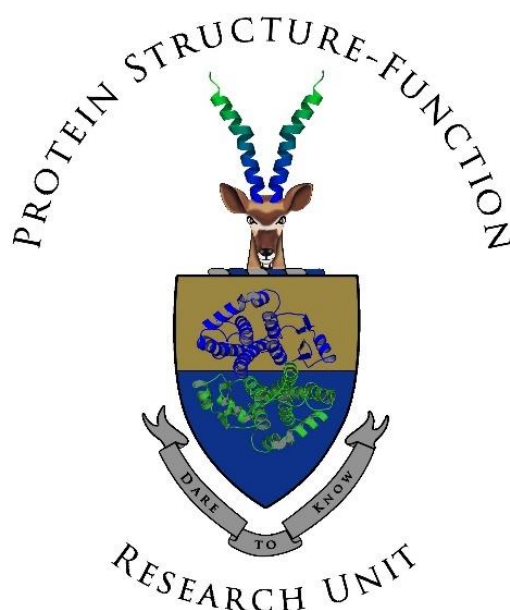
It is a principle of science that what comes before must determine what comes after.

This work is dedicated to my late father; he is responsible for all that I am and all that I do.

Table of Contents

List of Abbreviations

[Θ]	mean residue ellipticity
α9	α-helix 9
A_{xxx}	absorbance at xxx nm
CD	circular dichroism
CDNB	2,4- dinitrochlorobenzene
***C*m**	the denaturant concentration at the midpoint of the unfolding curve
EDTA	ethylenediaminetetraacetic acid
Em_{xxx}	emission of a fluorophore at xxx nm
Ex_{xxx}	excitation of a fluorophore at xxx nm
GS^-	anion of GSH after the thiol moiety is deprotonated
GSH	reduced glutathione
G-site	glutathione binding site
GST	glutathione transferase
GSTA1-1	class Alpha glutathione transferase with two type one subunits
GSTA3-3	class Alpha glutathione transferase with two type three subunits
HDX-MS	hydrogen-deuterium exchange mass spectrometry
HNE	4-Hydroxy-2-nonenal
H-site	hydrophobic electrophilic substrate binding site
IPTG	isopropyl β-D-1-thiogalactopyranoside
ITC	isothermal titration calorimetry
k_{cat}	turnover number
K_d	dissociation constant
kDa	kilodalton
K_i	inhibitor constant
K_M	Michaelis-Menten constant
KSI	α-ketosteroid isomerase
ln	natural logarithm
***m*-value**	dependence of free energy as a function of denaturant concentration
MWM	Molecular weight marker
OD	optical density

ORF	open reading frame
PDB	Protein Data Bank
pK_a	acid dissociation constant
R	molar gas constant ($1.987204118 \times 10^{-3}$ kcal.K^{-1}.mol^{-1})
R15A	arginine to alanine mutation at residue 15
SCOP	structural classification of proteins
SDS	sodium dodecyl sulfate
SDS-PAGE	sodium dodecyl sulfate polyacrylamide gel electrophoresis
T	temperature in kelvin
UV	ultraviolet
V_m	maximum velocity
Y9F	tyrosine to phenylalanine mutation at residue 9
Y9F/R15L	a double mutant, with a tyrosine to phenylalanine mutation at residue 9 and arginine to alanine mutation at residue 15
Δ^4-AD	Δ^4-androstene-3,17-dione
Δ^5-AD	Δ^5-androstene-3,17-dione
ΔG	Gibbs free energy
ΔG$_{H2O}$	change in free energy of unfolding in the absence of denaturant
ΔH	enthalpy change
ΔS	entropy change
ε	molar absorption coefficient
ε$_{xxx}$	molar absorption coefficient at xxx nm

The one- and three-letter symbolism for amino acids (IUPAC-IUB, 1984) and the one-letter symbolism for deoxyribonucleic acids (IUPAC-IUB, 1974) have been used in accordance with the IUPAC-IUBMB system of nomenclature.

List of Figures

List of Tables

Chapter 1
Introduction

1.1. Steroid biosynthesis

As a natural response to environmental pressures, evolution has over millennia resulted in the refinement of complex biological systems to improve their functionality and adaptability. Biological systems exist as a complex network of thousands of organic and inorganic compounds interacting to maintain homeostasis and/or to signal and carry out metabolism, growth and adaption.

Steroids are one such class of organic compounds participating in this complex network (Figure 1). Steroids have two primary functions: certain steroids (e.g. cholesterol) are important components of cell membranes which govern membrane fluidity[1] while other steroids (e.g. testosterone) act as signalling molecules which activate steroid hormone receptors.[2] Through these two functions steroids play important roles in regulating metabolic pathways, stress reactions, salt balance and sexual development. Steroids are common in almost all eukaryotic cells, including those of humans, animals, plants, fungi and insects.

Helping to regulate the complex network of organic compounds, including steroids, that life depends on are a different class of organic macromolecules called enzymes. Enzymes have evolved as powerful biological catalysts that have been optimised to allow a more efficient flow of energy and material through biological systems.[3,4] As catalysts, they act to reduce the activation energy of chemical reactions, making them indispensable to the proper metabolism of biological systems. The regulation of enzymes by activators, inhibitors, post-translational modifications and quantity in turn, therefore, controls metabolism. The regulation of enzymes can be carried out by positive or negative feedback loops as well as cell signalling molecules such as steroids.

The complex relationship between steroids and enzymes is a microcosm of the intricate relationship between the network of organic and inorganic compounds that create biological
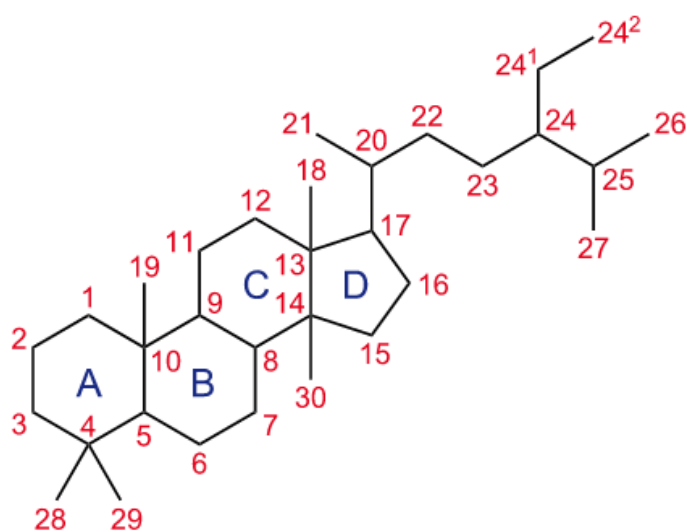
Figure 1: The steroid core structure. The core structure is composed of seventeen carbon atoms (numbered 1-17), bonded in four fused rings: three six-member cyclohexane rings (rings A, B and C) and one five-membered cyclopentane ring (ring D).[5] Carbon atoms 18 and above are not always present. Steroids vary by the functional groups attached to this four-ring core and by the oxidation state of the rings. Ketosteroids are forms of steroids with a ketone group, usually at positions 3 and/or 17.

systems in general but also serves to highlight the interconnectivity and dependence of the two classes of compounds on each other.

The production of steroid hormones such as testosterone and progesterone from cholesterol (itself the product of a complex metabolic pathway beginning with the mevalonate pathway[6]) proceeds via a complex series of oxidation and isomerisation reactions (Figure 2).[7] A critical step in the metabolic pathway is the isomerisation of the double bond of androst-5-ene-3,17-dione (Δ^5-AD) to the androst-4-ene-3,17-dione (Δ^4-AD) isomer. In bacteria, this isomerisation reaction is carried out by α-ketosteroid isomerase (KSI)[8,9] while in mammalian tissue the reaction is carried out by the close homologue glutathione *S*-transferase (GST) A3-3.[10-12] Although the reaction mechanism of bacterial KSI has been elucidated[8] the reaction mechanism of GSTA3-3 (the primary enzyme of interest to this study) remains indeterminate.

This introduction will demonstrate that a GST enzyme being responsible for the control and synthesis of steroid production is unusual and inconsistent with the typical function of the enzyme. Understanding the nature of this new function in GSTs is important, not only to understand an important biological process in humans, but to elucidate further the relationship between structure and function in proteins.

1.2. Glutathione *S*-transferase superfamily

The GST enzymes (EC 2.5.1.18) constitute a large and ancient protein superfamily of phase II detoxification enzymes best known for their ability to catalyse the conjugation of the reduced form of glutathione (γ-glutamylcysteinylglycine, GSH) to a wide variety of endogenous and exogenous compounds. The superfamily is, in turn, subdivided into three smaller protein families: the cytosolic, mitochondrial and microsomal GSTs.[13,14] The cytosolic GSTs (of interest to this study) are then further categorised into over 12 classes [structural classification of proteins (SCOP)♣].[15] GST enzymes are found in almost all aerobic organisms including bacteria, yeasts, plants, insects and vertebrates.[16] They are absent only in the Archaea domain which almost universally does not even produce the substrate of the enzyme.[17]

♣ http://scop.mrc-lmb.cam.ac.uk/scop/data/scop.b.b.gb.b.b.html
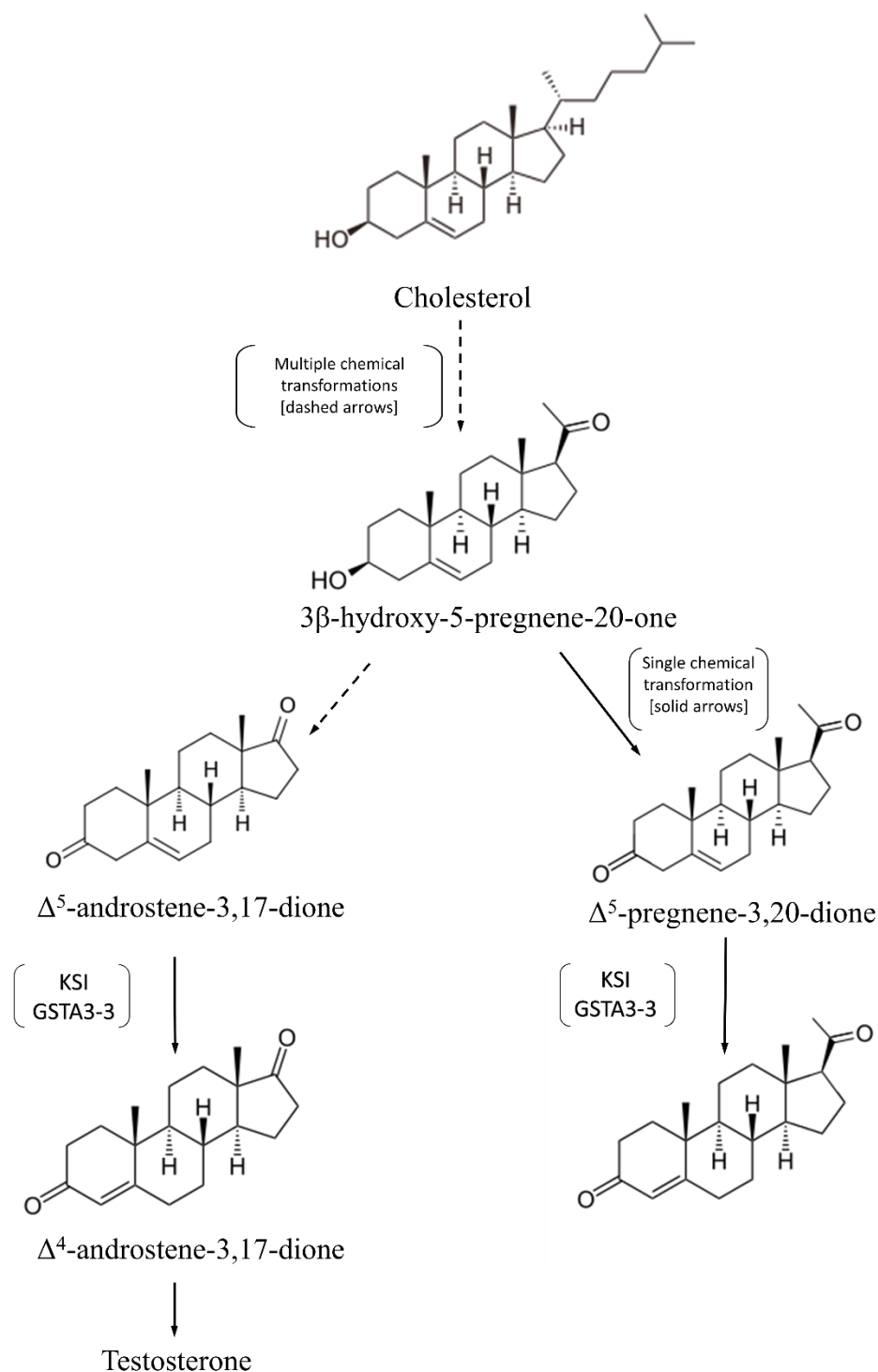
Figure 2: The biosynthesis of steroid hormones from cholesterol. Other hormones are produced from cholesterol or downstream products but have not been shown as they are outside the scope of this study. The role of KSI and GSTA3-3 in catalysing the formation of Δ^4-androstene-3,17-dione (which may subsequently be transformed into testosterone) and Δ^4-pregnene-3,20-dione is shown.[7]

1.2.1. Classification of the glutathione *S*-transferase enzymes

The cytosolic GSTs are categorised into classes according to a variety of factors including their sequence identity, structure, substrate specificity and immunological reactions.[14] The mammalian GSTs are grouped into nine species-independent gene classes designated by the names of Greek letters: Alpha, Mu, Pi,[18] Sigma,[19] Theta,[20] Kappa,[21] Zeta,[22] Beta[23] and Omega.[24] Additionally, there are classes of cytosolic GSTs unique to insects (Delta)[25] and plants (Phi and Tau).[26] Lastly, there are GST classes unique to and named for their organism of origin such as *Plasmodium falciparum*[27] and *Schistosoma.*[28]

GSTs are also classified according to their species of origin and the makeup of their dimeric structure. The large number of GST proteins; which must be identified by species of origin, class and the makeup of their subunits has necessitated the development of a precise GST nomenclature (Figure 3).[29]

The cytosolic GSTs may also be further subdivided in two major subgroups, namely the S/C-GSTs and the Y-GSTs.[30] Analysis of the sequence identity and structural similarity of the cytosolic GSTs combined with knowledge of the enzymatic mechanism of the enzymes has revealed that all the cytosolic GSTs bind and activate GSH through one of two ways: either a Cys/Ser residue (S/C-GSTs) or a Tyr residue (Y-GSTs). Members of the Y-GSTs include the Alpha, Mu, Pi, Sigma and *Plasmodium falciparum* GSTs whereas the C/S-GSTs are the Beta, Omega, Phi, Tau, Theta and Zeta GSTs. Members belonging to the same major subgroup are more closely related to each other than they are to any GST outside of their subgroup. In fact, evidence suggests that the Y-GSTs are a later evolutionary offshoot of the S/C-GSTs.[30]

1.2.2. The structure of cytosolic glutathione *S*-transferases

Though GSTs of different classes share little sequence similarity (~40%), crystal structures of the GST enzymes show that the structural fold of the proteins is highly conserved (Figure 4). Cytosolic GSTs have a dimeric quaternary structure (Mr ~ 50 kDa) and exist as obligate homo- or heterodimers,[31-33] though the subunits will always be from the same class (Figure 5A). Each subunit in turn may be subdivided into two distinct domains: Domain 1 or the N-terminal domain has a mixed α/β domain, topologically similar to the thioredoxin fold (a mixed β-sheet
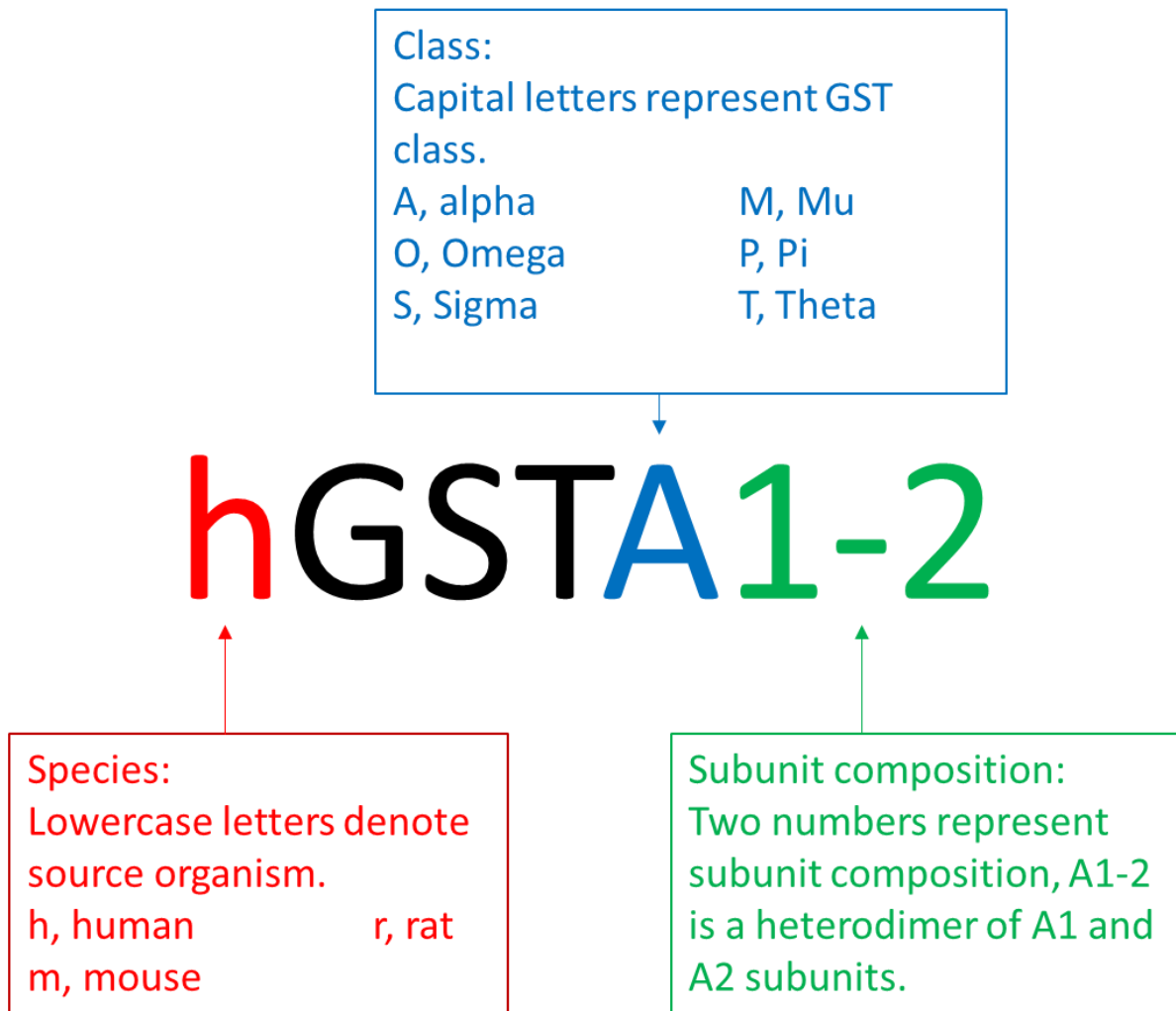
Figure 3: Nomenclature for cytosolic GSTs as laid out in Mannervik et al. (2005).[29] Many of the older references used in this study use an out-of-date nomenclature for GSTs, Mannervik et al. (2005)[29] also includes a list of the older nomenclatures and how they should be referenced today.
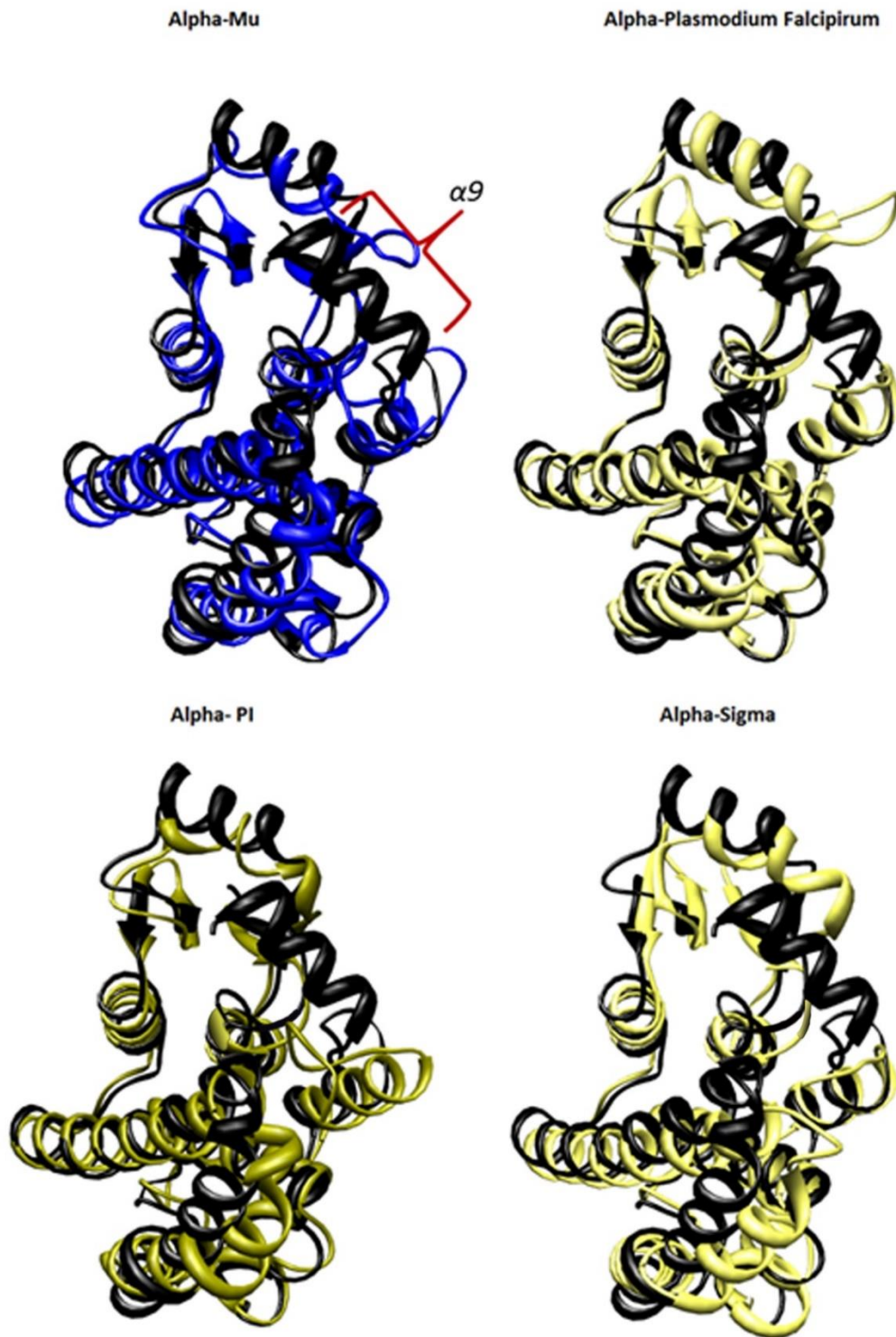
Figure 4: A structural alignment comparison subunits from five classes of Y-GSTs. Despite sharing a maximum of forty percent sequence identity, the structural folds of the subunits of Alpha (1K30, always coloured black), Mu (1GTU), Pi (16GS), *Plasmodium falciparum* (3FR6) and Sigma (2WB9) class GSTs can be seen to have very similar structural folds. Notice the lack of any comparable structure to the α9 of Alpha class GST. This figure was prepared using UCSF Chimera.[34]
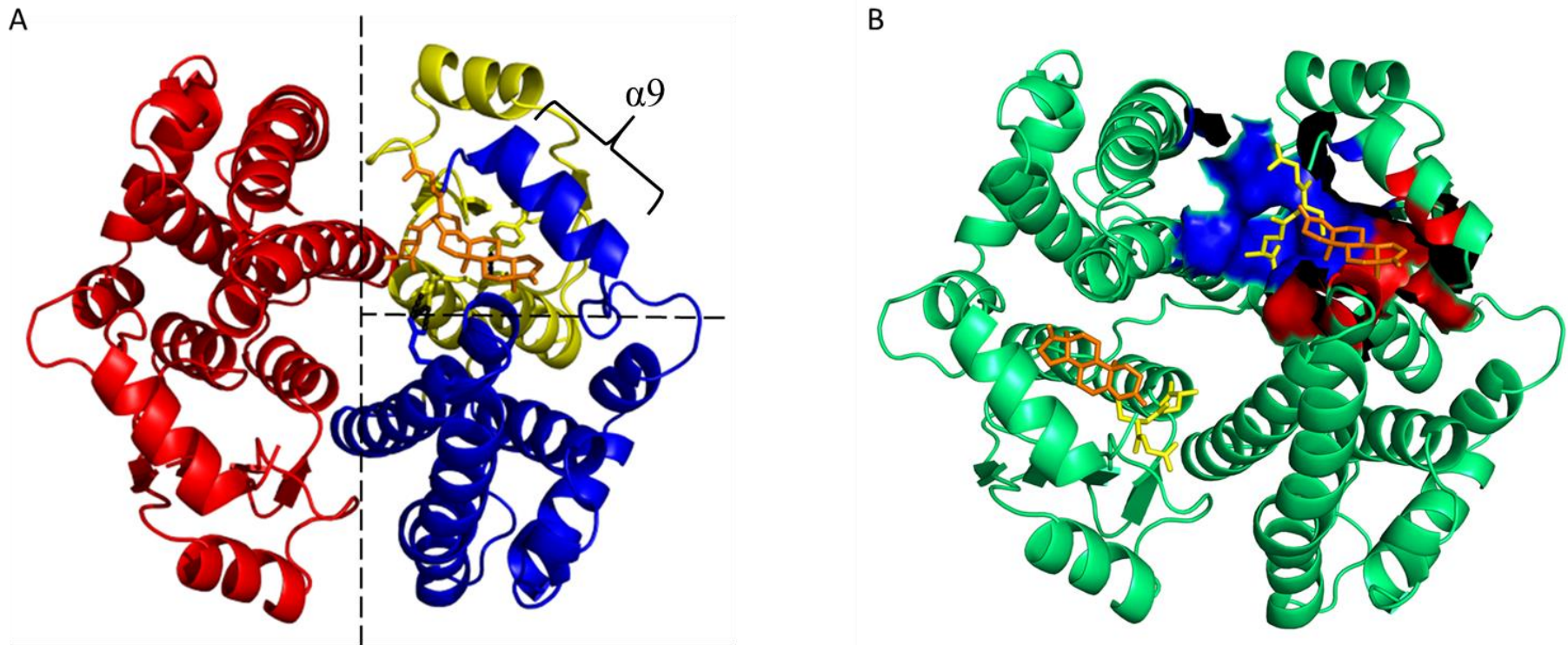
Figure 5: The crystal structure of the homodimer hGSTA3-3. (A) Showing a complete GSTA3 subunit in red, the second subunit is divided into domain 1 (yellow) and domain 2 (blue). The substrate / co-factor GSH and the product Δ^4-AD (orange), Tyr9, Arg15 on the active-site loop and its salt-bridge contact Glu104 are shown as stick models. The domain interface and the axis of symmetry at the subunit interface are signposted. This protein fold is indicative of the typical GST protein with the exception of the unique α9 of Alpha class GSTs. (B) The substrate / co-factor GSH (yellow) and the product Δ^4-AD (orange) are shown bound to the G-site (blue) and H-site (red), respectively in the top right corner. The second active site can be seen in the bottom left corner. Image generated from the PDB file 2VCV using the program PyMol.[35]

of four β-strands and three α-helices with a folding topology corresponding to βαβαββα), domain 2 or the C-terminal domain is entirely α-helical.[31 36]

Domain 1 of GSTs is always highly conserved and shows high sequence similarity even between GST classes.[37,38] Domain 2 by contrast shows far greater malleability in its structure and sequence and forms the distinguishing feature between most GST isoenzymes.[36] One such example is the unique α-helix 9 (α9) in domain 2 of the Alpha class GSTs.[39,40]

1.2.3. The active site

GST dimers contain two active sites (Figure 5B). Each active site is located at the confluence of the subunit and domain interfaces of GST. Each active site, therefore, is composed of structural elements of both domains of a subunit and from both subunits of the dimer.[31] Meaning, an active site requires proper domain association and dimerisation for full functionality (GSTs are obligate dimers).[31,41,42] Nevertheless, each active site of a dimer behaves independently of the other.[43]

Each GST active site may also be further subdivided into two binding sites (Figure 5B): the first is the hydrophilic G-site which is responsible for binding GSH, the defining substrate of the enzyme, and the second is the adjacent H-site which binds a widely diverse range of hydrophobic substrates.[32,36]

The G-site is highly specific for GSH and this can be explained in how the G-site is formed primarily form the highly conserved domain 1, thought to be descended and conserved from the single domain (an ancestral thioredoxin fold) protein ancestor of all GSTs.[36-38] Nevertheless, there are still some noteworthy differences between the classes. The binding of GSH to the G-site involves a network of polar interactions between GSH and domain 1 of a subunit and two salt-bridge interactions between both ends of the GSH tripeptide and two residues (Asp101 and Arg131)✤ of domain 2 of the second subunit of the GST enzyme. The latter interactions are not highly conserved however, while both are present in the Alpha class, there is only one interaction in the Mu, Pi and Sigma classes and none in the case of the Theta class by way of example.[31] Additionally, the sulfur atom of GSH forms a close contact with the hydroxyl group

---

✤ These residue numbers are based on the consensus sequence of Alpha class GSTs

of Tyr9 in the Y-GSTs[30] and in the case of the Alpha class of GSTs another close contact with the N^ε of Arg15.[44,45] Both residues are part of the so called active site loop connecting β-strand 1 with α-helix 1 in domain 1. Similarly, in the case of S/C-GSTs the sulfur atom of GSH will either form a hydrogen bond with the hydroxyl group of Ser13 or it will form a disulfide bond with Cys15.[30] Since the Alpha class GSTs are the primary concern of this study, it should be noted that Arg15 plays a role in stabilising the conformation of the active site loop by forming a salt-bridge with Glu104 of α-helix 4 in Alpha class GSTs.[39,40,44]

The H-site, in contrast, is a far less specific binding site.[32] The H-site of each GST isoenzyme is capable of binding a wide assortment of hydrophobic substrates with each isoenzyme within and across classes having its own unique, sometimes overlapping substrate specificities. The H-site is a solvent-exposed hydrophobic pocket that is formed between three sides. The active site loop (the loop connecting β-strand 1 with α-helix 1 in domain 1), the C-terminus of helix 4 and in the case of the Alpha class of GSTs the region immediately prior to and including α-helix 9 (Met208, Leu213, Ala216, Ala219 Phe220 and Phe222).[46]

1.2.4. The catalytic mechanism

GST enzymes perform a vital role in cellular defence against toxic physiological and xenobiotic compounds[16,32] as well as the harmful compounds created from oxidative stress.[47] In all cases, the enzyme performs its phase II detoxification[14] role by catalysing the conjugation of reduced glutathione (GSH) to the toxic compound. The conjugated product is far more soluble than the toxic substrate allowing for subsequent excretion by biological pathways such as the mercapturate pathway.[32,48]

The primary means by which GSTs catalyse the above reaction is to lower the energy required to deprotonate GSH.[49,50] The enzyme accomplishes this by lowering the pK_a of GSH after it binds the G-site, principally by stabilising the deprotonated anionic GS$^-$ form of GSH through interactions with either a Tyr, Cys or Ser residue (Section 1.2.1.).[30] The nucleophilic GS$^-$ anion then attacks the electrophilic centre of the hydrophobic substrate bound at the H-site and the two substrates are conjugated by nucleophilic substitution. The high cellular concentration of GSH (1-10 mM), at least three orders of magnitude higher than its K_d, makes it likely that GSH is always the first substrate to bind to the enzyme.[31,32] The sequential mechanism above may be represented as follows:[49-51]

$$E + GSH \rightleftharpoons E{\cdot}GS^- + H^+ \rightleftharpoons E{\cdot}GS^-{\cdot}R{\text-}X \rightleftharpoons E{\cdot}GSR{\cdot}X^- \rightleftharpoons E + GSR + H{\cdot}X$$
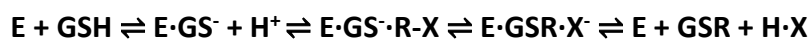
where E is the GST enzyme, R-X is the hydrophobic electrophilic substrate, GSH is the reduced glutathione, X is the leaving group and GS⁻ is the highly reactive thiolate anion. The reaction is hypothesised to pass through a transition state, an analogue of a Meisenheimer complex, which is typical of nucleophilic addition reactions.[49,52] Kinetic studies indicate the formation of the transition state is the rate limiting step. The conjugation of GSH to 2,4-dinitrochlorobenzene (CDNB), a reaction often used to assay the detoxifying catalytic efficiency of GST enzymes is shown as a specific example (Figure 6).[51]

The sulfhydryl group of free GSH in an aqueous solution has a pK_a of 9.2[53] and upon binding to the active site of a Y-GST the pK_a is lowered to between 6.2 and 7.1.[45,53,54] As revealed previously, the critical residue involved in Alpha class GSTs is Tyr9, which stabilises the deprotonated form of GSH by forming a hydrogen bond between the sulfur atom of GSH and its own hydroxyl group. It has been revealed, in the case of GSTA1-1, that Tyr9 is not fully responsible for lowering the pK_a of the GSH sulfhydryl group. The Arg15 residue (conserved in the Alpha class) through the positive electrostatic potential of its guanidinium group plays a significant role in stabilising the negatively charged thiolate form of GSH.[44,45] Indeed, it has been shown that the interaction between GSH and the Arg15 residue of GSTA1-1 lowers the pK_a of the GSH sulfhydryl group further than the interaction between GSH and Tyr9. It has been speculated that the role of Arg15 will be the same in GSTA3-3 though it has never been experimentally examined.

1.3. The dual roles of the GST enzymes

It is not unexpected that enzymes of the same protein superfamily would all share similar reaction chemistry and common mechanistic pathways.[55] Certainly this is the case of the GST enzymes which all share phase II detoxification activity. While there are differences in how each GST interacts with its substrates, and while GSTs may differ in their substrate specificity at their H-sites, each GST nevertheless performs the conjugation of GSH to a hydrophobic substrate as described above. More and more, however, researchers are discovering additional functions of the GST enzymes.
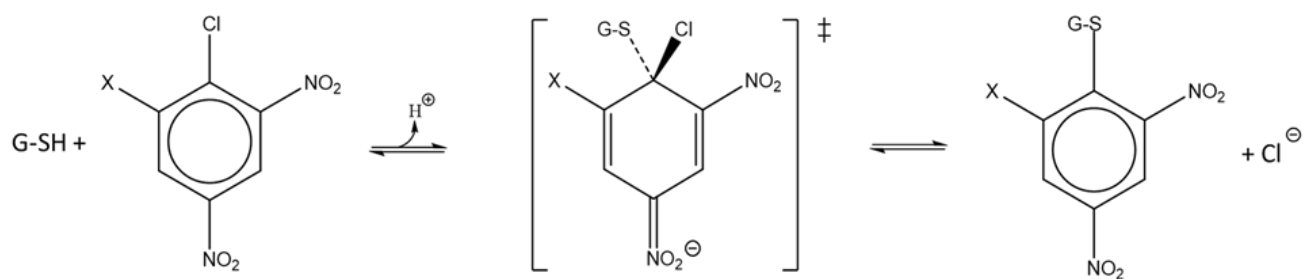
Figure 6: The glutathione *S*-transferase catalysed nucleophilic aromatic substitution reaction (S$_N$Ar) of GSH with CDNB to form S-(2,4-dinitrophenyl) glutathione, showing the putative transition state.[51]

Able to bind a wide variety of hydrophobic compounds at their H-site, GSTs play an important role in ligand transport and intracellular storage of a variety of non-substrate compounds such as hormones, metabolites, heme, steroids and drugs.[18,56-58] Further, some GSTs play an important role in signal transduction pathways by interacting with protein kinases.[11,59,60] Of interest to this study is that some GSTs have even evolved catalytic promiscuity. That is to say that despite a shared structural scaffold and similar reactive functional groups, some GSTs have evolved to catalyse distinct chemical reactions.[55,61] More precisely, they follow a catalytic pathway different to the one indicated by their Enzyme Commission number. There are GSTs that are able to catalyse the isomerisation 13-*cis*-retinoicacid, maleylacetoacetate and, particularly of interest to this study, ketosteroids.[62] Normally an enzyme responsibly for the isomerisation of a ketosteroid would have an EC 5.3.3.1 number. Enzyme plasticity is thought to give rise to promiscuous enzymes, the native catalytic activity of an enzyme is typically robust towards changes. That is to say point mutations at less well conserved regions of an active site often do not significantly diminish the native activity but may result in new functions.[62-64] Plasticity may also be the result of point mutations outside of the active site which may nevertheless result in enzyme repacking and changes in tertiary contacts within the protein resulting in structural or more ephemeral conformational dynamic changes at the active site that give rise to promiscuous reactions.[65] Promiscuous activities are typically slow relative to the main native activity; often so slow as to be physiologically irrelevant, and are under neutral selective pressure.[61,66] However, changes in selective pressures that infer a fitness benefit on the promiscuous activity may prompt an evolutionary refinement such that the promiscuous activity of the enzyme becomes its new main activity.[61,67]

An alpha class GST, GSTA3-3, is one of the most important steroid isomerase enzymes in humans.[10,11] That GSTA3-3 is selectively expressed in the testes, ovaries, adrenal glands and placenta argues that its role as a steroid isomerase enzyme has become its primary focus.[11] GSTA3-3 is still able to act as a detoxification enzyme but with reduced efficiency as compared to the rest of the Alpha class. Likewise, GSTA3-3 is not the only Alpha class GST that can act as a steroid isomerase but it has by far the greatest catalytic efficiency in regard to the reaction (see Table 1 for a comparison). In other words, plasticity in the Alpha class GSTs has allowed steroid isomerase activity to develop but only in the case of GSTA3-3 has that activity been selected for.

Table 1: Comparing the specific activities of Alpha class GST enzymes and KSI for the substrates CDNB and Δ^5-AD

Enzyme	Specific Activity (μmol.min^{-1}.mg^{-1})	
	CDNB	**Δ^5-AD**
GSTA1-1	111 ± 8[a]	12[b]
GSTA2-2	58 ± 4[a]	0.172[a]
GSTA3-3	23 ± 2[c]	197 ± 15[c]
GSTA4-4	7.5[d]	0.03[a]
KSI	NA	55000[e]

[a] Pettersson and Mannervik (2001)[53]
[b] Bjornestedt *et al.* (1995)[45]
[c] Johansson and Mannervik (2001)[11]
[d] Hubatsch *et al.* (1998)[68]
[e] Hawkinson *et al.* (1991)[69]
NA, not applicable

Previous studies have helped to elucidate the nature of how steroid isomerase activity has come about in the Alpha class of GSTs. Despite all Alpha class GSTs sharing over 80% sequence identity[70] there are important point mutations between them. Of particular note in this instance is that the H-site residues at positions 10, 12, 111, 208, 216 in the Alpha class GSTs are not conserved among GSTA1-1, GSTA2-2 and GSTA3-3 (Table 2).[70-72] These five residues account for 50% of the H-site. Comparing the crystal structures of the three isoenzymes indicated that only the H-site of GSTA3-3 is large enough to be able to accommodate the Δ^5-AD substrate such that is has a favourable orientation in regard to GSH at the G-site for the steroid isomerase reaction to be possible (see Figure 3C in Tars *et al.*, 2010).[72] GSTA1-1 which has the most comparable H-site to GSTA3-3 is able to accommodate both substrates at the active site simultaneously but with unfavourable orientations whereas GSTA2-2 by comparison is unable to bind both substrates simultaneously. In fact, it has been revealed that when five point mutations are made to GSTA2-2 to make its H-site match that of GSTA3-3, its steroid isomerase activity rises to be ~80% of GSTA3-3.[73] The five mutations uncover the potential steroid isomerase activity that exists within all Alpha class GSTs. Plasticity at the H-site, therefore, gives rise to steroid isomerase activity in the Alpha class GSTs, while the ability of the enzyme to bind and interact with GSH at the G-site remains.

It is worth mentioning that detoxification enzymes are among the most substrate and catalytically promiscuous enzymes known.[74-76] The nature of a detoxification enzyme requires that they protect an organism from a wide range of toxic compounds, even from xenobiotics foreign to the organism, necessitating broad substrate specificity/ambiguity.[75] It is speculated that detoxification enzymes are at the limits of substrate promiscuity attainable within the limits of a defined protein fold. Evidence has revealed that substrate promiscuity is often the first step towards catalytic promiscuity.[77-79] This is clearly demonstrated in the above case which demonstrated how five point mutations can lead to steroid isomerisation activity in GSTA2-2. Similarly, GSTA1-1 can be modified by only two point mutations to have greater catalytic activity for the 4-hydroxy-2-nonenal substrate, normally catalysed by GSTA4-4 with two-fold greater efficiency.[74] This latter case also illustrated that catalytic promiscuity must often be balanced against decreased stability.

The Alpha GSTs have far greater substrate promiscuity than other GST enzymes. This is due to greater conformational heterogeneity at the active site (specifically the unique and dynamic α-helix 9), but also throughout the protein structure.[74] In particular, flexibility at the domain

Table 2: Differences in the residue makeup of the H-sites of GSTA1-1, GSTA2-2 and GSTA3-3

Enzyme	Residue number				
	10	12	111	208	216
GSTA1-1	Phe	Ala	Val	Met	Ala
GSTA2-2	Ser	Ile	Phe	Met	Ser
GSTA3-3	Phe	Gly	Leu	Ala	Ala

interface around Trp21 was implicated in the broad catalytic range of hGSTA1-1. GSTs, therefore, provide an excellent model to study the nature of both substrate and catalytic promiscuity.

1.3.1. Isomerisation of Δ^5-AD by GSTs

GSTA3-3 uses the same structural scaffold common to all GSTs and more, it uses the same reaction machinery. That is to say, GSTA3-3 uses the same functional groups and residues to carry out its steroid isomerase reaction, as the Y-GSTs and more specifically the Alpha class GSTs use to catalyse their detoxification reactions. Nevertheless, there are important differences, perhaps the most obvious being that GSH is not a co-substrate in regard to the steroid isomerase reaction but instead acts as a cofactor.[40,72]

GSTA3-3 has attracted significant interest and research as a major player in steroid isomerisation, not only in the Alpha class of GSTs, but as the most efficient steroid isomerisation enzyme in humans.[11] The products of its steroid isomerisation reactions Δ^4-AD (the precursor to testosterone) and progesterone are essential to good health, so much so that both are included in the WHO Model List of Essential Medicines. Additionally, GSTA3-3 is a potential therapeutic drug target in the treatment of diseases characterised by excessive steroid hormone production such as polycystic ovary syndrome, Cushing's syndrome, congenital adrenal hyperplasia and some cancers of the sex organs.[80]

Yet, the steroid isomerase reaction mechanism of GSTA3-3 has yet to be resolved definitively. There are two major competing reaction mechanisms (Figure 7)[40,72] at present, each of which accounts for some of the observed experimental evidence, but not all. Both proposed mechanisms agree that GSH is an important cofactor. GSH will bind to the G-site (GSH is thought to bind the G-site first due to its high cellular concentration of between 1-10 mM in the cell) and will assume its deprotonated GS⁻ form which is stabilised by interactions with Tyr9. So far, the enzyme has behaved no differently than it would when performing its detoxification reaction. The changes are only evident when a ketosteroid binds to the H-site. The GSH in contrast to its previously established role as a nucleophilic attacker, instead acts a base catalyst that abstracts a proton from C4 of the Δ^5-AD substrate. There is a fine line between basicity and nucleophilicity (nucleophiles are weak Lewis bases) indicating that it is
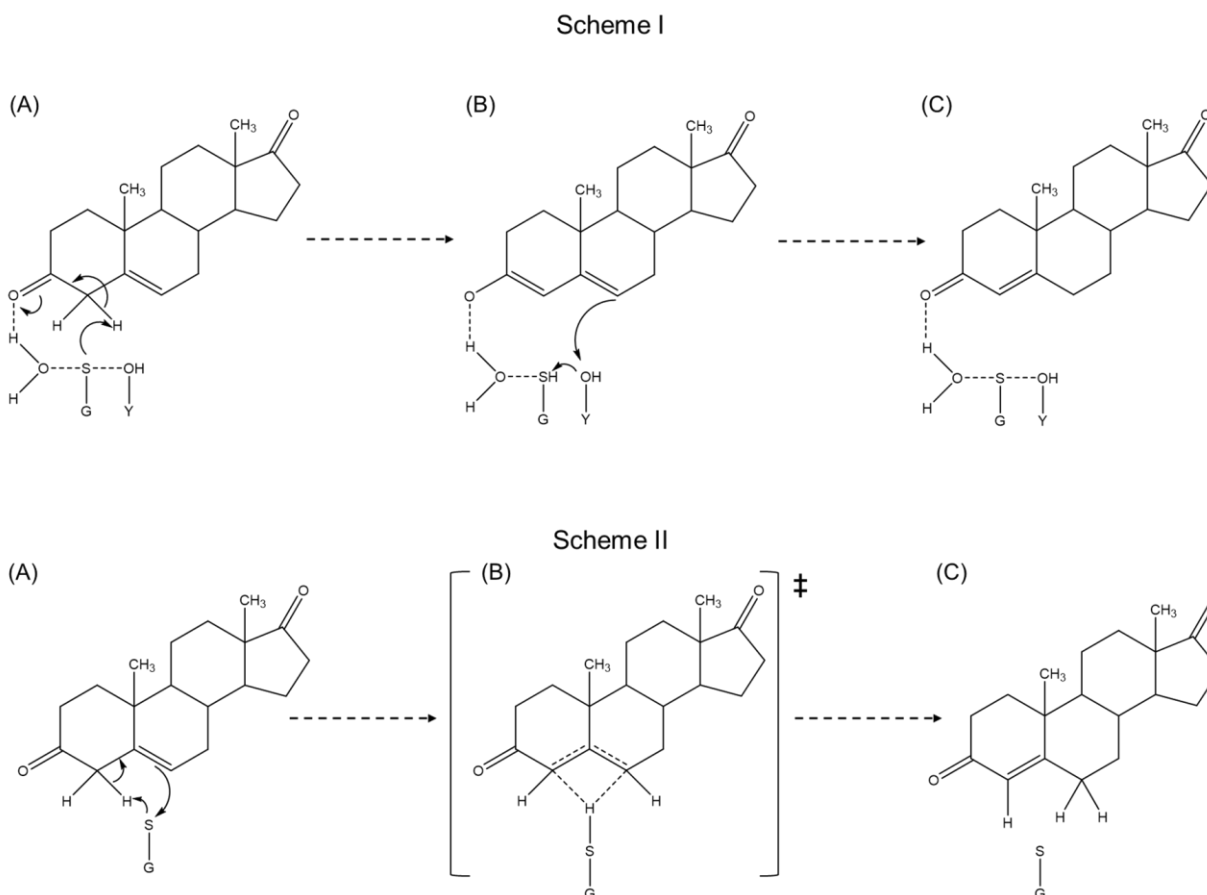
Figure 7: The two proposed reaction mechanisms for Δ^5-AD isomerisation by hGSTA3-3. In **Scheme 1**, [40] the deprotonated GS⁻ thiolate anion abstracts the carbon 4 proton of Δ^5-AD, a water molecule acts as a hydrogen bond donor, stabilising the negative charge of the dienolate intermediate (a,b). The keto form is regenerated by the transfer of the abstracted proton to carbon 6, by the transfer of negative charge via a conjugation system of π-bonds with Tyr9 acting as a proton shuttle (c). More recent evidence has found no proof of the proposed stabilising water molecule and it has been proposed that GSH plays a dual role of abstracting carbon 4 and stabilising the negative charge of O3 and the intermediate. [70] In **Scheme 2**, [72] GS⁻ abstracts a proton from carbon 4 while simultaneously transferring it to carbon 6. Bond formation and bond breaking occur simultaneously via a concerted single step mechanism, without a dienolate intermediate. In this mechanism, the role of Tyr9 is simply to help maintain the lower pK_a of GSH.

the lack of a proper leaving group in the steroid substrate that prevents the GS$^-$ anion from acting as a nucleophilic attacker.

At the moment that GS$^-$ deprotonates Δ^5-AD at C4, the competing reaction mechanisms begin to differ. In Scheme 1 (stepwise),[40] it was proposed that the reaction is step-wise and proceeds via a dienolate intermediate. It was proposed originally that electron delocalisation alone would stabilise the intermediate (via a conjugate system of vacant p-orbitals along O-C3-C4-C5-C6), but this explanation proved insufficient to explain the observed catalytic rates of GSTA3-3. A hypothetical water molecule was posited next that would act as a hydrogen bond donor to the carbonyl oxygen to stabilise the intermediate but no evidence of its existence has been discovered in crystal structures. Regardless, it was proposed that the intermediate is then protonated at C6 resulting in the product Δ^4-AD. Originally it was believed that the now protonated GSH would act as the proton donor but crystallographic data indicated it was too distant from C6 (~5 Å).[80] This data combined with experimental evidence that Tyr9 is itself deprotonated and reprotonated during the reaction[71] led to the conclusion that Tyr9 must act a proton shuttle. The hydroxyl group of Tyr9 protonates the intermediate at C6 and is in turn reprotonated by GSH. This leads to the deprotonation of GSH again, which after the product leaves and is replaced by fresh substrate at the H-site allowing the reaction to proceed again. This scheme remains contentious due to there being, as yet, no satisfactory explanation for how the intermediate might be stabilised.

In trying to address the shortcomings of the previous reaction mechanism a second reaction mechanism was proposed. Scheme 2 (concerted)[72] posits that that GSH does not merely act as a base catalyst but rather acts as an acid catalyst as well. GSH abstracts a proton from C4 while nearly simultaneously transferring it to C6. Bond breaking and bond formation occur via a single step concerted mechanism without a stable dienolate intermediate ever forming. Scheme 2 (concerted) successfully explains away the need for a stable intermediate but it fails to account for the distance between GSH and C6 in crystal structures, and evidence that Tyr9 may play a role beyond simply stabilising the GS$^-$ anion. Additionally, GSH has been shown not to be an obligate cofactor, even in the absence of GSH, GSTA3-3 is able to catalyse the isomerisation of Δ^5-AD to a significant degree, which seems to argue against GSH having such a prominent role in the reaction.[53]

1.3.1.1. Stepwise versus concerted reactions

Neither scheme is completely satisfactory and has left several details indeterminate. The critical difference between the two reaction schemes is the presence or absence of a stable intermediate during the reaction. That is, Scheme 1 proposes a stepwise reaction while Scheme 2 proposes a concerted single step mechanism.

Each type of reaction mechanism has its own advantages and disadvantages (Figure 8). For example, removing a H atom near the keto group of Δ^5-AD results in a negative charge imbalance in the steroid. The charge imbalance, in turn, results in electronic instability and an unfavourable high energy species (a transition state).[81] In a stepwise reaction, enzymes may make use of a variety of stratagems to stabilise the transition state. One approach is to use the functional group of a residue of opposite charge to the imbalance to stabilise it. The reduction in instability increases the lifetime of the species and it becomes an intermediate. The stabilisation of the intermediate can have many advantages for a catalysed reaction. In the case of multiple resonance forms, the enzyme may control the outcome of the reaction by stabilising a particular resonance form. Additionally, by completing the reaction over two or more steps, rather than one, the reaction can proceed through individual steps whose individual activation energies are lower than their sum. Intermediates also allow the enzyme to create kinetic and/or thermodynamic barriers which allows for greater control and can prevent reversible reactions.

This is the method used by KSI (EC 5.3.3.1). KSI shares ~43% sequence identity with GSTA3-3 and catalyses the same steroid isomerisation reaction, though without the use of a cofactor, with two orders of magnitude greater efficiency[8] (Figure 9; Table 1). After abstracting a proton from C4 of Δ^5-AD, KSI stabilises the resulting transition state by balancing the negative charge of the O3 oxyanion through two hydrogen bonds, C6 is then protonated forming the product. Discounting the role of GSH, this is similar to Scheme 1 (stepwise) proposed for GSTA3-3. Recall, however, that there is no known means by which GSTA3-3 may stabilise the transition state.

An alternative approach, the concerted mechanism,[82-84] is when two or more primitive changes such as bond-formation and bond-breaking occur within the same elementary reaction. Therefore, the reaction occurs through a single step passing through only one transition state, without any intermediates. The advantage of a concerted mechanism is that since the reaction
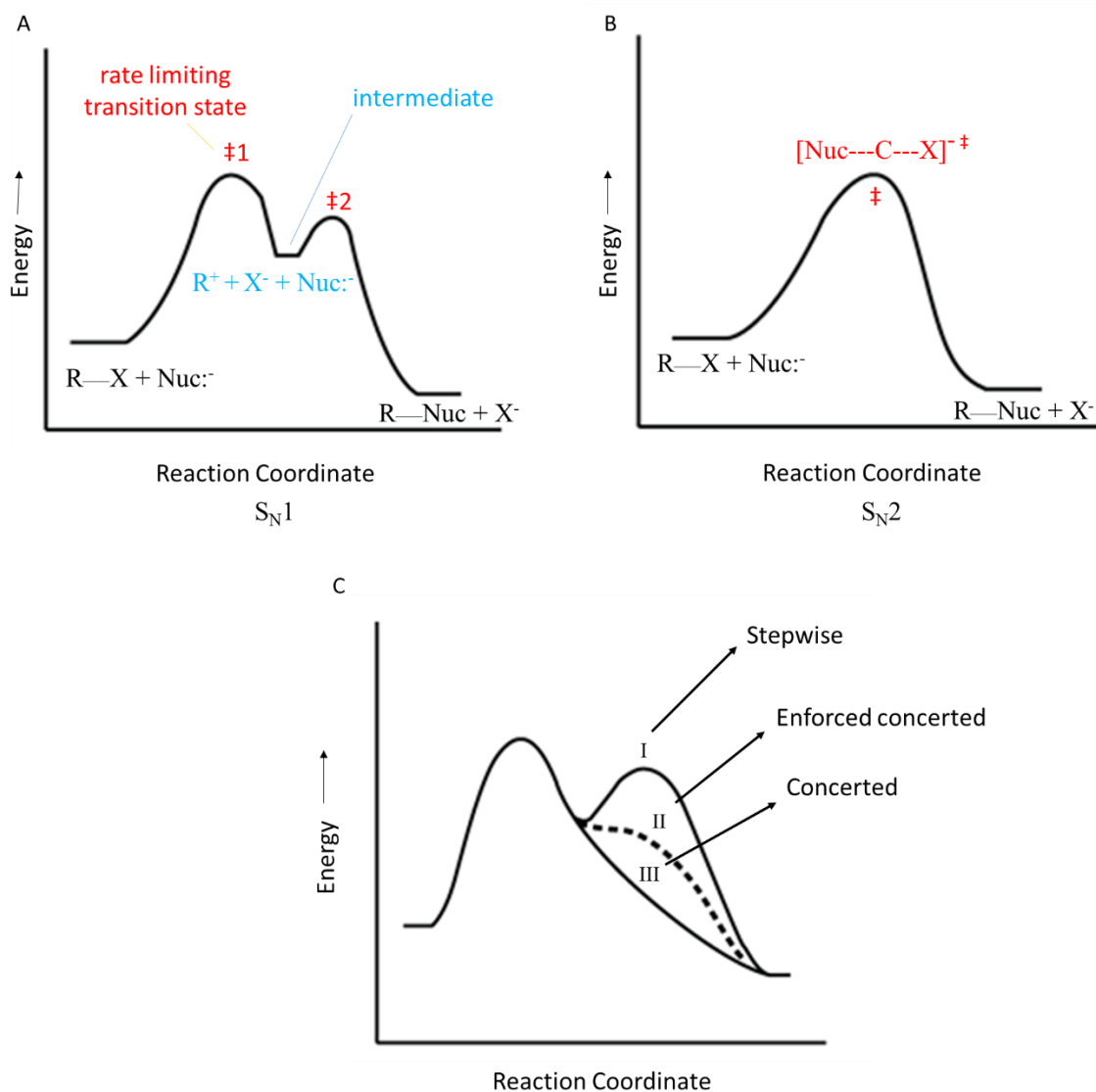
Figure 8: Comparing the energy diagrams of a stepwise, concerted and enforced concerted mechanism. (A) is a S_N1 reaction diagram representative of a stepwise mechanism. (B) is an S_N2 reaction diagram that is representative of a concerted mechanism. Both are nucleophilic substitution reactions that involve the removal of a leaving group (X^-) and replacing it with a nucleophile ($Nuc:^-$). In the S_N1 reaction, the leaving group leaves first creating a stable carbocation intermediate which is then bound to the nucleophile creating the product. In the S_N2 reaction, the leaving group leaves simultaneously to the nucleophile binding to the carbocation centre, the reaction has no intermediate and passes through a single transition state. Various conditions such as the strength of the nucleophile, the solvent (aprotic or protic) and the bulk of the alkyl groups attached to the electrophile will determine if the reaction proceeds through an S_N1 or S_N2 reaction. (C) Energy diagram showing an enforced concerted mechanism (II) on the borderline between stepwise (I) and concerted (III) mechanisms. A change in reaction conditions can reduce the energy barrier of the second transition state that the reaction proceeds immediately from the 'intermediate' to the product. This proceeds so quickly that the intermediate exists for so short a time that it arguably ceases to exist. Notice how the 'intermediate' no longer has a defined energy well between two transition states (the broken line - - -).
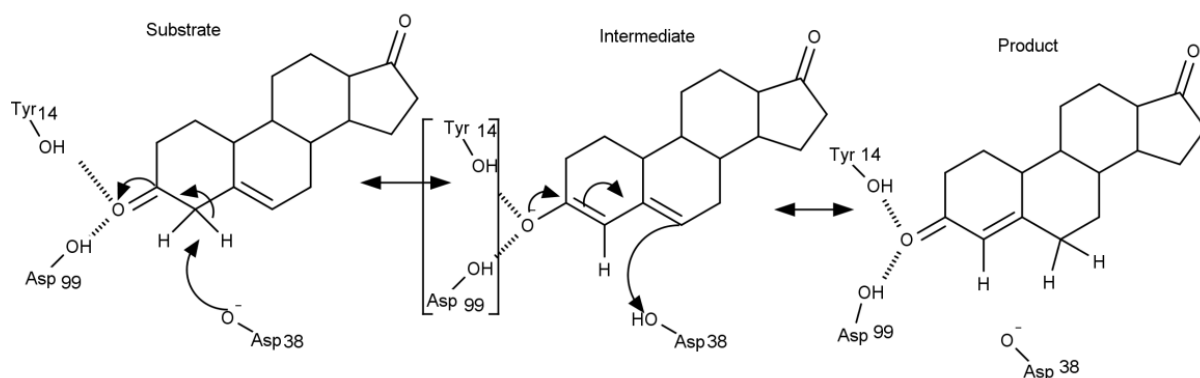
Figure 9: The catalytic mechanism of KSI. The reaction begins when a proton is abstracted from C4 of Δ^5-AD by Asp38 of KSI. The resulting dienolate intermediate is stabilised by two hydrogen bonds formed between the carbonyl oxygen of Δ^5-AD Tyr14 and Asp99 (the oxyanion hole). The abstracted proton is then transferred to C6 forming the product Δ^4-AD. This reaction mechanism is analogous to the proposed Scheme1 (stepwise) mechanism for GSTA3-3, the differences are that KSI does not need a cofactor and has an oxyanion hole to stabilise the intermediate. This figure is reproduced from Daka *et al.*, (2014).[85]

is so rapid no substantial charge imbalance can build and there is no need for stabilisation of the transition state.[83] Further, if the timing of the two steps is sufficiently synchronous they may become energetically coupled, so that the simultaneous progress of the primitive changes involves a transition state of lower energy than that for their successive occurrence.[83] For example, the energy released from bond formation may aid in bond breaking if both primitive changes occur simultaneously.[83]

It may be helpful to clarify the difference between a transition state and an intermediate. A transition state lies at a saddle point on potential-energy surface through which a reaction must pass on going from reactants to products. It has a fleeting existence and exists for less than the time of a bond vibration ($\sim 10^{-13}$ seconds).[82,86] An intermediate is a molecular entity with a lifetime appreciably larger than a molecular vibration that is formed from the reactants and reacts further to give products.

1.4. Does the dienolate intermediate exist?

Since the critical difference between the two reaction schemes is the presence or absence of a stable dienolate intermediate proof of its existence would be a strong indication that Scheme 1 (stepwise) is correct. Conversely, however, lack of proof of an intermediate may not always indicate a concerted mechanism.[83]

Pollack *et al*. (1989)[87] and Zeng *et al*. (1991)[88] have done extensive work in characterising the non-catalysed isomerisation of Δ^5-AD to Δ^4-AD under acidic and basic conditions. The non-catalysed isomerisation reaction passes through a dienolate intermediate under basic conditions and passes through a diene intermediate under acid conditions. Additionally, their work has shown that the ideal absorbance wavelength of the diene intermediate is 238 nm (ε_{13800} $M^{-1}.cm^{-1}$) but when the diene is ionised to its dienolate state it becomes 256 nm (ε_{15000} $M^{-1}.cm^{-1}$).

Recently, Daka *et al*. (2014)[85] found evidence of an intermediate during the steroid isomerisation reaction. Monitoring the GSTA3-3 catalysed isomerisation of Δ^5-AD to Δ^4-AD at either A_{238} and A_{256} they detected an increase in absorbance which subsequently decreased as the reaction continues to proceed, suggesting the formation of an intermediate which subsequently goes on to form product. Additionally, they note that when equilenin (an analogue

of the putative intermediate) is bound to GSTA3-3 it appears to be in its un-ionised form, suggesting that the intermediate, at least in the GSTA3-3 catalysed isomerisation reaction, is actually a diene[85] and not a dienolate as it is in KSI.[9] The detection of the intermediate (whether a diene or dienolate) strongly suggests Scheme 1 (stepwise).

Alternatively, a Quantum Mechanics/Molecular Mechanics (QM/MM) computational analysis of the GSTA3-3 catalysed steroid isomerisation mechanism by Calveresi *et al*., (2012) agrees that Scheme 1 (stepwise) is correct but suggests the reaction (based on the computationally predicted energy diagram of the reaction) is actually an enforced concerted mechanism which should not have a true intermediate.[80] The computational model suggests that GS$^-$ will deprotonate the C4 of Δ^5-AD nearly simultaneously to Tyr9 protonating Δ^5-AD at C6 to create the product. Interestingly, the calculated thermodynamics and energy diagrams of this computationally predicted model are in strong agreement with the experimentally determined values of Daka *et al.,* (2014). The computationally calculated thermodynamic parameters are nearly two-fold greater, because they were based on the dimeric structure of GSTA3-3 and not just a single active site.[89]

These two works, together, strongly suggest that Scheme 1 (stepwise) is correct but still leave the nature of the intermediate as contentious.

1.5.   Aim and objectives

The overriding aim of this study was to further elucidate the steroid isomerisation reaction mechanism of hGSTA3-3.

The two major competing reaction mechanisms (Figure 7), as well as more recent proposals, have left several details unanswered or controversial: (i) does the reaction proceed through a dienolate intermediate and, if so, how is it stabilised? (ii) what is the role of the GSH cofactor? (iii) what is the role of Tyr9? (iv) are there any other active site residues important to catalysis? Additionally, it needed to be examined what, if any differences, separates GSTA3-3 from the rest of the Alpha class?

In order to examine these questions, this study sought to examine the enzymatic, structural and conformational properties of the wild-type, Y9F, R15L and Y9F/R15L GSTA3-3 enzymes. The following general objectives were determined:

- Create plasmids which code for Y9F, R15L and Y9F/R15L hGSTA3-3
- Express and purify wild-type, Y9F, R15L and Y9F/R15L hGSTA3-3
- Determine the effects of the mutations on the structure of hGSTA3-3.
- Determine the effects of the mutations on the stability of hGSTA3-3.
- Determine the effects of the mutations on the conformational dynamics of hGSTA3-3.

The Y9F mutation was chosen because Tyr9 is highly conserved in GSTs and an important catalytic residue in GSTA3-3 which features prominently in the Scheme 1 (stepwise) reaction mechanism. The Y9F mutation removes the hydroxyl group of Tyr but otherwise does not affect the bulk of the residue. The R15L mutation was selected because Arg15 plays a significant role in the GSTA3-3 catalysed steroid isomerisation reaction. Arg15 is a highly conserved residue in Alpha GSTs which is important for lowering the pK_a of GSH but which has not undergone experimental evaluation in GSTA3-3. The R15L mutation was chosen because it removes the positive charge of the Arg residue but closely matches the bulk of the residue. Moreover, the R15L variant is a common natural substitution found in GST classes other than Alpha and has been the mutation of choice in other research works. As Arg15 is part of a salt-bridge it is necessary to examine if the mutation affects the structure, stability or conformational dynamics of the enzyme.

To answer the more specific questions, the following objectives were determined:

- Determine if the dienolate intermediate exists
- Determine if Tyr9 significantly contributes to the transformation of the intermediate to product

The experiments by Daka *et al*. (2014)[85] to detect the intermediate during the GSTA3-3 catalysed steroid isomerisation reaction can prove the existence of the dienolate intermediate along the reaction pathway. Additionally, Scheme 1 (stepwise) predicts Tyr9 is the major active site residue which protonates the intermediate at C6 to form the product. It was, therefore,

hypothesised that Y9F GSTA3-3 might be able to generate the intermediate but there should be evidence of the intermediate being converted to product at a decreased rate. This would provide strong evidence that Tyr9 acts a proton shuttle.

- Determine the effect of the mutations on the enzymatic properties of hGSTA3-3

To further investigate the role of the Tyr9 and Arg15 residues as well as the GSH cofactor, an extensive investigation into the enzymatic properties of GSTA3-3 was carried out. The role of the residues in binding and in lowering the pK_a of GSH were examined. Additionally, the specific activities of wild-type, Y9F, R15L and Y9F/R15L for the conjugation and steroid isomerisation reactions were examined.

Chapter 2
Experimental Procedures♠

2.1. Materials

The codon harmonised nucleic acid sequence encoding wild-type hGSTA3-3 with a N-terminal 6×His-tag and thrombin cleavage site was designed by Dr I. Achilonu (University of the Witwatersrand, South Africa). It was synthesised and sub-cloned into a pET-11a plasmid by GenScript Corporation (NJ, USA). The QuikChange II Site-Directed Mutagenesis Kit was purchased from Stratagene (La Jolla, CA, USA). Ampicillin and chloramphenicol were purchased from Roche Diagnostics (Mannheim, Germany). Inqaba Biotec (Pretoria, South Africa) conducted synthesis of the necessary oligonucleotide primers and performed all sequencing to confirm the identity of the plasmids. The *Escherichia coli* JM109 and BL21 (DE3) pLysS competent cells were obtained from Stratagene (La Jolla, CA, USA). The GeneJET™ Plasmid Miniprep Kit was obtained from Inqaba Biotec (Pretoria, South Africa). Sodium dodecyl sulfate polyacrylamide gel electrophoresis (SDS-PAGE) protein molecular weight markers (MWM; SM0431) and isopropyl-β-D-thiogalactoside (IPTG) were obtained from Fermentas Life Sciences (St. Leon-Rot, Germany). CDNB, GSH and D_2O were obtained from Sigma-Aldrich (St. Louis, MO, USA). The steroids, Δ^5-androstene-3,17-dione and Δ^4-androstene-3,17-dione, were obtained from Steraloids Inc (Newport, RI). All other reagents were of analytical grade. All solutions and media were prepared using distilled water and filtered through a 0.45 μm filter unless otherwise stated.

2.2. Preparation of mutant plasmids

The pET-11a plasmid coding for wild-type hGSTA3-3 (provided by Dr I. Achilonu) was modified to create three mutant plasmids encoding for Y9F, R15L and Y9F/R15L hGSTA3-3 according to the protocol of Papworth *et al*. (1996)[90] in conjunction with the QuikChange Site-

---

♠ Only those methods not covered in detail in the published paper in Chapter 4 are described here.

Directed Mutagenesis Kit. First, a reaction mix of 51 μl comprised of 5 μl (10× concentrate) reaction buffer, 1 μl (50 ng) double-stranded DNA template (pET-11a plasmid), 1 μl (125 ng) forward primer, 1 μl (125 ng) reverse primer, 1 μl dNTP mix, 41 μl milli-Q water and 1 μl (2.5 U/μl) Pfu DNA polymerase was set up. The reaction mix was subjected to a polymerase chain reaction (PCR) (Figure 10). Finally, the parental DNA template was digested with 1 μl (10 U/μl) DpnI, for one hour at 37 °C and one hour at 20 °C. DpnI targets methylated DNA only and, as such, only the parental DNA plasmid produced in a cellular environment was digested. Afterwards, the cells were transformed (Section 2.3.) with the remaining plasmids for the purposes of producing the variant proteins (Section 2.4.).

Primers, to create each mutant, were designed in accordance with the codon harmonised nucleic acid sequence encoding for GSTA3-3 (Figure 11) using Primer-X♦ and analysed for hairpins and loops by Gene Runner (V3.01, Hastings Software Inc., NY, USA). The primers are listed in Table 3. The primers to create Y9F and R15L mutant plasmids were applied to wild-type encoding pET-11a plasmid. The primer to create Y9F/R15L plasmid was applied to GSTA3-3 Y9F encoding pET-11a after it was created and expressed in *E. coli* JM109 cells (Section 2.3.) (this step is essential to ensure the base plasmid is made from methylated DNA).

2.3. Bacterial Transformation

Wild-type GSTA3-3 encoding pET-11a plasmid as well as the final DNA products of the above experiment (Section 2.2.) were used to transform JM109 *Escherichia coli* competent cells. The JM109 cell line was used to express and obtain high concentrations of quality plasmid DNA. Transformation was carried out by a one-step heat shock method.[91] All inoculation and growth procedures were conducted with sterilised media, containers and pipette tips using aseptic techniques under sterile conditions. Each plasmid (5 μl) was incubated on ice with 50 μl *Escherichia coli* cells which were subsequently heat shocked at 42 °C on a heating block for 45 s before being transferred back to ice for two minutes. Afterwards, 900 μl SOC expression recovery medium (super optimal broth with catabolite repression: 2% (w/v) tryptone, 0.5% (w/v) yeast, 10 mM NaCl, 2.5 mM KCl, 10 mM MgCl$_2$, 20 mM glucose) was added to each preparation, and thereafter incubated at 37 °C for 1 hour on a shaker (250 rpm).

♦ http://www.bioinformatics.org/primerx/
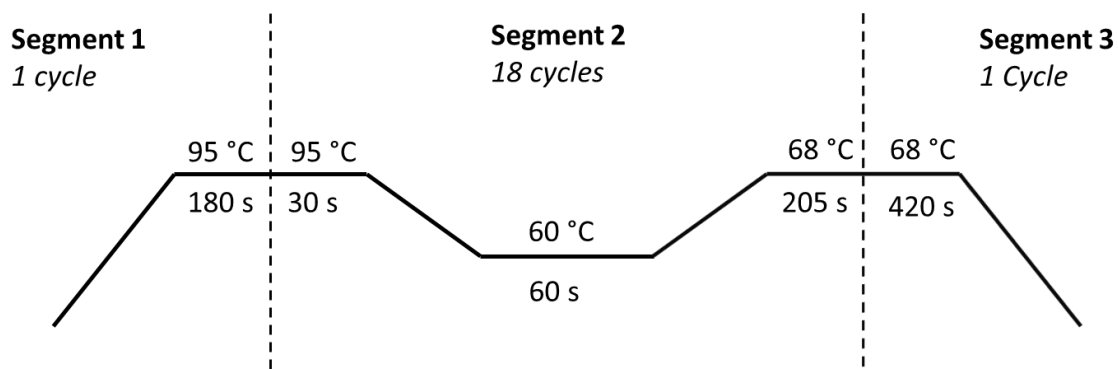
Figure 10: The polymerase chain reaction protocol used in conjunction with the QuikChange II Site-Directed Mutagenesis Kit. The procedure begins with an initialisation step (segment 1) whereby the temperature is raised to 95 °C for 180 s to denature the plasmid DNA into single strands. The reaction then proceeded to segment 2 which was repeated for 18 cycles, the 3 steps of the cycle are the denaturation step (same as segment 1), annealing step (the temperature is lowered just enough for the primers to anneal to the now single strands of the DNA plasmid) and elongation step (the temperature is raised slightly to promote optimum efficiency of the polymerase enzyme). The procedure ends on a long final elongation step (segment 3) to ensure any remaining single-stranded DNA is fully extended.

A

```
  1 CATATGGCTA GCATGACTGG TGGACAGCAA ATGGGTATGC ACCATCATCA TCATCATTCT
 61 TCTGGTCTGG TGCCACGCGG TTCTATGGCA GGGAAGCCCA AGCTTCACTA CTTCAATGGA
121 CGGGGCAGAA TGGAGCCCAT CCGGTGGCTC TTGGCTGCAG CTGGAGTGGA GTTTGAAGAG
181 AAATTTATAG GATCTGCAGA AGATTTGGGA AAGTTAAGAA ATGATGGGAG TTTGATGTTC
241 CAGCAAGTAC CAATGGTTGA GATTGATGGG ATGAAGTTGG TACAGACCAG AGCCATTCTC
301 AACTACATTG CCAGCAAATA CAACCTCTAC GGGAAAGACA TAAAGGAGAG AGCCCTAATT
361 GATATGTATA CAGAAGGTAT GGCAGATTTG AATGAAATGA TCCTTCTTCT GCCCTTATGT
421 CGACCTGAGG AAAAAGATGC CAAGATTGCC TTGATCAAAG AGAAACAAA AAGTCGCTAT
481 TTCCCTGCCT TCGAAAAAGT GTTACAGAGC CATGGACAAG ACTACCTTGT TGGCAACAAG
541 CTGAGCCGGG CTGACATTAG CCTGGTGGAA CTTCTCTACT ATGTGGAAGA GCTTGACTCC
601 AGCCTTATCT CCAACTTCCC TCTGCTGAAG GCCCTGAAAA CCAGAATCAG CAACCTGCCC
661 ACGGTGAAGA AGTTTCTACA GCCTGGCAGC CCAAGGAAGC CTCCCGCAGA TGCAAAAGCT
721 TTAGAAGAAG CCAGAAAGAT TTTCAGGTTT TAAGGATCC
```

B

Figure 11: The codon harmonised nucleic acid sequence encoding wild-type hGSTA3-3 with a N-terminal 6×His-tag and thrombin cleavage site. (A) The DNA sequence was codon harmonised to maximise protein expression in *Escherichia coli* cells. (B) The translated protein sequence. The thrombin cleavage site is highlighted in yellow, the thrombin enzyme will cleave the protein between the arginine and glycine residues marked with asterisks.

Table 3: Oligonucleotide primer sequences used for site-directed mutagenesis

Protein name	Fwd/Rev primer	Primer sequence	Codon change
hGSTA3-3 Y9F	Fw	5' CCCAAGCTTCAC<mark>TTC</mark>TTCAATGGACGGG 3'	TAC→ TTC
	Rev	5' CCCGTCCATTGAA<mark>GAA</mark>GTGAAGCTTGGG 3'	GTA→GAA
hGSTA3-3 R15L	Fw	5' CAATGGACGGGGC<mark>TTA</mark>ATGGAGCCCATCC 3'	AGA→TTA
	Rev	5' GGATGGGCTCCAT<mark>TAA</mark>GCCCCGTCCATTG 3'	TCT→TAA
hGSTA3-3 Y9F/R15L	Fw	5' CAATGGACGGGGC<mark>TTA</mark>ATGGAGCCCATCC 3'	AGA→TTA
	Rev	5' GGATGGGCTCCAT<mark>TAA</mark>GCCCCGTCCATTG 3'	TCT→TAA

The position of the desired altered nucleic acid sequence is highlighted in yellow.

Successful transformants were selected by plating the *Escherichia coli* cells on lysogeny broth (LB) agar [1% (w/v) tryptone, 0.5% (w/v) yeast, 0.5% (w/v) NaCl] containing 100 μg.ml⁻¹ampicillin. The plates were then incubated overnight (16-24 h). Only cells containing the pET-11a plasmid would have ampicillin resistance and be able to grow on the agar plate.

Plasmid DNA was extracted from the cells using the GeneJET™ plasmid miniprep kit (Fermentas, St. Leon-Rot, Germany) via the protocol of the kit.[92,93] The purified plasmid DNA was used in PCR (Section 2.2.), sequencing confirmation (Inqaba Biotec; Pretoria, South Africa) and transformation (via the same method already described) of BL21 (DE3) pLysS *Escherichia coli* competent cells for use in protein expression. When selecting for successful transformants of the BL21 (DE3) pLysS *Escherichia coli* competent cells, 30 μg.ml⁻¹ chloramphenicol was added to the agar plates because the pLysS plasmid also encodes for chloramphenicol resistance.

2.4. Heterologous protein expression and purification

The heterologous over-expression of wild-type and mutant GSTA1-1 encoding pET-11a plasmids was performed in BL21(DE3) pLysS *Escherichia coli* cells (Lucigen, Middleton, WI, USA) according to the method described by Daka *et al.* (2014).[85] BL21(DE3) pLysS *Escherichia coli* cells are suitable for the expression of non-toxic heterologous genes. The λ DE3 lysogen carries the gene for T7 RNA polymerase under control of the *lac*UV5 promoter, required for transcription of the pET-11a plasmid. The pLysS plasmid is important because it encodes T7 lysozyme which reduces basal polymerase transcription allowing the plasmid to become established and also provides chloramphenicol resistance to the cell.[94]

Since T7 RNA polymerase gene of DE3 lysogen is under *lacUV5* control its expression may be induced by the addition of IPTG.[95] IPTG binds to the lacI repressor, inhibiting it and allowing transcription via the *lacZ* promoter. Unlike the natural inducer of this gene (lactose), IPTG cannot be broken down in the cell, resulting in the genes becoming irreversibly over-expressed which, in turn, leads to the production of large amounts of T7 RNA polymerase. T7 RNA polymerase is extremely promoter specific and will transcribe only DNA that is downstream of a T7 promoter. In this case, the gene of interest on the pET-11a plasmid, and is

so prolific that most resources of a cell are converted to target gene expression. The desired gene product can comprise more than 50% of total cell protein a few hours after induction.

All inoculation and growth procedures described below were conducted in the presence of 100 μg.ml^{-1} ampicillin and 30 μg.ml^{-1} chloramphenicol, to create an environment hospitable only to the BL21 cells of interest. In addition, all procedures were carried out in Erlenmeyer flasks that were five times greater in volume than that of the culture to ensure adequate aeration during growth.

2.4.1. Induction studies

Induction studies were performed to determine if any changes needed to be made to the protocol of Daka *et al.* (2014)[85] to find the optimal conditions for the expression of wild-type, Y9F, R15L and Y9F/R15L GSTA3-3. Cultures of *Escherichia coli* BL21 (DE3) pLysS cells, already transformed with either wild-type, Y9F and R15L encoding pET-11a, in 2$\times$YT media [1.6% (w/v) tryptone, 1% (w/v) yeast extract, 0.5% (w/v) NaCl] were incubated at 20 or 37 $^{\circ}$C and 250 rpm until the start of the late-log phase (OD$_{600}$ = 0.6). IPTG was then added to cultures at final concentrations of 0-1 mM to induce over-expression of the pET-11a plasmids. After induction, the cultures were left to incubate between 4-16 h at 20 or 37 $^{\circ}$C and 250 rpm. Cells were then harvested from equal volumes of cell culture by centrifugation at 5000 g for 20 min at 10 $^{\circ}$C. The pellets were re-suspended in equilibration buffer (10 mM sodium phosphate, 1 mM ethylenediaminetetraacetic acid (EDTA), 0.02% sodium azide, pH 7.45), 0.02 mg.ml^{-1} DNAse, 0.02 mg/ml lysozyme and 2 mM MgCl$_2$ were added to further promote cell lysis and break down DNA, before lysis by sonication at 4 $^{\circ}$C. The lysate was centrifuged at 13 000 g at 4 $^{\circ}$C for 30 minutes and the supernatant and pellet collected. Samples of the supernatant and pellet were assessed by sodium dodecyl sulfate polyacrylamide gel electrophoresis (SDS-PAGE) according to the method of Laemmli (1970)[96] (Section 2.5.).

Subsequent over-expression procedures were conducted under those conditions which proved to be optimal.

2.4.2. Protein purification

The wild-type, Y9F, R15L and Y9F/R15L GSTA3-3 proteins were purified from their respective supernatants by immobilised metal affinity chromatography using a HisTrap FF 5 ml column (GE Healthcare Life Sciences, Uppsala, Sweden) charged with nickel according to the protocol of the column. The respective supernatants were diluted 1:1 with binding buffer (20 mM Tris-HCl, 200 mM NaCl, pH 7.4) and filtered through a 0.2 μm syringe filter to remove any large aggregates. The diluted supernatant was then loaded onto to the HisTrap column pre-equilibrated with 10 column volumes of binding buffer using an AKTA automated chromatographic system. The AKTA system monitored the eluate constantly via the on-board Jasco V-550 UV/Vis spectrometer and the column was washed with more binding buffer until an A_{280} reading of 0.000 was reached, indicating that weakly interacting, unbound, protein had already been eluted from the column. The column was then washed with elution buffer (20 mM Tris-HCl buffer containing 0.5 M imidazole at pH7.4) in a continuous gradient from 0-100% over 150 ml to elute bound protein. The eluent was collected in 2 ml fractions and spectroscopically assessed at 280 nm, again by the on-board spectrometer, for the presence of protein. To mitigate the risk of cross-contamination each protein was purified through use of its own HisTrap column.

Fractions containing pure protein, as assessed by SDS-PAGE, were pooled and concentrated on ice to a volume of 10 ml by ultra-filtration using a membrane with a molecular weight cut-off of 10 kDa.

2.4.3. Thrombin cleavage

After purification by IMAC, the protein underwent thrombin cleavage to remove the 6×His-tag and a second purification step to isolate the now cleaved protein. Purified wild-type, Y9F, R15L and Y9F/R15L protein were dialysed against thrombin cleavage buffer (20 mM Tris-HCl, 200 mM NaCl, 5 mM $CaCl_2$ at pH 8). After dialysis, 10 μl of a 1 U/μl stock of thrombin was adder per ml of protein solution and cleavage was allowed to proceed overnight (~12 h) at room temperature.

After the thrombin cleavage protocol was completed, the reaction mix was purified through a HisTrap FF and HiTrap benzamidine FF column (GE Healthcare Life Sciences, Uppsala,

Sweden) connected in series. Both columns were pre-equilibrated with binding buffer. The HisTrap column removes the cleaved 6×His-tag and the HiTrap benzamidine column removes thrombin from solution. Cleaved GSTA3-3 passed through both columns without binding and was collected in the eluate. The purity of thrombin cleaved protein was confirmed using 12% SDS-PAGE.

Pure, cleaved wild-type, Y9F, R15L and Y9F/R15L GSTA3-3 protein was dialysed against storage buffer (20 mM sodium phosphate buffer containing 1 mM EDTA and 0.02% (w/v) sodium azide at pH 7.45), concentrated to 10 ml and aliquoted in 1 ml volumes into cryogenic tubes, snap-frozen in liquid nitrogen and stored at -80 °C until use.

2.5. SDS-PAGE

Cell lysate obtained during induction studies and protein fractions obtained during the purification procedures were assessed by SDS-PAGE (Laemmli, 1970).[96] Cell lysate samples (10 µl) and protein samples (10 µl) were diluted two-fold with sample buffer [10% (w/v) glycerol, 2% (w/v) SDS, 5% (w/v) β-mercaptoethanol, 0.05% (w/v) bromophenol blue]. The samples were then heated at 95 °C for 5 minutes to ensure all protein was fully denatured and bound to SDS. SDS-PAGE is an electrophoretic technique wherein molecules are separated according to their electrophoretic mobility as they travel through a polyacrylamide matrix by the generation of an electric potential difference between either ends of the gel. Denaturing the protein gives them all a uniform shape and SDS is an anionic surfactant that binds to the protein and masks their natural charge. The result is that the electrophoretic mobility of the protein is a result of their size only, making the technique useful to determine the purity and size of a protein, which goes a long way in allowing the identity of a protein to be inferred.[97]

The samples were loaded into the wells of 12% (w/v) acrylamide/bis-acrylamide gels which were hand cast from a TGX™ FastCast™ Acrylamide kit (BioRad, California, U.S.). The gels were immersed in electrode buffer [1% (w/v) SDS, 0.192 M glycine and 0.025 M Tris, pH 8.5.] and electrophoresed at 180 V with discontinuous amperage for ~45 min using a Bio-Rad electrophoresis system (Bio-Rad, California, U.S.). A molecular weight marker (Fermentas Life Sciences, (cat. no.: SM0431), Ontario, Canada) was electrophoresed alongside the protein samples. The marker was a mixture of seven proteins: β-galactosidase (116 kDa), bovine serum

albumin (66.2 kDa), ovalbumin (45 kDa), lactate dehydrogenase (35 kDa), restriction endonuclease Bsp98I (25 kDa), β-lactoglobulin (18.4 kDa) and lysozyme (14.4 kDa). After electrophoresis, the gels were left in staining solution [2% (w/v) Coomassie Blue R250 staining solution containing 13.5% (v/v) glacial acetic acid and 18.75% (v/v) ethanol] for an hour and then de-stained with de-staining solution [40% (v/v) methanol and 10% (v/v) glacial acetic acid] until the background was clear to visualise the results.

Purity is indicated by a single band on the gel and identity of the proteins can be inferred by the distance the protein band travelled alongside a control lane containing a known pure solution of the protein, or protein markers of known molecular weight. Pure wild-type or any of the mutant GSTA3-3 proteins should correspond to a molecular weight of ~27 kDa uncleaved and 25.4 kDa post cleavage.

2.6. Protein concentration determination

The concentration of wild-type, Y9F, R15L and Y9F/R15L GSTA3-3 was determined spectrophotometrically using a Jasco V-630 UV-VIS spectrophotometer (Jasco Inc., Tokyo, Japan) and by applying the Beer-Lambert law:

$$A = \varepsilon c l \tag{1}$$

where A is the absorbance of the sample, ε is the molar extinction coefficient ($M^{-1}.cm^{-1}$), c is the concentration of the sample in solution (M) and l is the path length of the light passing through the solution (cm). An experimentally determined subunit molar extinction coefficient of 23900 M^{-1} cm^{-1} was used for wild-type GSTA3-3 and all three variant proteins.[11] The concentrations were determined by fitting a linear regression to five or more points from a serial dilution. All readings were corrected for the signal caused by the buffer alone. In the absence of an experimentally determined molar extinction coefficient, it may be calculated by using the formula described by Perkins (1986):[98]

$$\varepsilon = 5550\sum Trp + 1340\sum Tyr + 150\sum Cys \tag{2}$$

The formula indicates that wild-type GSTA3-3 should have a subunit molar extinction coefficient of 17760 $M^{-1}.cm^{-1}$ (only 74.3% of the experimentally determined value).

Nevertheless, it highlights that replacement of a Tyr residue with a Phe residue in the Y9F and Y9F/R15L variants may alter their determined subunit molar extinction coefficients. The accuracy of the calculated protein concentrations was, therefore, checked with the Bradford assay.

The concentration of stock solutions of GSH were also determined spectrophotometrically through use of Ellman's reagent to quantify the number of thiol groups in the stock solutions.[99,100]

2.6.1. Bradford assay

The Bradford assay is a colourimetric protein assay, based on the absorbance shift Coomassie Brilliant Blue G-250 dye experiences upon binding to Arg and other aromatic residues of a protein under acidic conditions; specifically, the absorbance properties of the dye undergo a hypsochromic shift.[101] This allows the protein concentration to be measured as a function of absorbance at 595 nm. Samples of both wild-type and variant protein shown to have an equal A_{280} were diluted 100 times, reacted with 100 µl of Bradford reagent (BioRad, California, USA) and measured at A_{595}.

While the R15L and Y9F/R15L variants have one less Arg residue than the wild-type, it is not expected that the loss of a single Arg residue would significantly affect the ability of the Bradford assay to act as a check.

2.7. Detecting the dienolate intermediate

The ideal absorbance wavelengths for the diene or dienolate intermediate generated during the conversion of Δ^5-AD to Δ^4-AD, in the absence of the enzyme, were found to be 238 and 256 nm respectively.[87,88] An enzyme-catalysed reaction was carried out using 10 µM Δ^5-AD and 2 mM GSH (personal communication with J. Daka[85]) in the presence of 1 µM GSTA3-3 and monitored by absorbance spectroscopy (A_{238}, A_{256}) in an attempt to detect the dienolate intermediate.[85]

2.8. Urea unfolding

2.8.1. Reversibility of unfolding

In order to calculate the change in Gibbs free energy during protein unfolding it must first be demonstrated that a state of equilibrium exists between the folded and unfolded states of the protein. This, in turn, requires the protein to be able to unfold reversibly and, further, that the protein refolds along the same path that it unfolds (i.e. there is no hysteresis effect).

All enzymes were confirmed to unfold reversibly, monitored by circular dichroism (CD), as described previously.[102] Samples of 20 μM unfolded wild-type, Y9F, R15L and Y9F/R15L protein, incubated in GST storage buffer with 8 M urea for 1 h at 20 °C, was achieved by a 10-fold dilution of each sample with GST storage buffer [20 mM sodium phosphate buffer containing 1 mM EDTA and 0.02% (w/v) sodium azide at pH 7.45] for 1 h at 20 °C. The refolded state of the protein was assessed using far-UV CD at 222 nm. All spectra were buffer corrected. The spectra were normalised by calculating the mean residue ellipticity, $[\Theta]$ $(deg.cm^2.dmol^{-1})$, using the following equation:[103]

$$[\Theta] = \frac{100 \times \theta}{Cnl} \tag{3}$$

where, Θ is the measured ellipticity signal in mdeg, C is the protein concentration in mM, n is the total number of residues in the protein chain, and l is the path length in cm. The amount of protein that was able to return to its native state was calculated by the comparison of the spectra of refolded protein with spectra of a control sample of 2 μM protein in 0.8 M urea, either wild-type, Y9F, R15L and Y9F/R15L variant as appropriate. The method to prove that the protein refolded along the same pathway on which it unfolds is described in Section 2.8.2.

2.8.2. Urea-induced equilibrium unfolding/refolding

Equilibrium unfolding studies were also performed as described previously.[104] Samples of 2 μM protein in 20 mM sodium phosphate buffer (pH 7.4), 1 mM EDTA, 0.02% (w/v) sodium azide and 0-8 M urea were used. Structural changes were monitored by far-UV CD at 222 nm and by fluorescence using excitation wavelengths of 280 and 295 nm with fluorescence emission recorded at 328 nm and 330 nm, respectively. The latter measurement is an excellent

local probe of the stability around the lone Trp21 residue of the protein subunits, which is near the active site. Rayleigh scatter plots of fluorescence (Ex_{340}; Em_{340}) were performed to monitor any protein aggregation. The experiment was performed in triplicate. Data were fitted and analysed using SigmaPlot v13.0 (Systat Software Inc; Chicago, IL, USA; Section 2.8.3.).

Refolding of the wild-type, Y9F, R15L and Y9F/R15L GSTA3-3 was also conducted over the same range of urea concentrations to prove equilibrium and the absence of hysteresis (Section 2.8.1.). Solutions of 20 µM wild-type, Y9F, R15L and Y9F/R15L GSTA3-3 protein in GST storage buffer with 8 M urea was diluted, with stocks of 10 M urea and GST storage buffer, as appropriate, to a protein concentration of 2 µM in various concentrations of urea and left to incubate for 1 hour at 20 ℃. The resultant unfolding and refolding curves were compared to identify whether the unfolding of the wild-type and variant hGSTA3-3 enzymes does indeed take place under equilibrium conditions.

2.8.3. Data fitting

All unfolding and refolding data obtained for the proteins were analysed according to a two-state unfolding process for a dimeric protein.

During a reversible two-state unfolding of a dimeric protein equilibrium is reached between the native (N) and the unfolded species (U):

$$N_2 \rightleftharpoons 2U \tag{4}$$

Furthermore, during a two-state unfolding transition, only the unfolded and native states are present at significant concentrations.[105] Hence, for a two-state mechanism:

$$f_N + f_U = 1 \tag{5}$$

where f_N is the fraction of folded or native protein and f_U is the fraction of unfolded protein. The recorded spectroscopic signal at any point during the unfolding of the samples is therefore in fact the sum of the signal of both species:

$$y_0 = y_N f_N + y_U f_U \qquad (6)$$

where y_0 is the signal obtained for the respective spectroscopic probe, f_N represents the fraction of folded protein, and f_U represents fraction unfolded protein. Further y_N represents the y value for the folded state and can be extrapolated from the linear pre-transition region of the unfolding data, while y_U represents the y value for the unfolded state and can be extrapolated from the linear post-transition region of the unfolding data (Figure 12).

By combining equations 5 and 6, the fraction of unfolded protein can be obtained:

$$f_u = \frac{(y_N - y)}{(y_N - y_U)} \qquad (7)$$

The equilibrium constant for the unfolding reaction (K_{eq}) is:

$$K_{eq} = \frac{[f_U]^2}{[f_N]} \qquad (8)$$

The total protein concentration, P_t, expressed in terms of the monomeric species is:

$$P_t = 2N_2 + U \qquad (9)$$

and the fraction of native dimeric species is:

$$F_N = 1 - F_U \qquad (10)$$

where:

$$F_U = \frac{[U]}{P_t} \qquad (11)$$
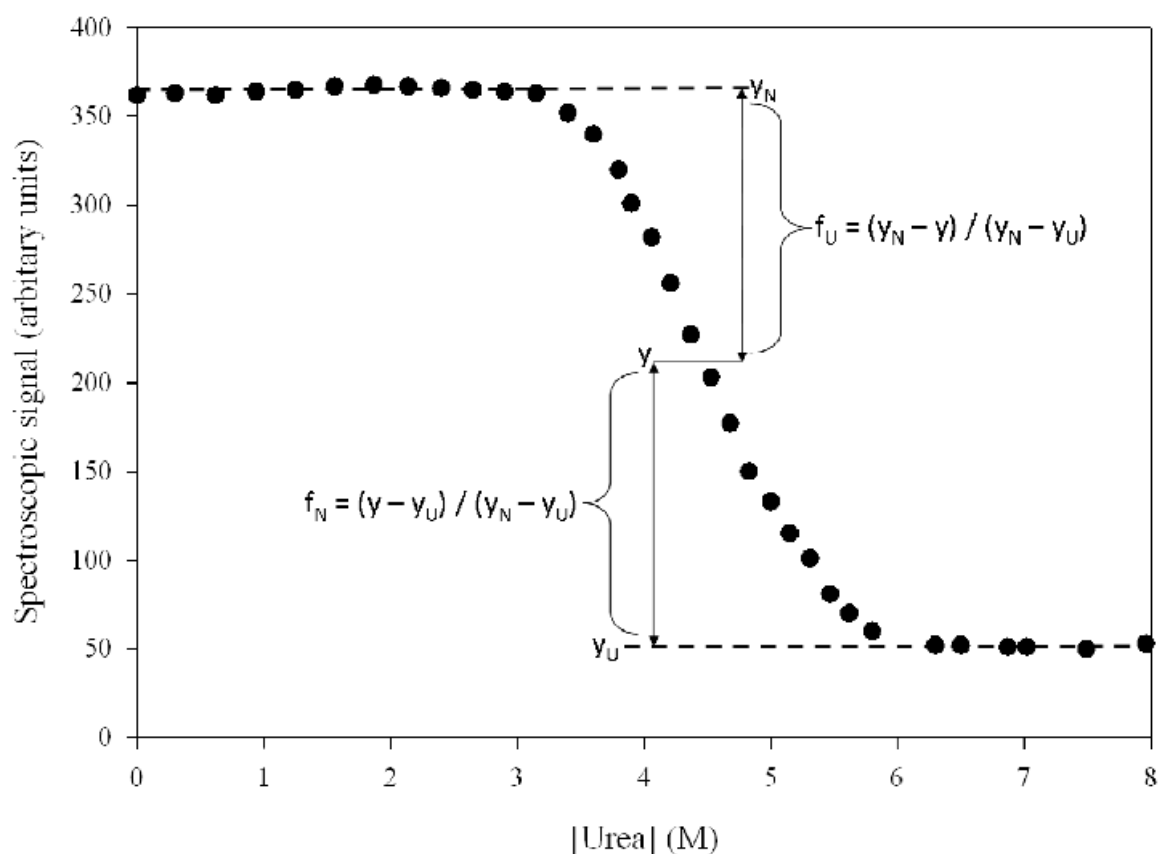
Figure 12: Representation of a typical two-state urea denaturation curve. The pre-transition region (plot of Y_N) where the protein remains folded, post transition region (plot of Y_U) where the protein is fully unfolded and the transition region where the protein is a state of equilibrium between the folded and unfolded states as a function of urea concentration are shown. Image adapted from Shirley (1995).[106]

Combining these equations and solving for F_U in terms of the equilibrium constant K_{eq} and P_t, one obtains the following equation:

$$F_U = \frac{\sqrt{K_{eq}^2 + 8K_{eq}P_t} - K_{eq}}{4P_t} \qquad (12)$$

Rearranging equation 7 yields the equation used for fitting the denaturation transitions:

$$y_0 = y_N(1 - f_U) + y_U(f_u) \qquad (13)$$

Substituting equation 13 allows the k_{eq} of unfolding to be calculated and hence $\Delta G°$ according to the equation:

$$\Delta G° = -RT\ln K_{eq} \qquad (14)$$

where $\Delta G°$ is the free energy of unfolding, R is the gas constant and T is temperature in Kelvin. In order to determine $\Delta G_{(H2O)}$ it is assumed that according to the linear free-energy model $\Delta G°$ has a linear dependence on denaturant concentration [D] for all urea concentrations (Tanford, 1968, 1970). Therefore:

$$\Delta G° = \Delta G_{(H2O)} + m[D] \qquad (15)$$

where $\Delta G_{(H2O)}$ represents the free energy difference between the folded and unfolded states in the absence of denaturant, m is the m-value for the dependence of free energy on denaturant concentration (calculated from the linear equation 15 which has the formulae $y = mx + c$) which is also an indicator of co-operativity and can be related to the change in solvent-accessible surface area ($\Delta SASA$),[107,108] and [D] is the denaturant concentration.

The equilibrium unfolding data obtained was fitted with these equations using SigmaPlot version 13.0 (Systat Software Inc; Chicago, IL, USA) and the parameters $\Delta G_{(H2O)}$ and the m-value were obtained.

Chapter 3
Results♥

3.1. Sequencing

The sequencing results of the open reading frame (ORF) for wild-type GSTA3-3 encoding pET-11a plasmid matched exactly to the sequence ordered by Dr I. Achilonu. The sequencing of the mutant plasmids indicated the desired mutations were successfully inserted and that no unwanted mutations had occurred (Figure 13).

3.2. Over expression and purification
3.2.1. Induction studies

Induction studies were performed to optimise the expression of Y9F and R15L GSTA3-3. The results of the induction studies were examined by SDS-PAGE (Figure 14). It was found in both cases that the optimum induction conditions were the same as that for the wild-type. Namely, cultures were induced by adding IPTG to a final concentration of 1 mM and incubated at 37 °C for ~16 h before cells were harvested. Similarly, like the wild-type, both Y9F and R15L GSTA3-3 was soluble in the supernatant fraction of the lysate. In light of this result no induction studies were performed on the Y9F/R15L GSTA3-3 mutant and it too was expressed under the same conditions.

3.2.2. Purification

Purified cleaved wild-type and mutant GSTA3-3 was obtained from cell lysate through a two-step process (Section 2.4.), first 6×His-tag wild-type and mutant GSTA3-3 was purified from cell lysate via IMAC using a HisTrap FF column (Figure 15). In the second step, this purified protein underwent thrombin cleavage to remove the 6×His-tag and then went through a second purification step to isolate wild-type and mutant GSTA3-3 from the cleaved tag and thrombin (Figure 16).

♥ Only those results not covered in sufficient detail in the published paper in Chapter 4 are reported here.
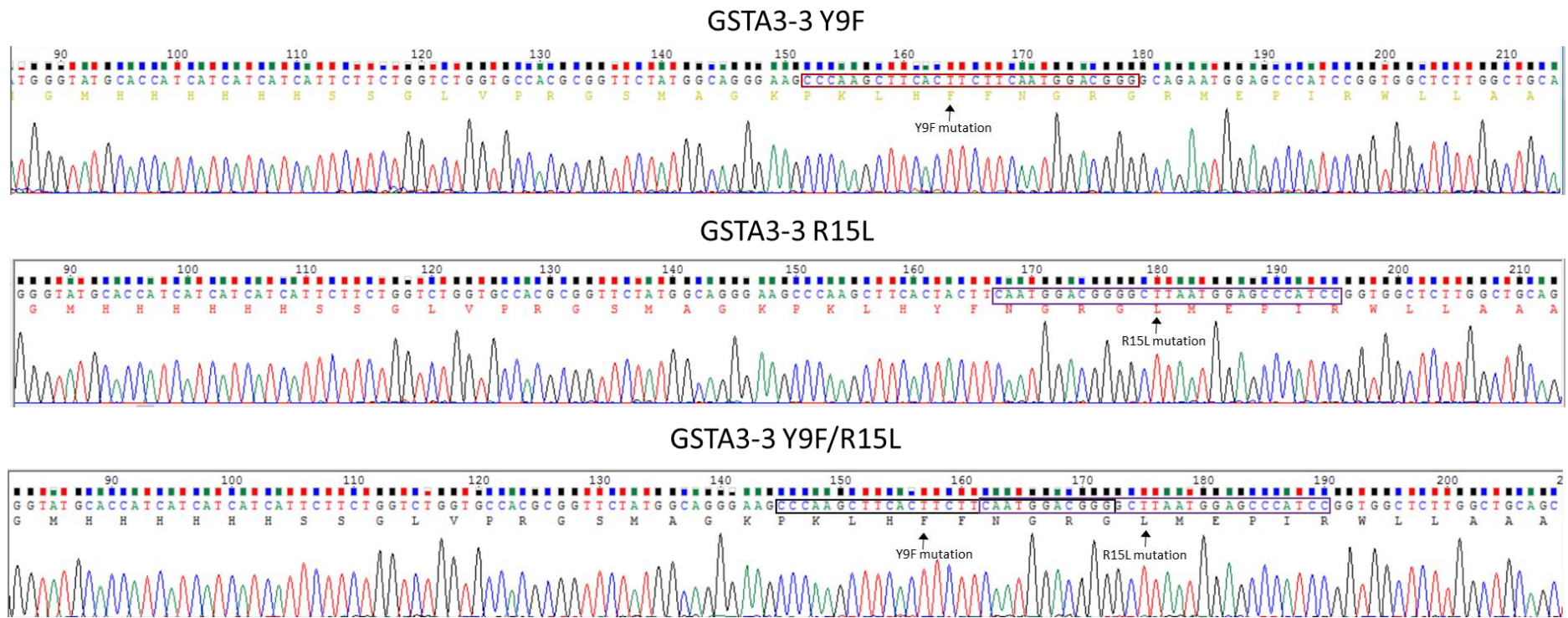
Figure 13: Extracts of the sequencing results showing successful site-directed mutagenesis creating plasmids which code for Y9F, R15L and Y9F/R15L GSTA3-3. The successful incorporation of the primer sequences is shown in boxes, the position and successful incorporation of the desired mutations are indicated by arrows. No unwanted mutations were incorporated into the sequences.
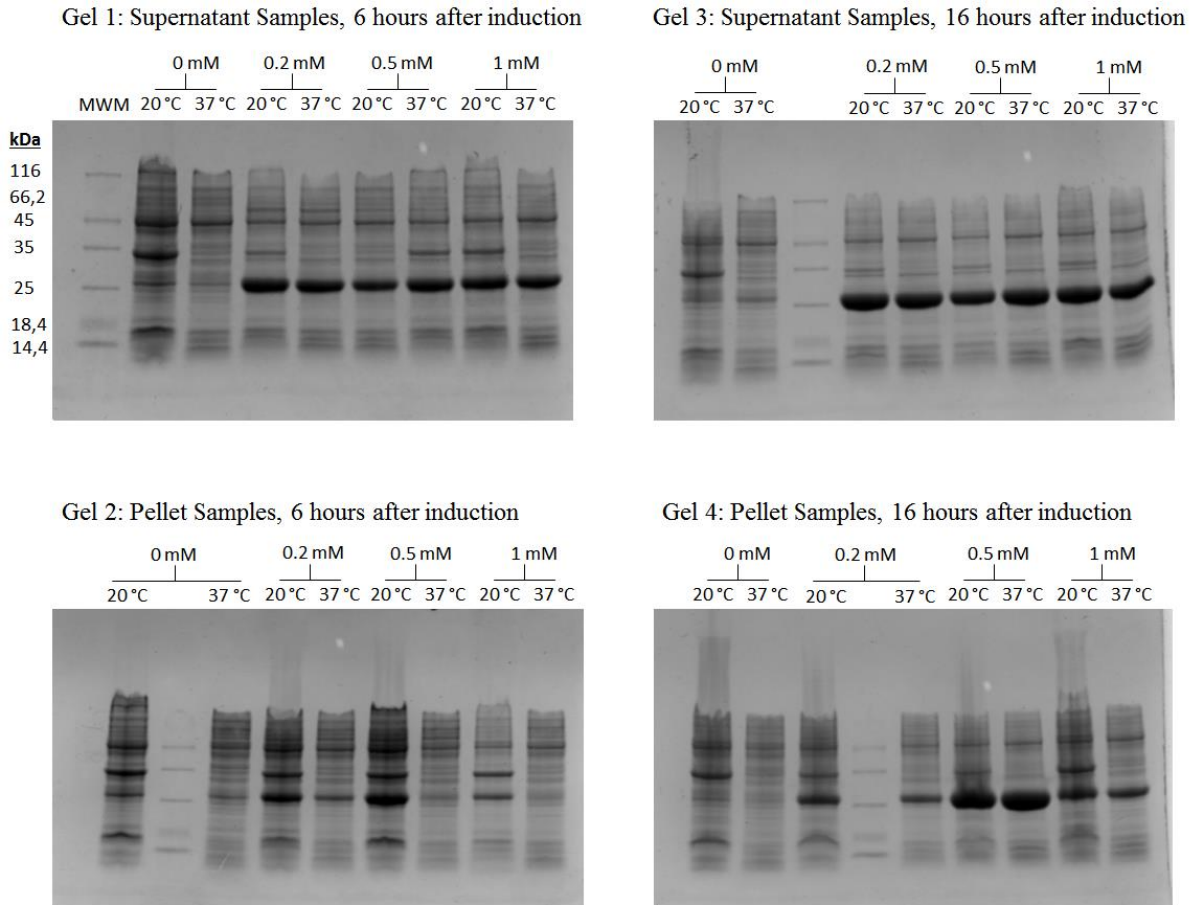
Figure 14: Expression patterns of Y9F GSTA3-3 at 20 °C and 37 °C and under induction from various concentrations of IPTG. The results indicate that Y9F GSTA3-3 has higher levels of expression in the presence of IPTG, though at concentrations between 0.2-1.0 mM the change in expression levels appears minimal. Significant amounts of Y9F GSTA3-3 were present in the supernatant with significant levels of Y9F GSTA3-3 present in the pellet only after 16 h. This data is also representative of the results seen for R15L GSTA3-3 (not shown). Optimal expression of Y9F GSTA3-3 occurred after 16 hours at 37 °C in the presence of 1 mM IPTG.
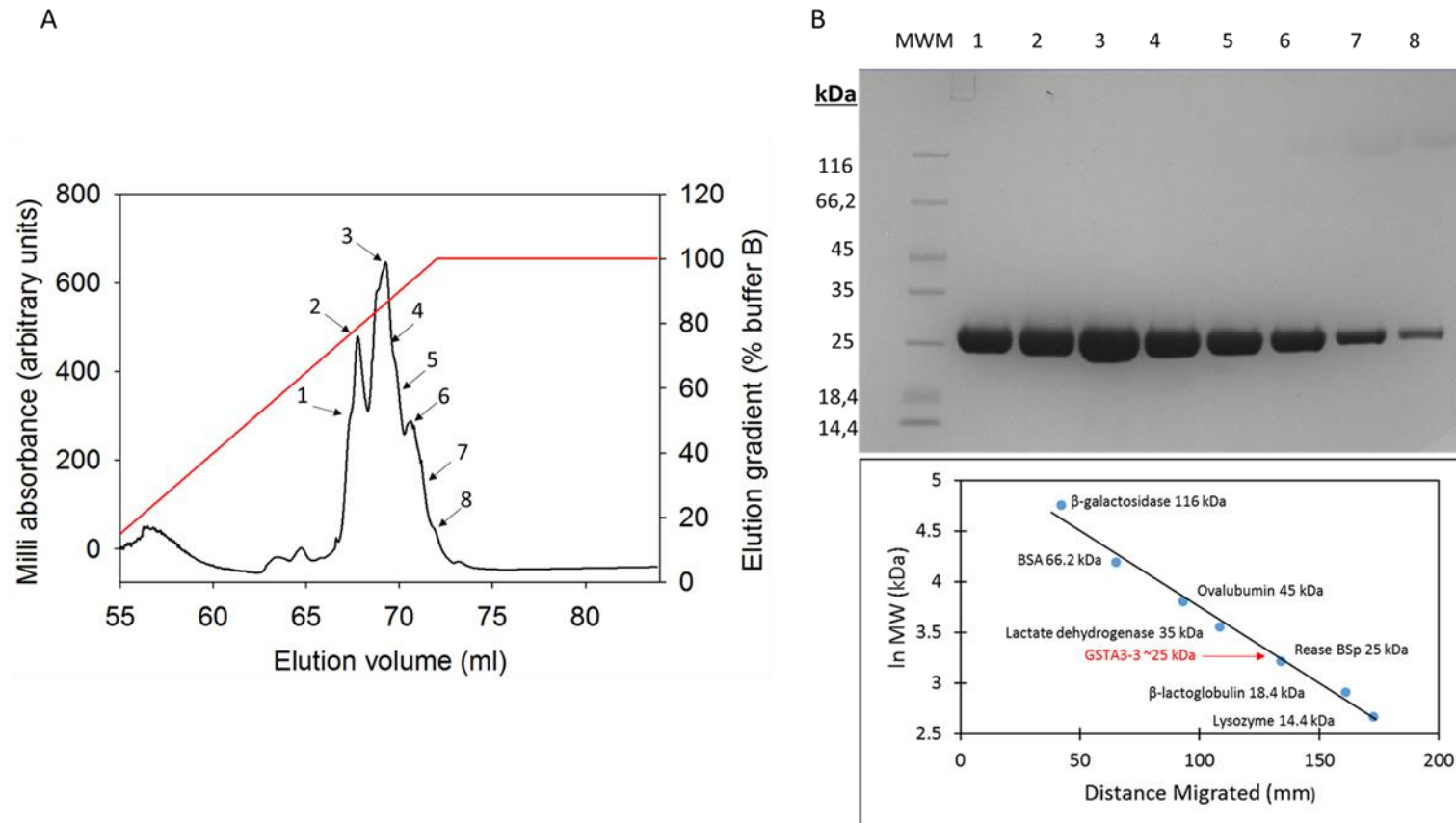
Figure 15: Elution profile of cell lysate containing wild-type GSTA3-3 during IMAC purification and proof of purity. (A) Elution was monitored at A_{280} (black), the position of the collected elute fractions suspected of containing pure wild-type GSTA3-3 are marked. Protein release was triggered by increasing concertation of Imidazole (Buffer B; Red). **(B)** SDS-PAGE analysis of the selected fractions. The analysis indicated pure protein of ~25 kDa which corresponds to the expected mass of 27 kDa for pure GSTA3-3. Similar results were obtained for the Y9F, R15L and Y9F/R15L.
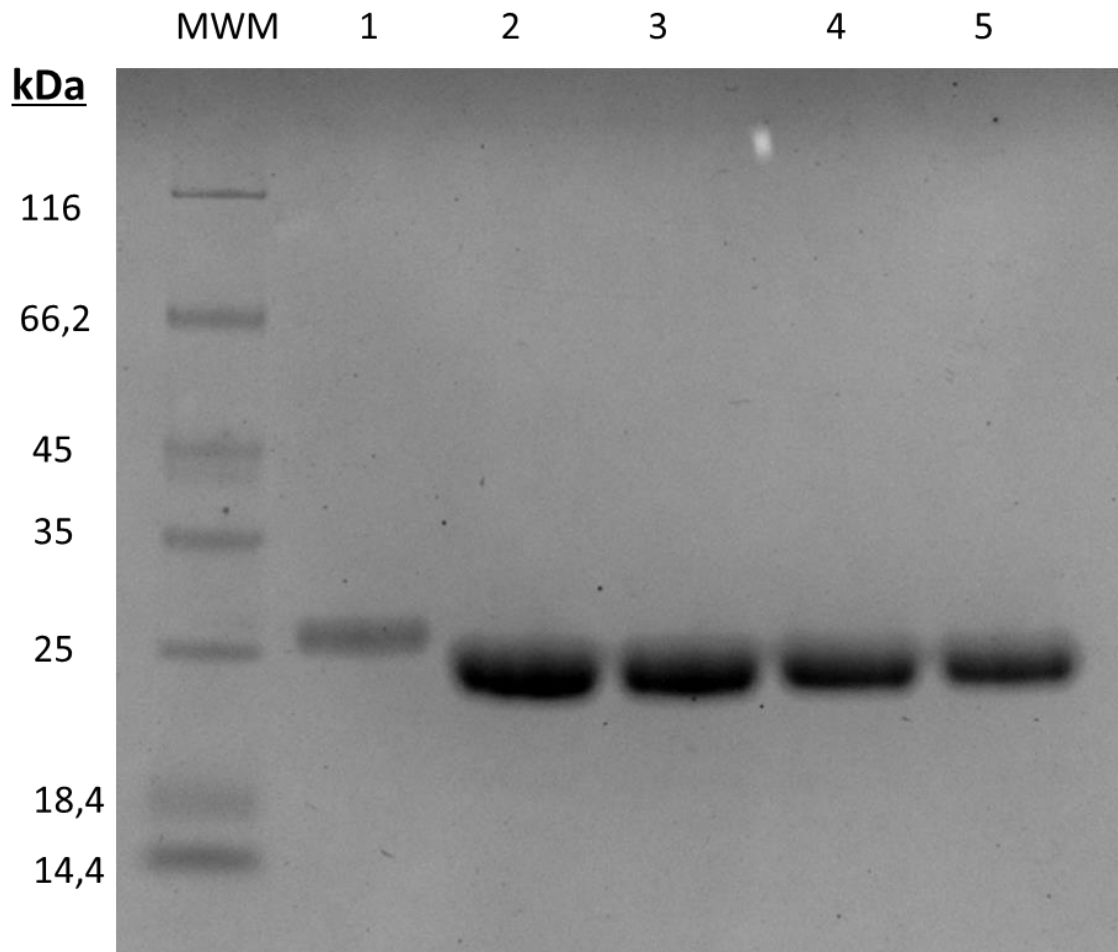
Figure 16: Showing purified wild-type, Y9F, R15L and Y9F/R15L GSTA3-3 post 6×His-tag cleavage. Lane 1 is 6×His-tagged wild-type GSTA3-3 and lanes 2-5 are wild-type, Y9F, R15L and Y9F/R15L GSTA3-3 (with the 6×His-tag removed), respectively. It can clearly be seen that the cleaved proteins travel further down the gel which is typical for proteins of a lower molecular weight. Cleavage of the 6×His-tag results in the removal of ~1.5 kDa.

SDS-PAGE was used to analyse the molecular mass and purity of wild-type, Y9F, R15L and Y9F/R15L GSTA3-3. After final purification, all proteins were judged to be pure as each protein showed as only a single band on SDS-PAGE gels. The molecular weight of the proteins was calculated by comparing the distances the GST proteins migrated in comparison to the set of known standards that migrated under the same conditions, was ~26 kDa (Figure 15). This corresponds to the expected value of 27 kDa.

3.2.3. Protein concentration determination

The concentration of wild-type and mutant GSTA3-3 was determined at 280 nm using the protein subunit molar extinction coefficient of 23900 $M^{-1}.cm^{-1}$. The Y9F point mutation was confirmed by the Bradford assay to not have any significant effect in altering the extinction co-efficient of the protein (Table 4).

The wild-type enzyme was purified from one litre of bacterial culture, yielding ~26 mg of purified protein. Whereas, one litre of bacterial culture yielded ~63, ~34 and ~49 mg of Y9F, R15L and Y9F/R15L GSTA3-3, respectively. This indicates that none of the mutations resulted in lowering the protein yield, suggesting that they do not significantly affect protein expression, folding and stability.

3.3. Detecting the dienolate intermediate

The presence or absence of an intermediate during the GSTA3-3 catalysed steroid isomerisation reaction has significant implications for determining the proper catalytic mechanism employed by the enzyme. Recently Daka *et al*. (2014)[85] reported for the first time, the detection of an intermediate, via absorbance spectroscopy, during the GSTA3-3 catalysed steroid isomerisation reaction. However, the results of Daka *et al*. (2014)[85] could not be reproduced in the current study. No intermediate was detected following their protocol with wild-type or Y9F GSTA3-3. This was true whether the detection of the intermediate was followed at 238 or 256 nm (Section 2.7.). Attempts to reproduce their results with varying concentrations of enzyme and Δ^5-AD also failed (Figure 17). These findings also made it impossible to investigate the importance of Tyr9 in converting the intermediate to product as hoped (Section 1.5.).

Table 4: Comparing the accuracy of the experimentally determined extinction co-efficient for GSTA3-3 for each of the variant proteins.

Protein	Concentration determined by absorbance (μM)	Absorbance of Bradford dye (arbitrary units)	Similarity to wild-type (%)
Wild-Type	2	0.1385	100
Y9F	2	0.1379	99
R15L	2	0.1339	96.6
Y9F/R15L	2	0.1352	97.6
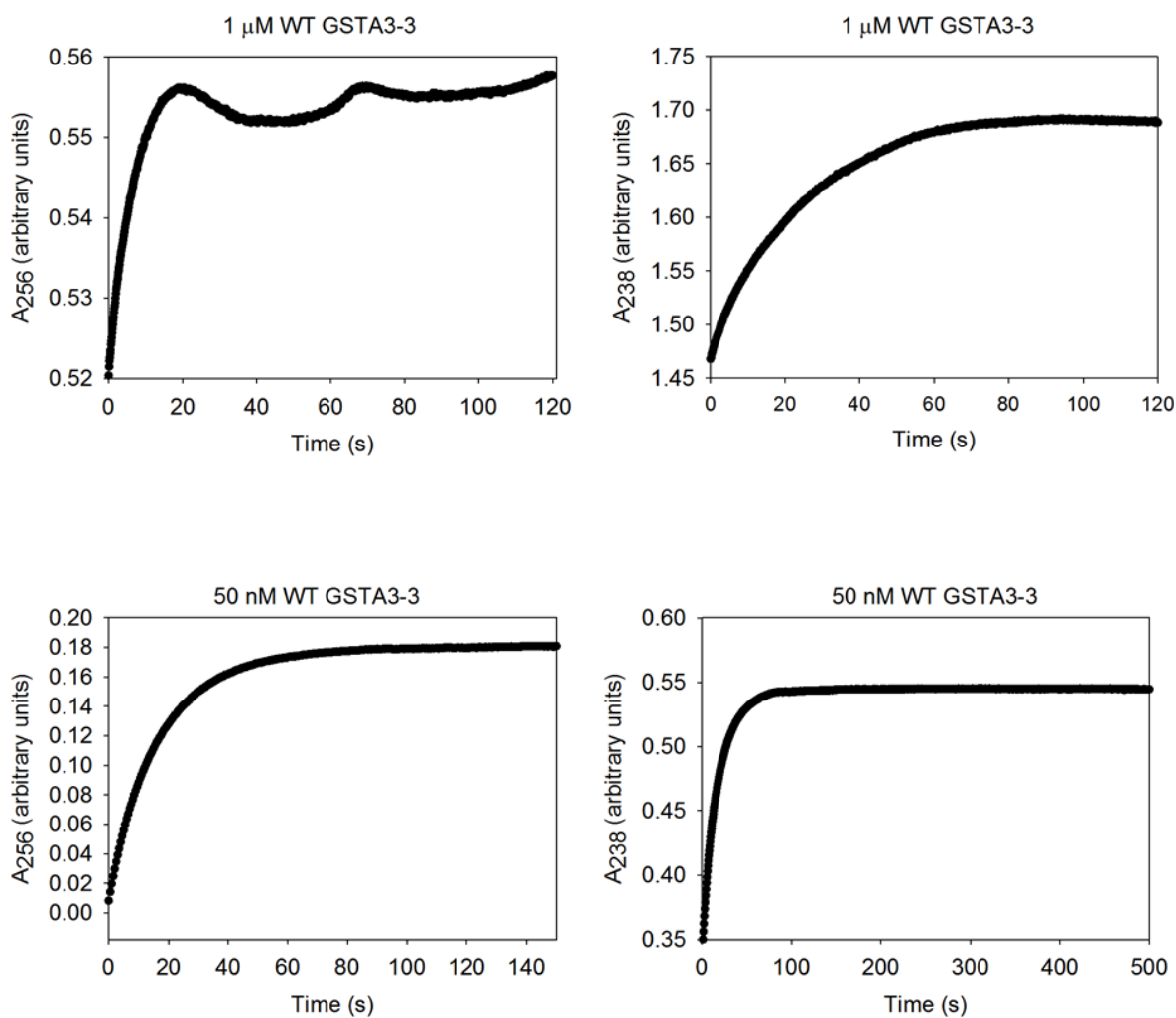
Figure 17: Attempts to detect the dienolate intermediate during GSTA3-3 catalysed steroid isomerisation by absorbance spectroscopy at A_{238} and A_{256}. If an intermediate was formed during the catalysed reaction, there would be an initial rise in the A_{238} or A_{256} followed by a subsequent decline as the intermediate was transformed into product. This is not the case in any of the reactions shown above where no intermediate was detected.

3.4. Conformational stability of wild-type, Y9F, R15L and Y9F/R15L GSTA3-3

3.4.1. Reversibility of urea-induced unfolding

The recovery of unfolded wild-type, Y9F, R15L and Y9F/R15L GSTA3-3 to its native, folded, state was established by far-UV CD ($[\Theta]_{222}$). In each case, after refolding (Section 2.8.1.), wild-type, Y9F, R15L and Y9F/R15L GSTA3-3 showed > 95% recovery (Figure 18). Additionally, it was established that the proteins refold reversibly without any hysteresis effect (Section 2.8.2.), the proteins refolded along the same pathway they unfold (Figure 18).

The data indicate that wild-type, Y9F, R15L and Y9F/R15L GSTA3-3 establish a state of equilibrium between their native and unfolded states in the presence of urea. Thus, the unfolding pathways of wild-type, Y9F, R15L and Y9F/R15L GSTA3-3 were analysed using thermodynamic principles to determine their conformational stabilities.

3.4.2. Urea-induced equilibrium unfolding

The urea-induced unfolding curves for wild-type, Y9F, R15L and Y9F/R15L GSTA3-3 were determined by far-UV CD (Figure 19) and fluorescence spectroscopy (Figure 20). In each case the unfolding curves are sigmoidal and monophasic, indicative of a highly co-operative and two-state unfolding curve.[109] Therefore, the unfolding curves as monitored by the probes of CD and fluorescence were fitted using a two-state model:

$$N_2 \rightarrow 2U$$
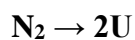
The free energy change in the absence of denaturant (ΔG_{H2O}), the dependence of free energy on denaturant concentration (m-value) and the midpoint of the unfolding transition (C_m) were calculated using SigmaPlot V13.0. The thermodynamic parameters are summarised in Tables 5 (far-UV CD) and 6 (fluorescence spectroscopy). The majority of the helical structure of GSTA3-3 is located in domain 2, whilst the lone tryptophan residue is located in domain 1. CD ellipticity is, therefore, primarily a probe of domain 2 unfolding/refolding, while selectively excited tryptophan fluorescence reports on the unfolding/refolding around Trp21, a highly
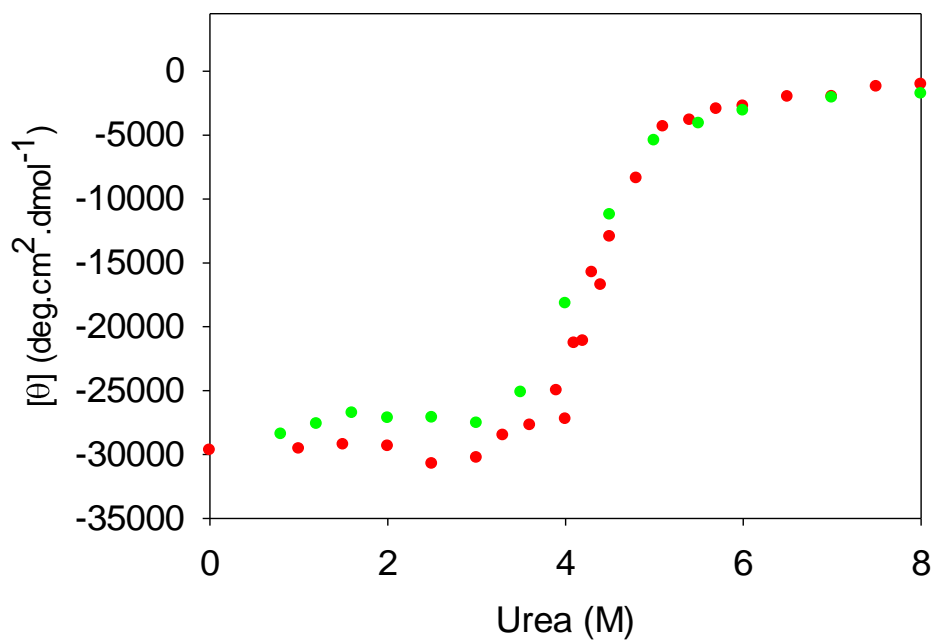
Figure 18: Reversibility of unfolding of wild-type GSTA3-3 monitored by far-UV CD. Overlay of an unfolding curve (red) with a refolding curve (green) of wild-type GSTA3-3. Similar data were obtained for Y9F, R15L and Y9F/R15L GSTA3-3.
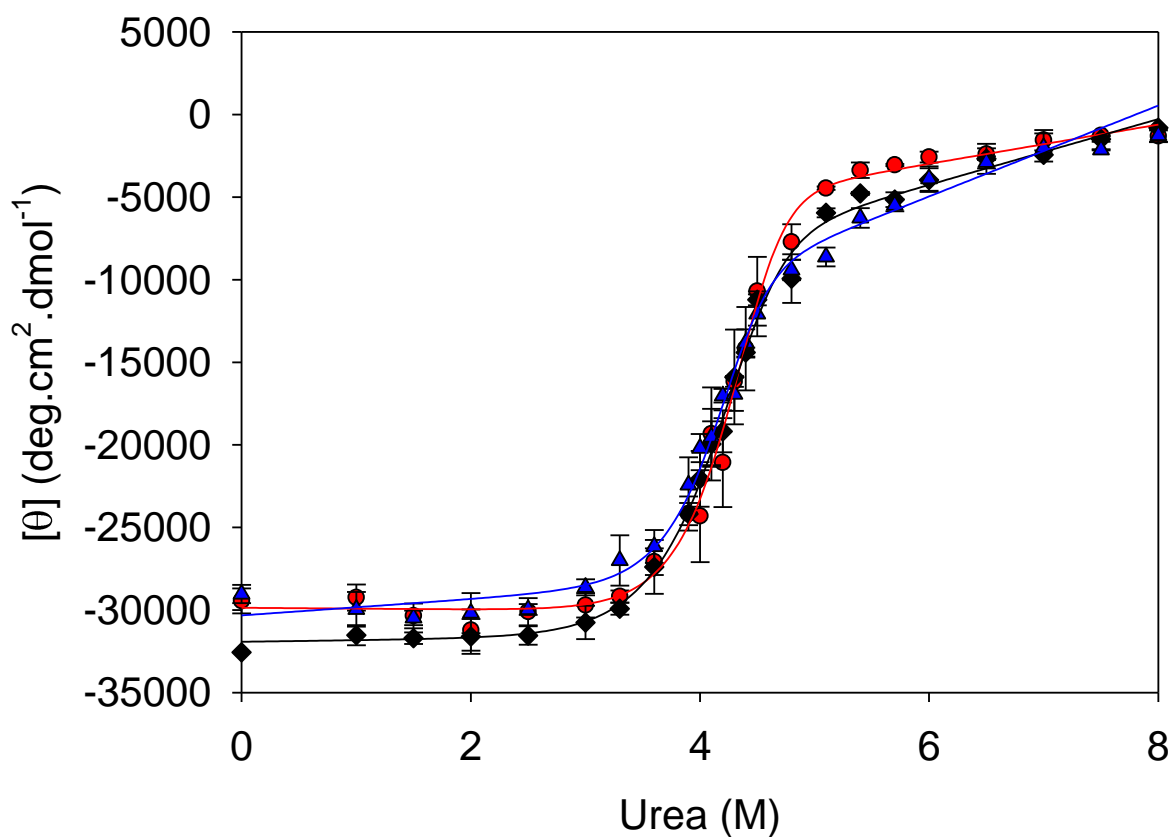
Figure 19: Urea-induced equilibrium unfolding of wild-type and mutant GSTA3-3 enzymes as monitored by circular dichroism at 220 nm. The wild-type (●), Y9F (♦) and Y9F/R15L (▲) GSTA3-3 concentration was 2 μM in 20 mM phosphate buffer, pH 7.4, containing 0.1 mM EDTA, and 0.02% (w/v) sodium azide. The points are the average of three replicates and error bars showing the standard deviation are shown. In each case, the R^2 value was > 0.95 and the p-value was < 0.0001 with a 5% confidence interval.
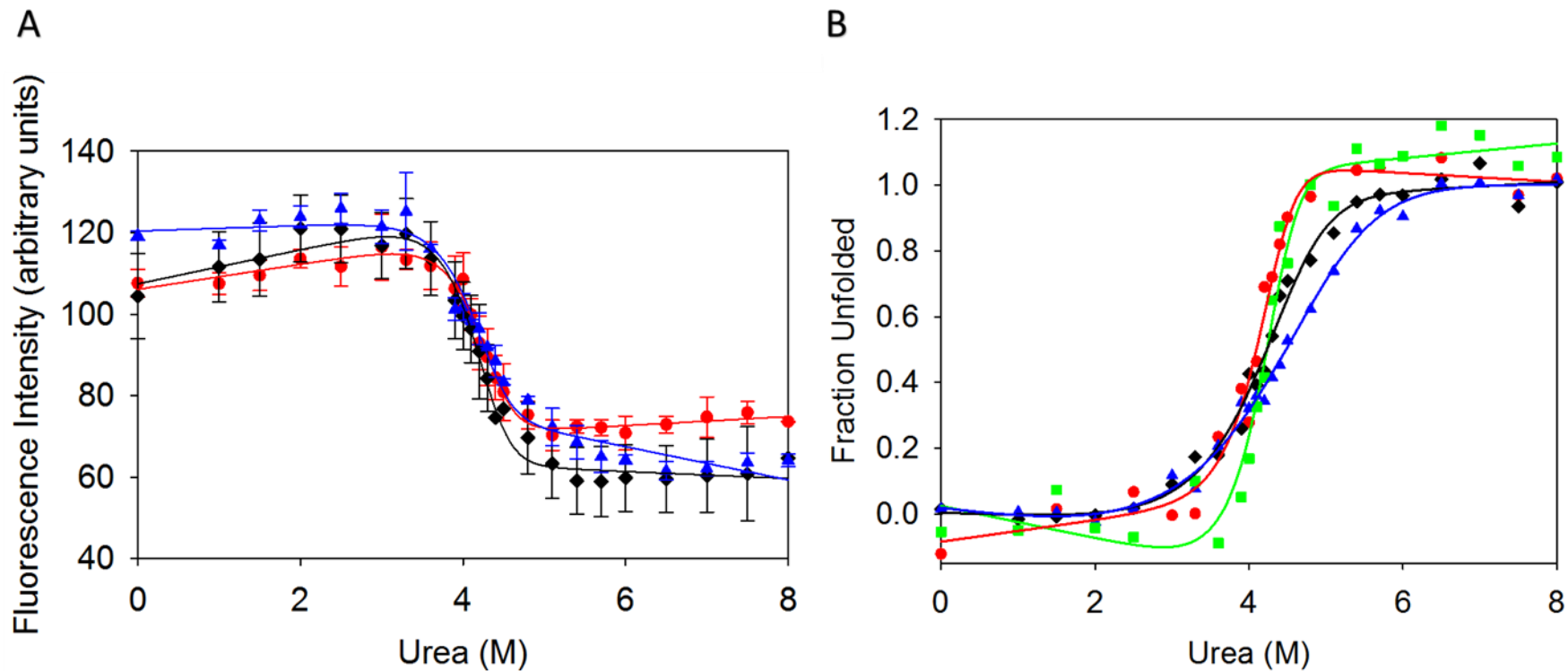
Figure 20: Urea-induced equilibrium unfolding of wild-type and mutant GSTA3-3 enzymes monitored by fluorescence spectroscopy. (A) represents the global unfolding of the enzyme monitored by excitation at 280 nm, (B) represents the unfolding around Trp21 located near the active site as monitored by excitation at 295 nm. The wild-type (●), Y9F (◆), R15L (■) and Y9F/R15L (▲) GSTA3-3 concentration was 2 μM in 20 mM phosphate buffer, pH 7.4, containing 0.1 mM EDTA, and 0.02% (w/v) sodium azide. The points are the average of three replicates and error bars showing the standard deviation are shown. In each case, the R^2 value was > 0.95 and the p-value was < 0.0001 with a 5% confidence interval.

Table 5: Thermodynamic parameters of two-state equilibrium unfolding for wild-type, Y9F, R15L and Y9F/R15L as monitored by circular dichroism

	Far – UV CD		
	Wild-type	**Y9F**	**Y9F/R15L**
$\Delta G_{(H2O)}$ (kcal.mol^{-1})	22.6 (±0.05)	23.2 (±1.88)	21.8 (±1.62)
m-value (kcal.mol^{-1}.M^{-1} urea)	3.6 (±0.03)	3.8 (±0.42)	3.5 (±0.38)
C_m (M urea)	4.2	4.2	4.2
R^2	0.96	0.99	0.99

Table 6: Thermodynamic parameters of two-state equilibrium unfolding for wild-type, Y9F, R15L and Y9F/R15L as monitored by fluorescence

	Intrinsic fluorescence at 280 nm			Intrinsic fluorescence at 295 nm			
	Wild-type	**Y9F**	**Y9F/R15L**	**Wild-type**	**Y9F**	**R15L**	**Y9F/R15L**
$\Delta G_{(H2O)}$ (kcal.mol^{-1})	22.9 (±2.48)	21.9 (±0.60)	21.6 (±2.33)	23.1 (±0.01)	22.0 (±0.23)	21.9 (±0.12)	12.6 (±1.08)
m-value (kJ.mol^{-1}.M^{-1} urea)	3.7 (±0.58)	3.5 (±0.12)	3.5 (±0.54)	3.8 (±0.08)	3.5 (±0.02)	3.5 (±0.06)	1.2 (±0.22)
C_m (M urea)	4.2	4.2	4.2	4.2	4.2	4.2	4.5
R^2	0.97	0.96	0.95	0.95	0.99	0.94	0.99

conserved residue located near the active site that forms part of an inter-domain lock-and-key motif.[42]

Neither the Y9F nor Y9F/R15L mutations had any effect on the unfolding of domain 2 of GSTA3-3 (ellipticity at 222 nm) (Table 5). Similarly, neither mutation affected the global unfolding of the enzyme as monitored by fluorescence (excitation 280 nm) (Table 6). Since the wild-type, Y9F and Y9F/R15L mutations had such similar unfolding properties it was unnecessary to examine the R15L mutation. However, when unfolding was monitored through the selective excitation of Trp21 it was seen that while neither mutation alone affected the stability of the enzymes, the double mutation caused a decrease in stability (excitation 295 nm) (Table 6). Additionally, the lower *m*-value could indicate the possibility of intermediates along the unfolding path becoming more significantly populated.

The stability of GSTA3-3 closely matches that of GSTA1-1 and the effects of the Y9F and R15L mutations are the same as they had on GSTA1-1 as well.[44] The data strongly suggest that neither Tyr9 nor Arg15 are required for structure or stability of the Alpha class GSTs. In the case of Arg15, this result is perhaps surprising as it indicates that the Arg15-Glu104 salt-bridge has no significant structural or stabilising role.

Chapter 4
Publication

The effects of mutating Tyr9 and Arg15 on the structure, stability, conformational dynamics and mechanism of GSTA3-3

GARY J. ROBERTSON, STOYAN STOYCHEV, YASIEN SAYED, IKECHUKWU ACHILONU AND HEINI W. DIRR
Biophysical Chemistry (Accepted pending revision)

In this publication, the effects of Y9F, R15L and Y9F/R15L mutations on GSTA3-3 were determined. Data indicate that neither the structure, stability nor conformational dynamics of GSTA3-3 are affected. Results from this study show that Arg15 is critical to proper catalytic function of the GSTA3-3, and as important as the Tyr9 residue.

Author Contributions: G. J. Robertson performed all experimental work, analysed the data and wrote the manuscript. S. Stoychev provided guidance and training in regard to performing the HDX-MS experiments at the CSIR. I. Achilonu and Y. Sayed supervised the project and assisted in data analysis and interpretation. H.W. Dirr is the Unit leader and provided the initial impetus to begin work on GSTA3-3.

The effects of mutating Tyr9 and Arg15 on the structure, stability, conformational dynamics and mechanism of GSTA3-3

Gary J. Robertson [a], Stoyan H. Stoychev [b], Yasien Sayed [a], Ikechukwu Achilonu [a], Heini W. Dirr [a,*]

[a] Protein Structure-Function Research Unit, School of Molecular and Cell Biology, University of the Witwatersrand, Johannesburg 2050, South Africa
[b] CSIR Biosciences, Pretoria, South Africa

ABSTRACT

Glutathione S-transferase A3-3 is the most catalytically efficient steroid isomerase enzyme known in humans, transforming Δ^5-androstene-3-17-dione into Δ^4-androstene-3-17-dione. GSTA3-3 catalyzes this reaction with ten-fold greater efficiency than GSTA1-1, its closest competitor in the Alpha class of GSTs. In order to examine the differences between Alpha class GSTs and to better elucidate the mechanism of GSTA3-3 the roles of Tyr9 and Arg15 were examined. Tyr9 is the major catalytic residue of Alpha class GSTs and Arg15 is proposed to be catalytically important to GSTA3-3 but never before experimentally examined. While the structure and stability of the Alpha class enzymes are highly comparable, subtle differences at the G-site of the enzymes account for GSTA3-3 having a ten-fold greater affinity for the substrate GSH. Y9F and R15L mutations, singly or together, have no effect on the structure and stability of GSTA3-3 (the same effect they have on GSTA1-1) despite the R15L mutation removing an interdomain salt-bridge at the active site. Hydrogen-deuterium exchange mass spectrometry also revealed that neither mutation had a significant effect on the conformational dynamics of GSTA3-3. The R15L and Y9F mutations are equally important to the specific activity of the steroid isomerase reaction; however, Arg15 is more important for lowering the pK_a of GSH. Lowering the pK_a of GSH being how GSTs catalyze their reactions. Additionally, there is evidence to suggest that Arg15 is integral to allowing GSTA3-3 to differentiate between Δ^5-androstene-3-17-dione and Δ^4-androstene-3-17-dione, indicating that Arg15 is a more important active-site residue than previously known.

© 2016 Elsevier B.V. All rights reserved.

Enzymes are perhaps the most vital component of life and have been refined over millennia to maximize the efficiency of biological systems. The glutathione S-transferase superfamily (GSTs, EC 2.5.1.18) is one such group of enzymes. Divided into over 13 classes of cytosolic enzymes, the members of this protein superfamily all share a highly conserved topological fold and mechanistic role [1,2]. Common to almost all aerobic organisms [3], GSTs play a vital role in the detoxification of endogenous and exogenous compounds [1]. GSTs are dimeric enzymes composed of two subunits [4,5]. Each subunit, in turn, is composed of a highly conserved thioredoxin-like domain containing the glutathione-binding site (G-site) and a less highly conserved all alpha helical secondary domain which makes up most of the H-site (Fig. 1). The detoxification reaction involves the conjugation of a diverse range of nonpolar electrophilic compounds (which bind at the H-site) to the tripeptide co-substrate glutathione (GSH) of the enzyme, which binds at the G-site. The enzyme promotes the conjugation reaction by lowering the pK_a of GSH; thus, reducing the energetic barrier for the deprotonated GS⁻ anion to attack the H-site substrate [6]. The conjugated product is, in general, less reactive and more soluble and can be further metabolized and eventually excreted by the organism [5].

While it is not unexpected for proteins belonging to the same superfamily to share similar reaction chemistry, and even common mechanistic pathways [7], new research continues to bring to light additional functions of the GST enzymes. They are known to play a role in ligand transport [8–11] and to interact with the protein kinases of signal transduction pathways [12,13], amongst other functions [14]. Furthermore, in some instances, the GST enzymes are promiscuous, having the capacity to catalyze supplementary reactions in addition to their main, classical catalytic activity [7,15]. In some instances, the secondary role of GSTs becomes more important than its classical detoxification role.

An example of this behavior is the Alpha class of GSTs [16,17]. All the enzymes in this class are, in addition to their classical role, able to catalyze a steroid isomerization reaction. Specifically, they catalyze the isomerization of the β,γ double bond of Δ^5-androstene-3,17-dione (Δ^5-AD) to the α,β isomer Δ^4-androstene-3,17-dione (Δ^4-AD). This

Fig. 1. The crystal structure of the homodimer hGSTA3-3. (A) A complete GSTA3 subunit is shown in red, the second subunit is divided into domain 1 (yellow) and domain 2 (blue). The substrate/co-factor GSH and product Δ^4-AD (orange) is shown bound at the active site. The domain interface and the axis of symmetry at the subunit interface are signposted. (B) Highlighting the active site. GSH (Orange) and the residues Tyr9, Arg15 and Glu104 (blue) are shown as stick models. The hydrogen bonds between the hydroxyl group of Tyr9 and the Sulphur atom of GSH and between the hydroxyl group and Arg15 are shown. Additionally, the salt bridge formed between Arg15 and Glu104 is shown. Image generated from the PDB file 2VCV using the program PyMol (www.pymol.sourceforge.net). (For interpretation of the references to color in this figure legend, the reader is referred to the web version of this article.)

reaction is critical in metabolic pathways that produce steroid hormones such as testosterone and progesterone from cholesterol. However, the Alpha GSTs perform each catalytic role with widely varying levels of efficiency. GSTA3-3 displays the highest isomerase activity in the alpha class; ten-fold greater than GSTA1-1 and 5000-fold greater than GSTA2-2 [18]. Inevitably though, as GSTA3-3 has evolved to optimize its isomerase activity, its efficiency regarding its classical detoxification role has diminished. GSTA3-3 also has the lowest activity in its class for to the conjugation of 1-chloro-2,4-dinitrobenzene (CDNB) to GSH which is representative of its ability to act as a detoxification enzyme [18]. These significant differences in the capabilities of the enzymes exist despite sharing >80% sequence identity. In fact, it has already been shown that just five point mutations in the H-site of the enzyme accounts for the majority of these differences [18].

GSTA3-3 is the most efficient steroid isomerization enzyme in the Alpha class and a major player in steroid isomerization in humans. It has, therefore, has attracted significant interest and research as a potential therapeutic drug target in the treatment of diseases characterized by excessive steroid hormone production such as polycystic ovary syndrome, Cushing's syndrome, congenital adrenal hyperplasia and some cancers of the sex organs [19]. Rational drug design would be greatly aided by a thorough understanding of the reaction mechanism of GSTA3-3. Additionally, knowing the differences that exist between the GST enzymes is important in avoiding any unwanted side-effects.

Nevertheless, there are many questions regarding the reaction mechanism. Currently, there are two major competing viewpoints regarding the reaction mechanisms (Fig. 2) [19–22], which have left several details unresolved. These are: (i) does the reaction proceed through a dienolate intermediate and, if so, how is it stabilized? (ii) what is the role of the GSH cofactor? (iii) what is the role of Tyr9? (iv) are there any other active site residues important to catalysis? In regards to the first question, more recent evidence has suggested that Scheme 1 may also proceed via an enforced concerted mechanism with the putative intermediate existing for only a short time (less than ~10^{-13} s) [19,23]. In order to address the questions above, this study examined the enzymatic properties of the wild-type, Y9F, R15L and Y9F/R15L GSTA3-3 enzymes. Arg15 was chosen to be examined as it has long been suspected to play a catalytic role, lowering the pK_a of GSH, as it does in GSTA1-1 [24,25]. However, the Arg15 residue of GSTA3-3 has as yet, never been experimentally examined.

Many aspects of GSTA3-3, such as stability and substrate affinities, have also gone un-investigated. Instead researchers have inferred

information about GSTA3-3 from our knowledge of the rest of the GST Alpha class. Given the highly conserved sequence identity and topological fold within the Alpha class, such inference is justified. However, given the evolutionary divergence between GSTA3-3 and the rest of the GST Alpha class, there may be significant differences which have gone unnoticed. In support of this supposition, it is worth noticing that despite all the Alpha class GSTs sharing an identical G-site, GSTA3-3 is reported to lower the pK_a of GSH to a greater degree than the other Alpha class GSTs [26]. This indicates possible differences, even at the G-site of the enzymes, which are otherwise strictly identical in the makeup of their residues [22]. Also, since Arg15 forms an interdomain salt-bridge with Glu104 at the active site, the contribution of this salt-bridge needs to be examined [25]. Even though in GSTA1-1 no role in protein stability could be ascribed to it [25]. This study, therefore, was aimed at gaining additional insights into the structure, stability and conformational dynamics of GSTA3-3 through the examination of Y9F, R15L and Y9F-R15L mutants of GSTA3-3.

1. Experimental procedures

1.1. Materials

CDNB, GSH and D$_2$O and were obtained from Sigma-Aldrich (St. Louis, MO, USA). The steroids Δ^5-androstene-3,17-dione and Δ^4-androstene-3,17-dione were obtained from Steraloids Inc. (RI, USA). All oligonucleotide primers were purchased from Inqaba Biotechnical Industries (Pty) Ltd. (Pretoria, South Africa). All other reagents were of analytical grade.

1.2. Mutagenesis, expression and purification

The codon harmonized nucleic acid sequence encoding wild-type GSTA3-3 with a N-terminal His6-tag and thrombin cleavage site was designed by Dr I. Achilonu (University of the Witwatersrand, South Africa). It was synthesized and subcloned into a pET-11a plasmid by GenScript Corporation (NJ, USA). The wild-type encoding vector was used with a QuikChange™ site-directed mutagenesis kit (Stratagene, La Jolla, CA) to create vectors encoding for the Y9F, R15L and Y9F/R15L GSTA3-3 enzymes. Each insert in the vector was confirmed by nucleotide sequencing performed by Inqaba Biotechnical Industries (Pty) Ltd. (Pretoria, South Africa). All the proteins were over-expressed as described previously [23], with one modification. Cells were incubated at 37 °C for a
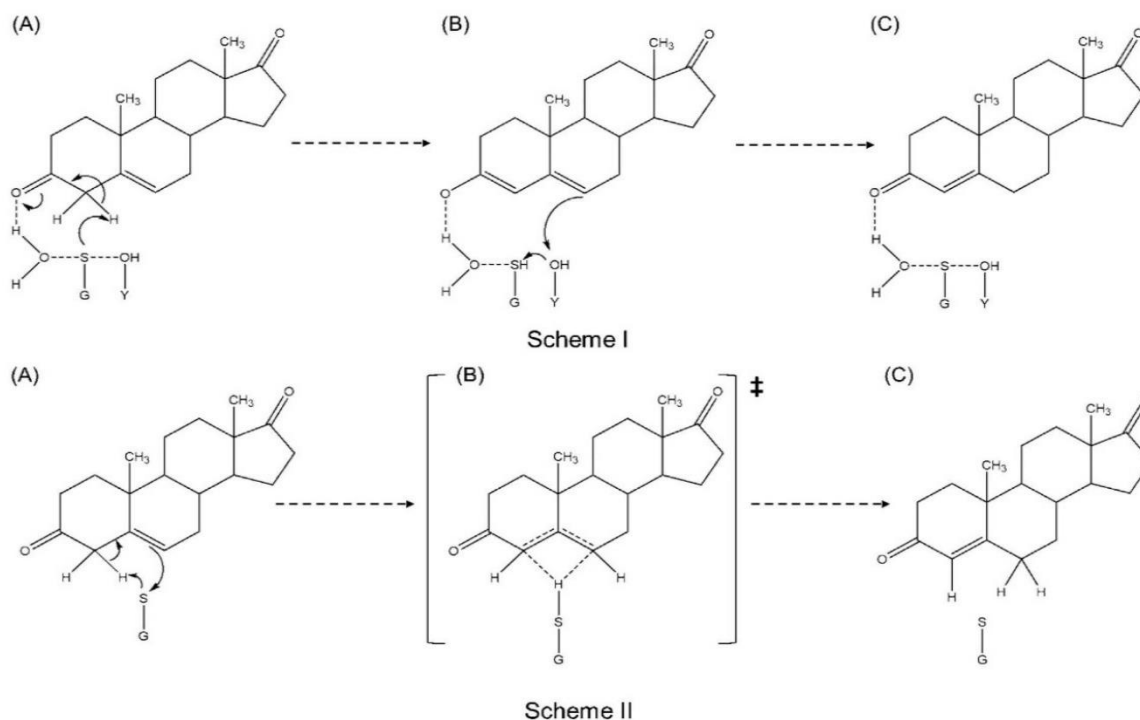
Scheme I

Scheme II

Fig. 2. The two proposed reaction mechanisms for Δ^5-AD isomerization by hGSTA3-3. In Scheme 1 [21], the deprotonated GS$^-$ thiolate anion abstracts the carbon 4 proton of Δ^5-AD, a water molecule acts as a hydrogen bond donor, stabilizing the negative charge of the dienolate intermediate (A, B). The keto form is regenerated by the transfer of the abstracted proton to carbon 6, by the transfer of negative charge via a conjugation system of π-bonds with Tyr9 acting as a proton shuttle (C). More recent evidence has found no proof of the proposed stabilizing water molecule and it has been proposed that GSH plays a dual role of abstracting carbon 4 and stabilizing the negative charge of O_3 and the intermediate [22]. In Scheme 2 [20], GSH abstracts a proton from carbon 4 while simultaneously transferring it to carbon 6. Bond formation and bond breaking occur simultaneously via a concerted single step mechanism, without a dienolate intermediate. In this mechanism, the role of Tyr9 is simply to help maintain the lower pK_a of GSH.

minimum of 6 hour post-induction before they were harvested and lysed by ultra-sonication. Purification of the proteins from the cell lysate then proceeded as described previously [23]. The concentration of pure dimer was determined from absorbance spectroscopy at 280 nm using the subunit molar extinction coefficient of 23,900 $M^{-1} \cdot cm^{-1}$ [17]. The Y9F mutation did not affect the molar extinction coefficient.

1.3. Spectroscopic methods

Fluorescence measurements were performed using a Jasco FP-6300 spectrometer with Spectra Manager software v1.5.00 (Jasco Inc., Tokyo, Japan). The intrinsic fluorescence of the purified enzymes was measured using excitation wavelengths of 280 nm and 295 nm; the latter to selectively excite the lone Trp residues of GSTA3-3 subunits. The protein concentration was 2 μM in 20 mM sodium phosphate buffer (pH 7.4), 1 mM EDTA, 0.02% sodium azide.

Far-UV circular dichroism (CD) (190–250 nm) measurements were conducted at 20 °C using a Jasco model 810 CD spectropolarimeter with Spectra Manager software v1.5.00 (Jasco Inc., Tokyo, Japan) and a path length of 2 mm. The protein concentration was 2 μM in 20 mM sodium phosphate buffer (pH 7.4), 1 mM EDTA, 0.02% sodium azide. The raw data, corrected for solvent effects, was converted to mean residue ellipticity [θ] (deg·cm²·dmol^{-1}) using the equation:

$$[\theta] = \frac{100 \times \theta}{Cnl}$$

where C is the concentration of protein in mM, θ is the measured ellipticity in millidegrees, n is the number of amino acid residues in the polypeptide chain and l is the path length in cm.

1.4. Equilibrium unfolding studies

All enzymes were confirmed to unfold reversibly, monitored by CD, as described previously [27]. Equilibrium unfolding studies were also performed as described previously [28]. Samples of 2 μM protein in 20 mM sodium phosphate buffer (pH 7.4), 1 mM EDTA, 0.02% sodium azide and 0–8 M urea were used. Structural changes were monitored by far-UV CD at 222 nm and by fluorescence using an excitation wavelength of 280 nm with fluorescence emission recorded at 328 nm. Rayleigh scatter plots of fluorescence (λex = 340; λem = 340) were performed to monitor any protein aggregation. The experiment was performed in triplicate. Data were fitted and analyzed using SigmaPlot v13.0 (Systat Software Inc.; Chicago, IL, USA).

1.5. Hydrogen deuterium exchange mass spectrometry (HDX-MS)

Deuterium labelling, quenching as well as proteolytic cleavage were all performed in an automated manner using a LEAP PAL HD-X system (Leap Technologies, USA). LC-MS analyses were performed on an Agilent 1100 HPLC system coupled to an AB Sciex 6600 TripleTOF, to initiate on-exchange reactions, 10 μL of wild-type or Y9F/R15L GSTA3-3 at a concentration of 10 mg/mL in 20 mM phosphate buffer (pH 7.4), 2 mM EDTA, and 0.02% (w/v) sodium azide in the presence or absence of 65 mM GSH at 20 °C was transferred to a vial containing 40 μL of 100% D_2O. After a set labelling time (15–3600 s), the protein – deuterium mix was transferred to a vial containing quench buffer (2 M guanidine hydrochloride, 100 mM TCEP) in a pre-chilled compartment held at 0 °C. For the fully deuterated control, deuteration was conducted overnight in a buffer supplemented with 0.02% (v/v) formic acid. The non-

deuterated control experiment was performed as described above except that MilliQ H_2O was used in place of D_2O. Following quenching of 45 s, samples were injected onto a Poroszyme immobilized pepsin column 2.1×5 mm (Life Technologies, USA) at a flow rate of 100 µL/min using 0.1% formic acid. The resulting peptides were desalted on an Acclaim PepMap trap column (0.3×5 mm) for 2 min using 0.1% formic acid and separated at 200 µL/min using a linear gradient of 5–40% B (B: 80% ACN/0.1% FA) using a Phenomenex Kinetex C18 column (2.1×5 mm). Proteolysis, desalting as well as peptide separation were all performed in a column oven operated at 4 °C. For peptide identification the 6600 TipleTOF mass spectrometer was operated in Data Dependent Acquisition (DDA) mode while measuring deuterium incorporation only a precursor scan was collected. In DDA mode precursor scans were acquired from m/z 360–1500 using an accumulation time of 250 ms followed by 30 product scans, acquired from m/z 100–1800 at 100 ms each, for a total scan time of 3.3 s. Charge ions (1^+–5^+, that fall in the mass range 360–1500 m/z) were automatically fragmented in Q2 collision cells using nitrogen as the collision gas. Collision energies were chosen automatically as function of m/z and charge. Dynamic exclusion was set to 15 s. PEAKS 6 (Bioinformatics Solutions Inc.) was used for peptide identification using the following parameters: enzyme specificity none, a precursor mass error of 5 ppm and product mass error of 0.1 Da. Level of deuterium incorporation was calculated using HDExaminer 1.3 (Sierra Analytics).

1.6. Determination of the pK_a of the thiol group of free and enzyme bound GSH

The pK_a of the thiol group of free and enzyme bound GSH was calculated from a plot of its thiolate form (monitored by absorbance at 239 nm) versus pH according to protocols described previously [6,23]. The pH range used was 5–11 and was maintained by 0.1 M MES (5.0–6.5), HEPES (6.5–8.0) and Tris-HCl (8.0–9.5) buffers. The enzyme concentration was 9 µM, and the GSH concentration was kept at 250 µM. For the R15L enzyme, to enhance the signal, the concentrations were doubled.

1.7. Isothermal titration calorimetry

The energetics of complex formation between the purified enzymes and GSH were determined using a Nano ITC calorimeter (TA instruments, DE, USA). Wild-type and mutant GST enzyme (0.05 mM subunit concentration) in the sample cell was titrated with 3 µL aliquots of (2 mM) GSH at 20 °C. Raw data were integrated, corrected for heats of dilution, and analyzed using the NanoAnalyze software (TA instruments, DE, USA).

1.8. Enzyme assays

The specific activities of the purified enzymes were measured with two different substrates in the presence of GSH by spectrophotometric assays described by Stenberg et al. [29]. Conjugation activity, representing the classical detoxification reaction of the enzyme, was measured using 1 mM CDNB in the presence of 1 mM GSH. Steroid isomerase activity was measured using 200 µM Δ^5-androstene-3,17-dione in the presence of 1 mM GSH [16]. 200 µM Δ^5-androstene-3,17-dione is ten times the calculated K_M of wild-type GSTA3-3 and is near the solubility limit [17,23]. All assays were carried out at 20 °C. For the CDNB-GSH conjugation reaction, enzyme concentrations were between 1 and 7 nM. For the steroid isomerization reaction, enzyme concentrations were between 0.5 and 3.5 nM for wild-type and between 7 and 75 nM for the mutants. Specific activity ($\mu mol \cdot min^{-1} \cdot mg^{-1}$) was determined by linear regression, using SigmaPlot v13.0 (Systat Software Inc.; Chicago, IL, USA), of the slope of a plot between the initial velocities of product formation ($\mu mol \cdot min^{-1}$) versus the mass of protein (mg). The rate of product formation was calculated by monitoring the increase in product absorbance after correcting for the non-enzymatic reaction. All CDNB-GSH conjugation reaction rates were linear over the monitored 100 second period. For the steroid isomerization reaction, the wild-type and Y9F GSTA3-3 catalyzed reactions were linear for at least the first 50 s but the R15L GSTA3-3 catalyzed reaction was only linear for ~10 s. Only the initial linear reaction rates were used to calculate specific activity. Since previous studies have shown that the GSTA3-3 catalyzed steroid isomerization reaction does not have a burst phase [18] and since the enzyme catalyzed reaction was carried out in the presence of substrate concentrations that far exceed K_M, the initial rates are a good approximation of V_{max} and suitable for calculating specific activity [30].

2. Results

2.1. The structure and stability of GSTA3-3 is not adversely affected by the mutations

The far-UV CD and fluorescence spectra of wild-type, Y9F, R15L and Y9F/R15L GSTA3-3 show no significant differences, with <5% difference between the spectra (Figs. S1 and S2, respectively). Additionally, there were no changes in secondary structural content between the enzymes as calculated from their far-UV CD spectra using Dichroweb analysis [31]. This indicates that neither Y9F nor R15L mutations singly or together have any significant effect on the global/overall protein structure. These findings concur with similar experiments performed on GSTA1-1 [25].

To analyze the effect of the mutations on the stability of GSTA3-3, unfolding equilibrium was probed using far-UV CD and fluorescence spectroscopy (Figs. S3 and S4, respectively). In all cases, the proteins refold reversibly without hysteresis or aggregation. All proteins displayed a sigmoidal, co-operative transition, indicating a two-state unfolding pathway. The majority of the helical structure of GSTA3-3 is located in domain 2, making CD ellipticity primarily a probe of domain 2 unfolding/refolding. Neither the Y9F nor Y9F/R15L mutations had any effect on the unfolding of domain 2 of GSTA3-3 (ellipticity at 222 nm) (Table 1). Similarly, the mutations did not affect the global unfolding of the enzyme as monitored by fluorescence (excitation at 280 nm) (Table 1). Since the wild-type, Y9F and Y9F/R15L mutations had such similar unfolding properties we did not consider it necessary to examine the R15L mutation. The stability of GSTA3-3 closely matches that of GSTA1-1 and the effects of the Y9F and R15L mutations are the

Table 1
Thermodynamic parameters of two-state equilibrium unfolding for wild-type, Y9F, R15L and Y9F/R15L as monitored by circular dichroism and fluorescence.

	Far – UV CD			Intrinsic fluorescence 280 nm		
	Wild-type	Y9F	Y9F/R15L	Wild-type	Y9F	Y9F/R15L
ΔG (H_2O) (kcal·mol^{-1})	22.6 ($\pm$0.05)	23.2 ($\pm$1.88)	21.8 ($\pm$1.62)	22.9 ($\pm$2.48)	21.9 ($\pm$0.60)	21.6 ($\pm$2.33)
m-Value (kJ·mol^{-1}·M^{-1} urea)	3.6 ($\pm$0.03)	3.8 ($\pm$0.42)	3.5 ($\pm$0.38)	3.7 ($\pm$0.58)	3.5 ($\pm$0.12)	3.5 ($\pm$0.54)
C_m (M urea)	4.2	4.2	4.2	4.2	4.2	4.2
R^2	0.96	0.99	0.99	0.97	0.96	0.95

same for GSTA1-1 [25]. The data strongly suggests that neither Tyr9 nor Arg15 are required for structure nor stability of the Alpha class GSTs. In the case of Arg15, this result is perhaps surprising because it suggests that the Arg15-Glu104 salt-bridge has no significant structural or stabilizing role.

2.2. The conformational dynamics of GSTA3-3 is not significantly affected by the double mutation

The conformational dynamics of the wild-type and Y9F/R15L double mutant were probed using amide HDX-MS (Fig. 3). The deuteration maps reveal that α9 rapidly exchanged nearly all of its amide protons. Additionally, α2 and the loop region between α4 and α5 experienced equally fast and high levels of deuteration. This data is in agreement with what is known about the highly disordered nature of α9 and α2 helices as well as the high B-factor of these regions in the crystal structures of these proteins [20,21]. In contrast, the helical bundle comprising domain 2 is relatively stable in both proteins and in agreement with HDX-MS data for other GST proteins [32–34].

The deuteration difference maps reveal no substantial differences in amide hydrogen exchange behavior when comparing wild-type and Y9F/R15L GSTA3-3 to each other, in the absence (Fig. 4) or presence of GSH (Fig. S5). Although the binding of GSH to the enzymes did cause a decrease in deuteration at the G-site and α9 (not shown) indicating the binding of the ligand shielded or decreased the flexibility of these regions it affected both enzymes approximately equally (Fig. S5). Comparison of the apoenzymes revealed that the active-site loop (residues 9–15), containing both mutations, experienced an increase in deuteration at its already most flexible region (residues 11–12). However, there were no significant changes (<10%) in deuteration at/or around the Y9F (residues 8–10) and R15L sites (residues 14–17) of interest at any of the observed time points. Breaking the Arg15-Glu104 salt-bridge did not result in an increase in deuteration at Glu104, or at α4 (of which it is apart). The changes in deuteration that were observed at positions 11–12 disappeared in the presence of the GSH co-factor. This data suggests that neither Tyr9 and Arg15 residues nor the Arg15-Glu104 salt-bridge are important in maintaining the proper conformational dynamics of the GSTA3-3 enzyme. Further, since the specific sites of the Tyr9 and the Arg15 mutations did not experience a significant change in their conformational flexibility and these residues are

responsible for directly interacting with GSH they do not have a role in maintaining the proper conformational dynamics of the active-site loop, despite the changes that occur at residues 11–12.

### 2.3. The binding and activation of GSH is significantly altered by the mutations

To examine the effects of the mutations on the binding and activation of GSH, the affinity of each enzyme for GSH was examined by ITC (Fig. S6). The ability of the enzymes to lower the pK_a of enzyme bound GSH was examined by differential absorbance spectroscopy (Fig. S7).

During data analysis of the integrated ITC profiles (Fig. S6) stoichiometry (N) was fixed. This was necessary because the experiments had low Wiseman c-values (~3.5), which resulted in erroneous curve-fitting unless N is kept constant [35,36]. The Wiseman c-value was calculated using the following equation:

$$c = nK_a[M]$$

where K_a is the dissociation constant and n is the number of binding sites per receptor M (molar concentration). The stoichiometry was fixed at one GSH ligand binding to one subunit of GST based on crystallographic data [20,21]. Under these conditions it has been experimentally proven that ITC experiments with low c-values [1–10] may still provide valuable and accurate K_a ($K_d = 1/K_a$) and ΔG data [35,37]. ITC data revealed that wild-type GSTA3-3 has an approximately ten-fold greater affinity for GSH as compared to GSTA1-1 [25,38–40] (Table 2) and that it has a binding affinity more comparable to that of the Mu class of GSTs [6,41]. While the binding affinity of GSTA3-3 for GSH is different compared to GSTA1-1 the trends caused by the mutations are similar to those observed for GSTA1-1 [25,38]. The Y9F mutation results in a greater affinity for GSH [38] while the R15L mutation causes a weaker affinity [25]. Interestingly, the two mutations together result in a greater affinity for GSH than that caused by Y9F alone. Since the c-values were low, necessitating the stoichiometry to be fixed, the ΔH and ΔS values are not as reliable as the K_d [35] and, therefore, their significance will not be speculated upon further.

The GST detoxification reaction mechanism and the steroid isomerization reaction mechanism, regardless of which reaction scheme is used, require GSH deprotonation [6,20,21]. When GSH binds to the G-site of a GST enzyme, the pK_a of the thiol group is reduced significantly
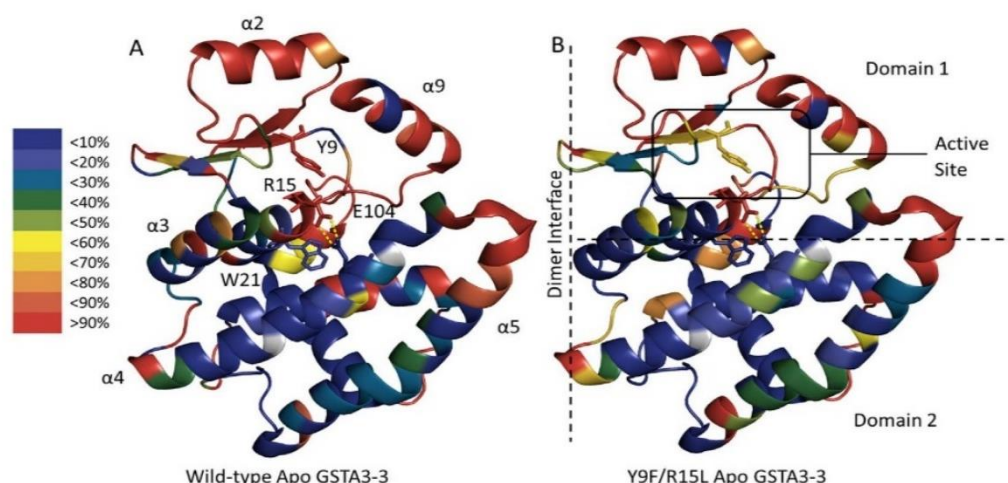
Fig. 3. Conformational dynamics of wild-type and Y9F/R15L GSTA3-3 probed by HDX-MS. The percentages of deuteration of (A) wild-type and (B) Y9F/R15L GSTA3-3 after 90 s are mapped onto the structure of a single subunit of the protein (PDB entry 1TDI). The positions of the Tyr9 residue, the Arg15-Glu104 salt-bridge and Trp21 are indicated. The helices as well as the loop connecting the helices experienced the most deuteration which matches closely with the regions with the highest B-factor in the crystal structures.
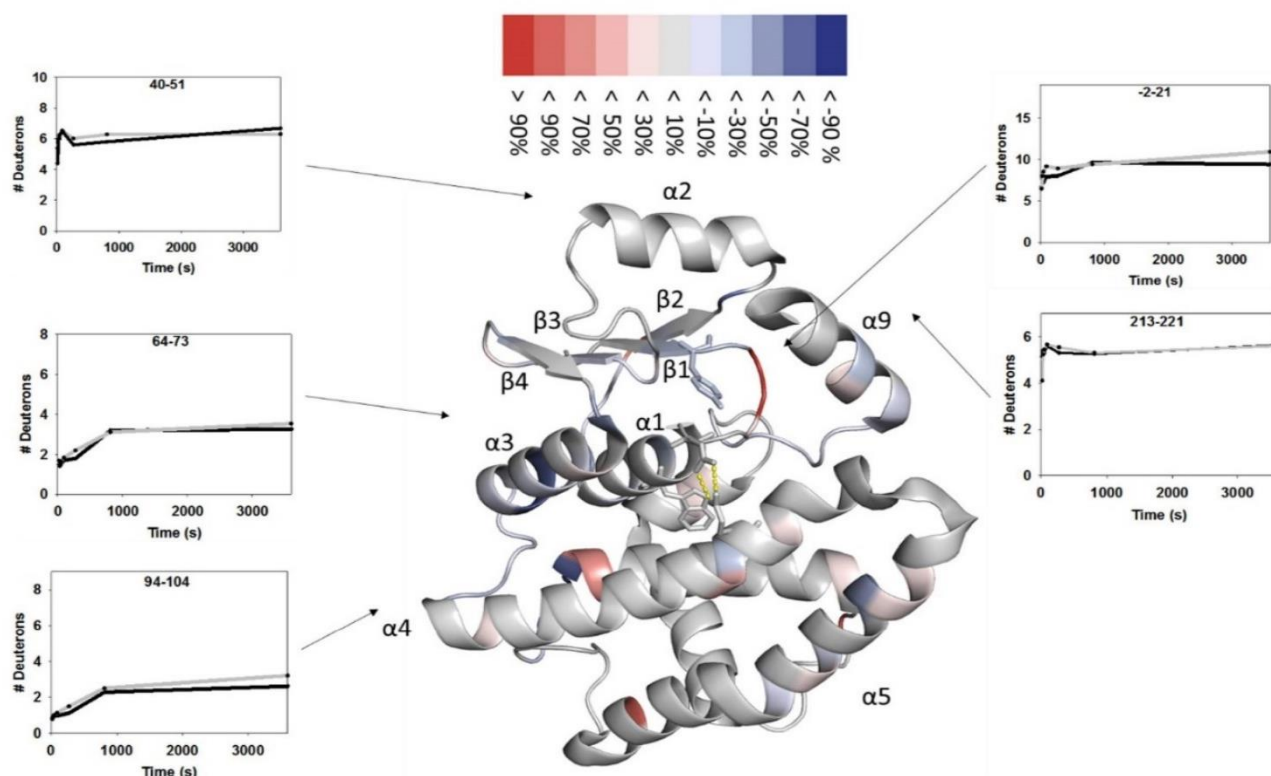
Fig. 4. The Y9F/R15L double mutation has only a negligible change on the conformational flexibility of GSTA3-3. The percentage differences in deuteration between wild-type and Y9F/R15L GSTA3-3 after 90 s are mapped onto the structure of dimeric GSTA3-3 (PDB entry 1TDI), calculated as the percentage of deuteration (Y9F/R15L) minus the percentage of deuteration (wild-type). Red coloring indicates that the level of deuterium exchange is higher for the mutant protein, while blue coloring indicates that the level of deuterium exchange is higher for the reduced protein. Helices and β-sheets are labelled, and the positions of the Tyr9 residue, the Arg15-Glu104 salt-bridge and Trp21 are indicated. The deuterium uptake plots compare deuterium incorporation of wild-type (●) and Y9F/R15L (○) GSTA3-3 over time for representative peptides. The plots are scaled according to the maximum number of exchangeable amide hydrogens for that peptide, assumed to equal the number of non-proline residues in the peptide minus the first two residues, which are subject to rapid back exchange. (For interpretation of the references to color in this figure legend, the reader is referred to the web version of this article.)

[26,42]. This is one way in which the GST enzymes lower the activation energy of their reactions. Differential absorbance spectroscopy indicates that free GSH has a pK_a of 9.2, a value closely supported by that of literature [26]. When GSH is bound to wild-type GSTA3-3 its pK_a is reduced by 2.6 pH units to 6.6, equivalent to a ΔG of −14,8 kJ·mol^{-1} (ΔG = $RT\ln K_a$, at 25 °C ΔG in kJ·mol^{-1} = 5.708 pK_a) [43]. GSH bound to Y9F and R15L GSTA3-3 has pK_a values of 7 and 7.5, respectively. This indicates that Tyr9 contributes 2.3 kJ·mol^{-1} and Arg15 contributes 5.2 kJ·mol^{-1} towards stabilizing the GS$^-$ anion. These data indicate that both Tyr9 and Arg15 are important in the activation of GSH but that Arg15 is more important. These data also follow the same trends as those seen in GSTA1-1. However, these results do not agree with previous literature indicating that GSTA3-3 lowers the pK_a of GSH to a greater extent than GSTA1-1 [25,26]. A complete record of the pK_a values of the proteins, as determined in this study and others, is shown in Table 3. The pK_a of the Y9F/R15L double mutant could not be determined. As the pK_a of bound GSH more closely approaches that of the pK_a of free GSH in solution it becomes more difficult to

Table 2
Thermodynamic parameters for the binding of GSH to wild-type and R15LhGST A1-1 at 25 °C.

Protein	ΔH (kJ·mol^{-1})	K_d (μM)	ΔS (kJ·mol^{-1}·K^{-1})
Wild-type	−16.7 (±0.6)	24.4 (±7.4)	0.03 (±0.004)
Y9F	−21.4 (±1.2)	16.6 (±4.7)	0.02 (±0.002)
R15L	−27.7 (±3.2)	64.5 (±4.3)	−0.01 (±0.01)
Y9F/R15L	−26.7 (±1.61)	12.5 (±1.0)	0.003 (±0.006)

Stoichiometry was fixed at N = 1.

Values in parentheses represent the standard error calculated from duplicate experiments for wild-type, R15L and Y9F/R15L GSTA3-3. For Y9F GSTA3-3 the error was calculated from Monte Carlo simulations performed using NanoAnalyze software.

Table 3
The pK_a of GSH in solution and bound to wild-type and mutant forms of the Alpha class GSTs.

Complex	pK_a of GSH	
	This study	Previous literature[a]
Free GSH	9.25 (±0.07)	9.17 (±0.04)[b,c]
GSTA3-3	6.59 (±0.05)	6.2 (±0.12)[b,d]
GSTA3-3 Y9F	6.98 (±0.01)	6.5 (±0.2)[d]
GSTA3-3 R15L	7.53 (±0.07)	–
GSTA3-3 Y9F/R15L	ND	–
GSTA1-1	ND	6.58 (±0.2)[c,e]
GSTA1-1 Y9F	ND	7.2(±0.1)[c]
GSTA1-1 R15L	ND	7.6[f]

ND: not determined.
[a] The values are the average of the values from the cited references.
[b] Daka et al. [23].
[c] Pettersson and Mannervik [26].
[d] Johansson and Mannervik [18].
[e] Caccuri et al. [42].
[f] Gildenhuys et al. [25].

differentiate between the signal of deprotonated GSH bound to the enzyme and the signal due to the contribution of deprotonated free GSH in solution.

2.4. The enzymatic activity of GSTA3-3 is severely impacted by the mutations

The Y9F, R15L and Y9F/R15L mutations all have a deleterious effect on the catalytic activity of the GSTA3-3 enzyme. This is true both for the CDNB-GSH conjugation assay and the steroid isomerization reaction assay (Table 4).

The CDNB-GSH conjugation assay (Fig. S8) revealed substantial decreases of 97.3% and 92.6% in the specific activity of the Y9F $(0.4 \ \mu mol \cdot min^{-1} \cdot mg^{-1})$ and R15L $(1.11 \ \mu mol \cdot min^{-1} \cdot mg^{-1})$ variant enzymes, respectively, as compared to that of the wild-type $(15 \ \mu mol \cdot min^{-1} \cdot mg^{-1})$. The Y9F/R15L mutation completely inactivated the enzyme. In the case of Y9F, these findings are comparable to those of previous studies on GSTA3-3 [18] while R15L and the double mutant show a similar effect on GSTA3-3 as they have on GSTA1-1 [24].

For the steroid isomerization reaction assay (Fig. S9), the Y9F mutation causes a decrease of 97.6% in the specific activity of the enzyme $(3.0 \ \mu mol \cdot min^{-1} \cdot mg^{-1})$ compared to that of the wild-type $(127.1 \ \mu mol \cdot min^{-1} \cdot mg^{-1})$, equivalent to its effect reported in literature [18]. Interestingly, the R15L mutation caused a similar decrease of 92.5% in the specific activity of the enzyme $(9.6 \ \mu mol \cdot min^{-1} \cdot mg^{-1})$. While the effects of this mutation on the steroid isomerization reaction of GSTA1-1 have been observed, where it caused a decrease of 90% [24], the effects on GSTA3-3 are reported here for the first time. Its effect on the catalytic activity of GSTA3-3 is more severe due to the ten-fold greater efficiency of wild-type GSTA3-3 to catalyze the steroid isomerization reaction [21]. Additionally, monitoring the formation of product during the steroid isomerization reaction catalyzed by R15L GSTA3-3 revealed the reaction rate declined sooner and before a comparable amount of product was formed, as compared to wild-type GSTA3-3 (Fig. 5A). The reaction catalyzed by R15L GSTA3-3 declined after ~10 s whereas the reaction catalyzed by wild-type GSTA3-3 remained steady for 60 s. In Fig. 5A, wild-type GSTA3-3 (in the first 60 s) converts 2.35% of the Δ^5-AD substrate and generated 1.36 μg of the product Δ^4-AD (4.7 μM) before experiencing a decline in reaction rate. By comparison, R15L GSTA3-3 (in the first 10 s), before it experiences a dramatic decline in its reaction rate, only consumed 0.24% of the substrate and generated 0.14 μg of the product Δ^4-AD (0.49 μM). Comparing 15 nM of Y9F and R15L GSTA3-3 (Fig. 5B) reveals a similar result with 15 nM of Y9F GSTA3-3 able to maintain its initial reaction rate for 100 s, consuming 0.93% of the substrate and generating 0.53 μg of the product Δ^4-AD (1.85 μM) in this time. Therefore, despite identical enzyme concentrations, R15L GSTA3-3 showed a reaction rate that declined sooner and before a comparable amount of product was formed as compared to Y9F GSTA3-3. Even at concentrations as low as 1.5 nM, R15L GSTA3-3

cannot maintain a linear reaction rate for the steroid isomerization reaction for a period longer than 20 s (Fig. S10). The data indicate that the catalytic properties of R15L GSTA3-3 have been significantly altered by the mutation. Lastly, the Y9F/R15L mutation caused a complete loss of activity in the enzyme in the steroid isomerization reaction.

3. Discussion

The GSTA3-3 enzyme shares a high sequence similarity as well as near identical topological fold when compared to other members of the GST Alpha class and GST proteins, in general. However, this paper adds to a growing list of evidence suggesting that GSTA3-3 has diverged from the rest of the Alpha class. There is clear evidence that despite residues which interact directly with GSH at the G-site being strictly identical across the Alpha class, there are still major differences in how the enzymes bind and interact with GSH. Previous studies have consistently reported that GSH bound to wild-type or mutated GSTA3-3 has a lower pK_a value when compared to wild-type bound GSH or identically mutated GSTA1-1. However, the findings of this study disagree and show closely matching values between GSTA3-3 and GSTA1-1. Lowering the pK_a of GSH is one of the primary ways by which the GSTA3-3 enzyme reduces the energy barrier of the enzymatic reactions. Differences in the pK_a values of GSH between the Alpha class GSTs could have accounted for some of the differences in their enzymatic activities between but this does not appear to be the case.

Nevertheless, we have now shown that GSTA3-3 has a ten-fold greater affinity for GSH as compared to GSTA1-1. It is likely the enhanced affinity of GSTA3-3 for GSH is due to the larger than typical active site of the enzyme compared to the rest of the Alpha class, due to the five variant residues at the H-site of the enzyme. Note that both Mu and Pi GSTs have active sites that are larger than typical class Alpha GSTs [44] and each has a greater binding affinity for GSH [40]. The non-additive effects of the mutations on the affinity of GSH binding to the mutants are unclear at this stage.

3.1. Structure, stability and conformational dynamics of GSTA3-3

The structure and stability of GSTA3-3 closely matches that of GSTA1-1. Additionally, neither the Y9F nor R15L mutations, singly or together, seem to affect the structure, stability or conformational dynamics of the protein. In the case of mutating the Tyr9 residue, this outcome is not surprising. That Arg15 does not appear important to these properties is, since mutating Arg15 disrupts the salt-bridge with Glu104. In the case of GSTA1-1, crystallographic data indicates that the R15L mutation results in a cavity that is filled by three water molecules [25]. The hydrogen bonding requirements of Glu104 are satisfied by binding two of the water molecules. It seems likely that the same would occur in the case of R15L GSTA3-3. It may be that the salt-bridge is important for correct packing specificity and protein folding, but there were no significant differences in yield during protein expression and purification to support this idea. It may be that the salt-bridge is important for either partly neutralizing the charge of Arg15 or maintaining a specific conformation of Arg15 that promotes catalytic efficiency but this would need to be examined through mutation of Glu104.

It must be noted that while Tyr9 is highly conserved [2], the same is not true for Arg15, which is a residue practically unique to the Alpha class of GSTs [25,45]. The Arg15 residue is sometimes naturally a Leu [4], as in the Class Mu GSTs. Furthermore, even when Arg15 is conserved, it does not always form a salt-bridge. This is a strong point against either Arg15 or its salt-bridge being of particular importance to GSTA3-3 stability.

3.2. The catalytic activity of GSTA3-3

It is clear that each mutation, Y9F and R15L, singly or combined, has a deleterious effect on the catalytic activity of the enzymes. Therefore,

Table 4
Specific activity of wild-type and mutant forms of the Alpha class GSTs.

Enzyme	Specific activity $(\mu mol \cdot min^{-1} \cdot mg^{-1})$[a]	
	Δ^5-AD	CDNB
GSTA3-3	127.1 ($\pm$4.34)	15.0 ($\pm$0.86)
GSTA3-3 Y9F	3.0 ($\pm$0.16)	0.4 ($\pm$0.2)
GSTA3-3 R15L	9.6 ($\pm$0.73)	1.1 ($\pm$0.11)
GSTA3-3 Y9F/R15L	Inactive	Inactive
GSTA1-1	12[b]	75[b]
GSTA1-1 Y9F	0.2[b]	1.9[b]
GSTA1-1 R15L	1.2[b]	3.1[b]
GSTA2-2	0.17 ($\pm$0.003)[c]	58 ($\pm$4)[c]

[a] Values are means $\pm$ S.E. of at least triplicate measurements.
[b] Bjornestedt et al. [24].
[c] Pettersson and Mannervik [26].
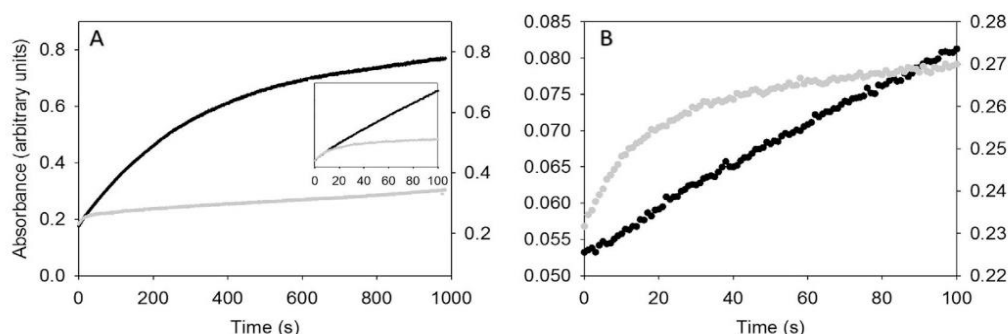
Fig. 5. A comparison of the reaction rates of wild-type, Y9F and R15L GSTA3-3 during the steroid isomerase assay monitored by absorbance at A_{248}. (A) The steroid isomerization reaction rate of 1.5 nM wild-type (black, left axis) in comparison to 15 nM R15L (grey, right axis) GSTA3-3 over 1000 s, the insert shows a zoomed in portion of the first 100 s. In the first ten seconds the reaction rates were nearly identical ($\sim$0.1 $\Delta A \cdot min^{-1}$). After only 10 s, however, the reaction rate of R15L GSTA3-3 begins to decline dramatically whereas wild-type GSTA3-3 maintained its initial reaction rate for at least 60 s and the reaction rate does not decline as rapidly or as significantly as for R15L even during the final 100 s. (B) The steroid isomerization reaction rate of 15 nM Y9F (black, left axis) in comparison to 15 nM R15L (grey, right axis) GSTA3-3.

Tyr9 and Arg15 are important to both the mechanisms of CDNB-GSH conjugation and steroid isomerization and are consistent with the active site of GSTA3-3 slowly evolving away from its classical activity towards a new one, while simultaneously using the same reaction machinery. The data indicate that by whichever means the mutations affect the catalytic activity of the enzymes they do so entirely through the way they interact with the substrates.

Our study has shown, for the first time, Arg15 is as important to the catalytic activity of the steroid isomerization reaction as Tyr9 is in GSTA3-3. The R15L mutation significantly increases the pK_a of bound GSH from 6.6 to 7.5. This is the probable cause of the deleterious effect of the mutation on the catalytic activity of the enzyme. The rapid decline in the reaction rate of the R15L GSTA3-3 enzyme in regards to the steroid isomerization reaction is particularly noteworthy. The decline may be attributed to a number of factors: (i) substrate depletion (ii) R15L GSTA3-3 is more susceptible to product inhibition (iii) R15L GSTA3-3 is unable to release the product efficiently after formation (iv) the enzyme becomes deactivated as the reaction proceeds, (v) the end of a burst-phase. Considering point (i), this is clearly not the case since the activity of R15L GSTA3-3 begins to decline before it has produced a comparable amount of product as compared to the wild-type or Y9F enzyme. Additionally, the concentrations of the Δ^5-AD and GSH substrates were both at least ten times higher than the calculated K_M values for wild-type GSTA3-3. Under such conditions it is unlikely for a decline in substrate concentrations of <1% to cause a significant decline in reaction rates [30]. It is also unlikely to be a result of (iv) as it has already been established that neither the structure nor the stability of the enzyme was affected by the R15L mutation. Nor is it likely to be point (v), the end of a burst phase, previous experiments have concluded that wild-type GSTA3-3 catalyzed steroid isomerization has no discernible burst phase [18]. Further as the initial rate lasts ~10 s, this is too long to be due to pre steady-state reaction conditions [46]. It is, therefore, most likely that either (ii) or (iii) or a combination thereof is the cause [47,48]. The binding between R15L GSTA3-3 and Δ^4-AD is, however, certainly not irreversible as the concentration of product formed does exceed the concentration of enzyme as a function of time. Additionally, computational models have also predicted that Arg15 is important to the binding of Δ^5-AD [19]. The K_M of wild-type GSTA3-3 for Δ^5-AD is 22.5 $\pm$ 4.3 μM, [23] conversely, the K_i of the enzyme for Δ^4-AD is 25 μM [17], suggesting the enzyme has a near identical affinity for substrate as it does for product. Any change to this fine balance could have a considerable impact on the catalytic properties of GSTA3-3. The low K_i value is also likely what caused the eventual decline in the reaction rate of wild-type and Y9F GSTA3-3.

3.3. The role of Arg15

The Arg15 residue (and the Arg15-Glu104 salt-bridge) is unique to Alpha class GSTs and is highly conserved. There is, however, growing evidence that Arg15 is part of an electron-sharing network conserved in all GSTs (there is evidence of the network in Alpha, Delta, Mu, Omega, Pi, Sigma, Tau and Theta GSTs) [45,49]. Although the residues which make up this electron-sharing network are not conserved in the primary sequences of GSTs, the presence of the network can be mapped to the same region in all GSTs. This further supports the idea that Arg15 is not important for structural or stability reasons but is necessary because of the charge of its side chain group. Indeed, experiments have previously determined that the charge of Arg15 is more catalytically significant than its bulk [45]. The conservation of this electron-sharing network, which nevertheless demonstrates plasticity in its make up, may be indicative of the robust nature of GSTs against point mutations which may nevertheless lead to novel functions. In conclusion, the Arg15 residue may have been integral to the evolution of steroid isomerization in the Alpha class of GSTs. The R15L mutation has certainly revealed that Arg15 is as important, if not more so, as the typical major active site residue Tyr9 [2].

Conflict of interest

The authors declare no competing financial interest.

### Appendix A. Supplementary data

Circular dichroism and fluorescence spectra of GSTA3-3 and variants (Figs. S1 and S2), urea-induced equilibrium unfolding of spectra of GSTA3-3 and variants as monitored by circular dichroism and fluorescence (Figs. S3 and S4), HDX-MS deuteration difference map comparing wild-type and Y9F/R15L GSTA3-3 in the presence of GSH (Fig. S5),

isothermal calorimetric profile (Fig. S6), pK_a spectra (Fig. S7), GSH-CDNB conjugation and steroid isomerization specific activity of GSTA3-3 and variants (Figs. S8 and S9) and the steroid isomerization reaction rate of 1.5 nM R15L GSTA3-3 (Fig. S10). Supplementary data associated with this article can be found in the online version, at 10.1016/j.bpc.2017.02.004.

References

[1] D. Sheehan, G. Meade, V.M. Foley, C.A. Dowd, Structure, function and evolution of glutathione transferases: implications for classification of non-mammalian members of an ancient enzyme superfamily, Biochem. J. 360 (2001) 1–16.

[2] H.J. Atkinson, P.C. Babbitt, Glutathione transferases are structural and functional outliers in the thioredoxin fold, Biochemistry 48 (2009) 11108–11116.

[3] S.D. Copley, J.K. Dhillon, Lateral gene transfer and parallel evolution in the history of glutathione biosynthesis genes, Genome Biol. 3 (2002) (research0025.0021-research0025.0016).

[4] H. Dirr, P. Reinemer, R. Huber, X-ray crystal structures of cytosolic glutathione S-transferases. Implications for protein architecture, substrate recognition and catalytic function, Eur. J. Biochem. 220 (1994) 645–661.

[5] M.C. Wilce, M.W. Parker, Structure and function of glutathione S-transferases, Biochim. Biophys. Acta 1205 (1994) 1–18.

[6] G.F. Graminski, Y. Kubo, R.N. Armstrong, Spectroscopic and kinetic evidence for the thiolate anion of glutathione at the active site of glutathione S-transferase, Biochemistry 28 (1989) 3562–3568.

[7] P.C. Babbitt, J.A. Gerlt, Understanding enzyme superfamilies. Chemistry as the fundamental determinant in the evolution of new catalytic activities, J. Biol. Chem. 272 (1997) 30591–30594.

[8] I. Listowsky, M. Abramovitz, H. Homma, Y. Niitsu, Intracellular binding and transport of hormones and xenobiotics by glutathione-S-transferases, Drug Metab. Rev. 19 (1988) 305–318.

[9] D.P. Danger, W.S. Baldwin, G.A. LeBlanc, Photoaffinity labelling of steroid-hormone-binding glutathione S-transferases with [3H]methyltrienolone. Inhibition of steroid-binding activity by the anticarcinogen indole-3-carbinol, Biochem. J. 288 (1992) 361–367.

[10] B. Mannervik, The isoenzymes of glutathione transferase, Adv. Enzymol. Relat. Areas Mol. Biol. 57 (1985) 357–417.

[11] B. Mannervik, C. Guthenberg, Glutathione transferase (human placenta), Methods Enzymol. 77 (1981) 231–235.

[12] V. Adler, Z. Yin, S.Y. Fuchs, M. Benezra, L. Rosario, K.D. Tew, M.R. Pincus, M. Sardana, C.J. Henderson, C.R. Wolf, R.J. Davis, Z. Ronai, Regulation of JNK signaling by GSTp, EMBO J. 18 (1999) 1321–1334.

[13] S.G. Cho, Y.H. Lee, H.S. Park, K. Ryoo, K.W. Kang, J. Park, S.J. Eom, M.J. Kim, T.S. Chang, S.Y. Choi, J. Shim, Y. Kim, M.S. Dong, M.J. Lee, S.G. Kim, H. Ichijo, E.J. Choi, Glutathione S-transferase mu modulates the stress-activated signals by suppressing apoptosis signal-regulating kinase 1, J. Biol. Chem. 276 (2001) 12749–12755.

[14] Y. Kanaoka, H. Ago, E. Inagaki, T. Nanayama, M. Miyano, R. Kikuno, Y. Fujii, N. Eguchi, H. Toh, Y. Urade, O. Hayaishi, Cloning and crystal structure of hematopoietic prostaglandin D synthase, Cell 90 (1997) 1085–1095.

[15] O. Khersonsky, D.S. Tawfik, Enzyme promiscuity: a mechanistic and evolutionary perspective, Annu. Rev. Biochem. 79 (2010) 471–505.

[16] A.M. Benson, P. Talalay, J.H. Keen, W.B. Jakoby, Relationship between the soluble glutathione-dependent delta 5-3-ketosteroid isomerase and the glutathione S-transferases of the liver, Proc. Natl. Acad. Sci. U. S. A. 74 (1977) 158–162.

[17] A.S. Johansson, B. Mannervik, Human glutathione transferase A3-3, a highly efficient catalyst of double-bond isomerization in the biosynthetic pathway of steroid hormones, J. Biol. Chem. 276 (2001) 33061–33065.

[18] A.S. Johansson, B. Mannervik, Active-site residues governing high steroid isomerase activity in human glutathione transferase A3-3, J. Biol. Chem. 277 (2002) 16648–16654.

[19] M. Calvaresi, M. Stenta, M. Garavelli, P. Altoé, A. Bottoni, Computational evidence for the catalytic mechanism of human glutathione S-transferase A3-3: a QM/MM investigation, ACS Catal. 2 (2012) 280–286.

[20] K. Tars, B. Olin, B. Mannervik, Structural basis for featuring of steroid isomerase activity in alpha class glutathione transferases, J. Mol. Biol. 397 (2010) 332–340.

[21] Y. Gu, J. Guo, A. Pal, S.S. Pan, P. Zimniak, S.V. Singh, X. Ji, Crystal structure of human glutathione S-transferase A3-3 and mechanistic implications for its high steroid isomerase activity, Biochemistry 43 (2004) 15673–15679.

[22] D.F.A.R. Dourado, P.A. Fernandes, B. Mannervik, M.J. Ramos, Isomerization of Δ5-androstene-3,17-dione into Δ4-androstene-3,17-dione catalyzed by human glutathione transferase A3-3: a computational study identifies a dual role for glutathione, J. Phys. Chem. A 118 (2014) 5790–5800.

[23] J.L. Daka, I. Achilonu, H.W. Dirr, The isomerization of delta5-androstene-3,17-dione by the human glutathione transferase A3-3 proceeds via a conjugated heteroannular diene intermediate, J. Biol. Chem. 289 (2014) 32243–32252.

[24] R. Bjornestedt, G. Stenberg, M. Widersten, P.G. Board, I. Sinning, T.A. Jones, B. Mannervik, Functional significance of arginine 15 in the active site of human class alpha glutathione transferase A1-1, J. Mol. Biol. 247 (1995) 765–773.

[25] S. Gildenhuys, M. Dobreva, N. Kinsley, Y. Sayed, J. Burke, S. Pelly, G.P. Gordon, M. Sayed, T. Sewell, H.W. Dirr, Arginine 15 stabilizes an S(N)Ar reaction transition state and the binding of anionic ligands at the active site of human glutathione transferase A1-1, Biophys. Chem. 146 (2010) 118–125.

[26] P.L. Pettersson, B. Mannervik, The role of glutathione in the isomerization of delta 5-androstene-3,17-dione catalyzed by human glutathione transferase A1-1, J. Biol. Chem. 276 (2001) 11698–11704.

[27] L.A. Wallace, H.W. Dirr, Folding and assembly of dimeric human glutathione transferase A1-1, Biochemistry 38 (1999) 16686–16694.

[28] L.A. Wallace, N. Sluis-Cremer, H.W. Dirr, Equilibrium and kinetic unfolding properties of dimeric human glutathione transferase A1-1, Biochemistry 37 (1998) 5320–5328.

[29] G. Stenberg, P.G. Board, I. Carlberg, B. Mannervik, Effects of directed mutagenesis on conserved arginine residues in a human Class Alpha glutathione transferase, Biochem. J. 274 (Pt 2) (1991) 549–555.

[30] H.B. Brooks, S. Geeganage, S.D. Kahl, C. Montrose, S. Sittampalam, M.C. Smith, J.F. Weidner, Basics of enzymatic assays for HTS, Assay Guidance Manual, 2012 (Internet).

[31] L. Whitmore, B.A. Wallace, DICHROWEB, an online server for protein secondary structure analyses from circular dichroism spectroscopic data, Nucleic Acids Res. 32 (2004) W668–W673.

[32] D. Balchin, L. Wallace, H.W. Dirr, S-nitrosation of glutathione transferase P1-1 is controlled by the conformation of a dynamic active site helix, J. Biol. Chem. 288 (2013) 14973–14984.

[33] L.C. Thompson, J. Walters, J. Burke, J.F. Parsons, R.N. Armstrong, H.W. Dirr, Double mutation at the subunit interface of glutathione transferase rGSTM1-1 results in a stable, folded monomer, Biochemistry 45 (2006) 2267–2273.

[34] S.H. Stoychev, C. Nathaniel, S. Fanucchi, M. Brock, S. Li, K. Asmus, V.L. Woods, H.W. Dirr, Structural dynamics of soluble chloride intracellular channel protein CLIC1 examined by amide hydrogen—deuterium exchange mass spectrometry, Biochemistry 48 (2009) 8413–8421.

[35] W.B. Turnbull, A.H. Daranas, On the value of c: can low affinity systems be studied by isothermal titration calorimetry? J. Am. Chem. Soc. 125 (2003) 14859–14866.

[36] T. Wiseman, S. Williston, J.F. Brandts, L.N. Lin, Rapid measurement of binding constants and heats of binding using a new titration calorimeter, Anal. Biochem. 179 (1989) 131–137.

[37] J. Tellinghuisen, Designing isothermal titration calorimetry experiments for the study of 1:1 binding: problems with the "standard protocol", Anal. Biochem. 424 (2012) 211–220.

[38] D. Balchin, H.W. Dirr, Y. Sayed, Energetics of ligand binding to human glutathione transferase A1-1: Tyr-9 associated localisation of the C-terminal helix is ligand-dependent, Biophys. Chem. 156 (2011) 153–158.

[39] S. Mosebi, Y. Sayed, J. Burke, H.W. Dirr, Residue 219 impacts on the dynamics of the C-terminal region in glutathione transferase A1-1: implications for stability and catalytic and ligandin functions, Biochemistry 42 (2003) 15326–15332.

[40] M. Widersten, R. Bjornestedt, B. Mannervik, Involvement of the carboxyl groups of glutathione in the catalytic mechanism of human glutathione transferase A1-1, Biochemistry 35 (1996) 7731–7742.

[41] I. Jakobson, M. Warholm, B. Mannervik, The binding of substrates and a product of the enzymatic reaction to glutathione S-transferase A, J. Biol. Chem. 254 (1979) 7085–7089.

[42] A.M. Caccuri, G. Antonini, P.G. Board, M.W. Parker, M. Nicotra, M. Lo Bello, G. Federici, G. Ricci, Proton release on binding of glutathione to alpha, Mu and Delta class glutathione transferases, Biochem. J. 344 (1999) 419–425.

[43] R.N. Goldberg, N. Kishore, R.M. Lennen, Thermodynamic quantities for the ionization reactions of buffers, J. Phys. Chem. Ref. Data 31 (2002) 231–370.

[44] I. Sinning, G.J. Kleywegt, S.W. Cowan, P. Reinemer, H.W. Dirr, R. Huber, G.L. Gilliland, R.N. Armstrong, X. Ji, P.G. Board, et al., Structure determination and refinement of human alpha class glutathione transferase A1-1, and a comparison with the Mu and Pi class enzymes, J. Mol. Biol. 232 (1993) 192–212.

[45] D.F. Dourado, P.A. Fernandes, B. Mannervik, M.J. Ramos, Glutathione transferase A1-1: catalytic importance of arginine 15, J. Phys. Chem. B 114 (2010) 1690–1697.

[46] K. Hiromi, Recent developments in the stopped-flow method for the study of fast reactions, Methods of Biochemical Analysis, John Wiley & Sons, Inc. 2006, pp. 137–164.

[47] K.F. Tipton, Enzyme assays: a practical approach, in: Robert Eisenthal, Michael J. Danson (Eds.),The Practical Approach Series, Volume 257, second ed., The Quarterly Review of Biology, 78, 2003 (89-89).

[48] S. Cha, Tight-binding inhibitors-I. Kinetic behavior, Biochem. Pharmacol. 24 (1975) 2177–2185.

[49] P. Winayanuwattikun, A.J. Ketterman, An electron-sharing network involved in the catalytic mechanism is functionally conserved in different glutathione transferase classes, J. Biol. Chem. 280 (2005) 31776–31782.

Supplementary Figures:
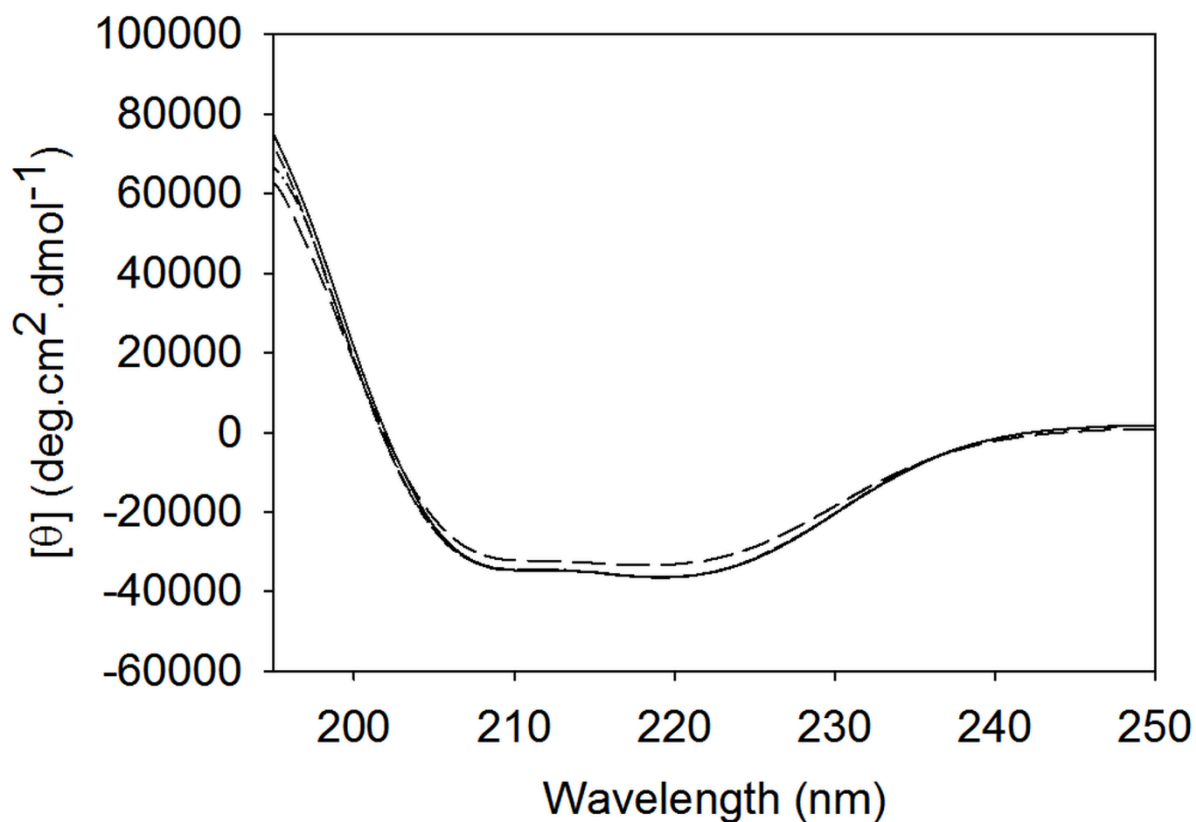
Figure S1: Far-UV circular dichroism spectra of wild-type and mutant GSTA3-3 enzymes. Spectra were collected using samples of 2 μM wild-type (‐ ‐ ‐), Y9F (——), R15L (‐ ‐) and Y9F/R15L (— —) GSTA3-3 protein in 20 mM phosphate buffer containing 1 mM EDTA and 0.02% (w/v) sodium azide, pH 7.4. The near perfectly overlapping spectra indicate that all the proteins have similar secondary structure.
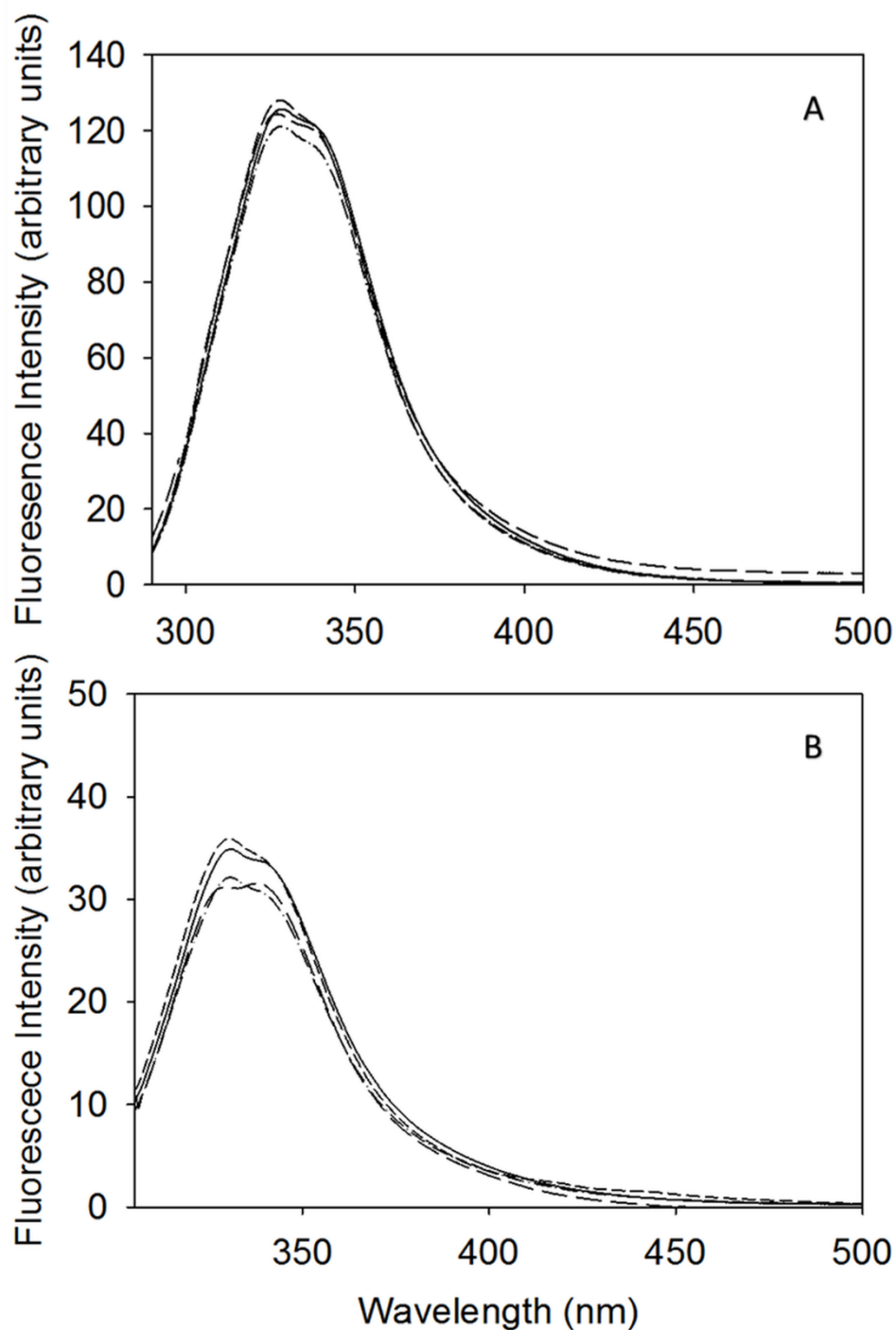
Figure S2: Fluorescence emission spectra of wild-type and mutant GSTA3-3 enzymes. Spectra were collected using 2 μM wild-type (– – –), Y9F (——), R15L (– · –) and Y9F/R15L (— —) GSTA3-3 protein in 20 mM phosphate buffer containing 1 mM EDTA and 0.02% (w/v) sodium azide, pH 7.5. Excitation at 280 nm (A) and 295 nm (B). The near perfectly overlapping spectra indicate that all the proteins have similar tertiary structure.
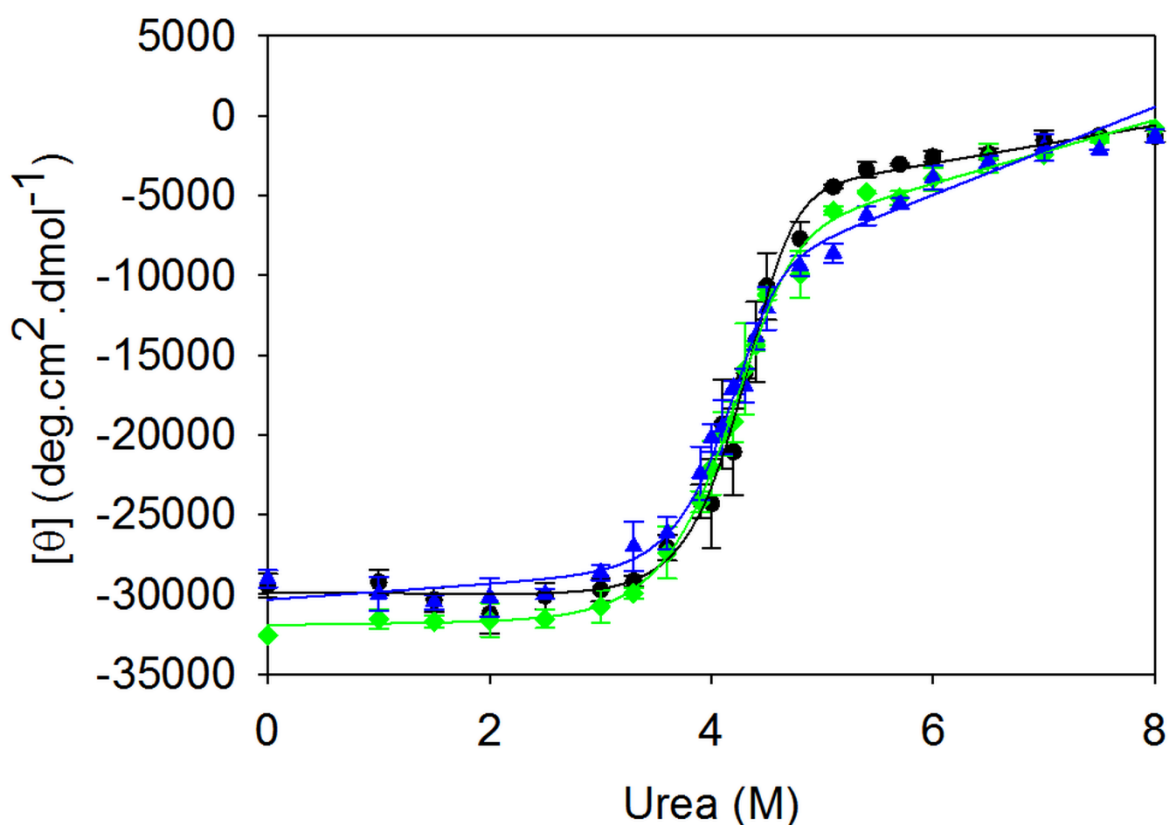
Figure S3: Urea-induced equilibrium unfolding of wild-type and mutant GSTA3-3 enzymes as monitored by circular dichroism at 220 nm. The wild-type (●), Y9F (♦) and Y9F/R15L (▲) GSTA3-3 concentration was 2 μM in 20 mM phosphate buffer, pH 7.4, containing 0.1 mM EDTA, and 0.02% (w/v) sodium azide. The points are the average of three replicates and error bars showing the standard deviation are shown.
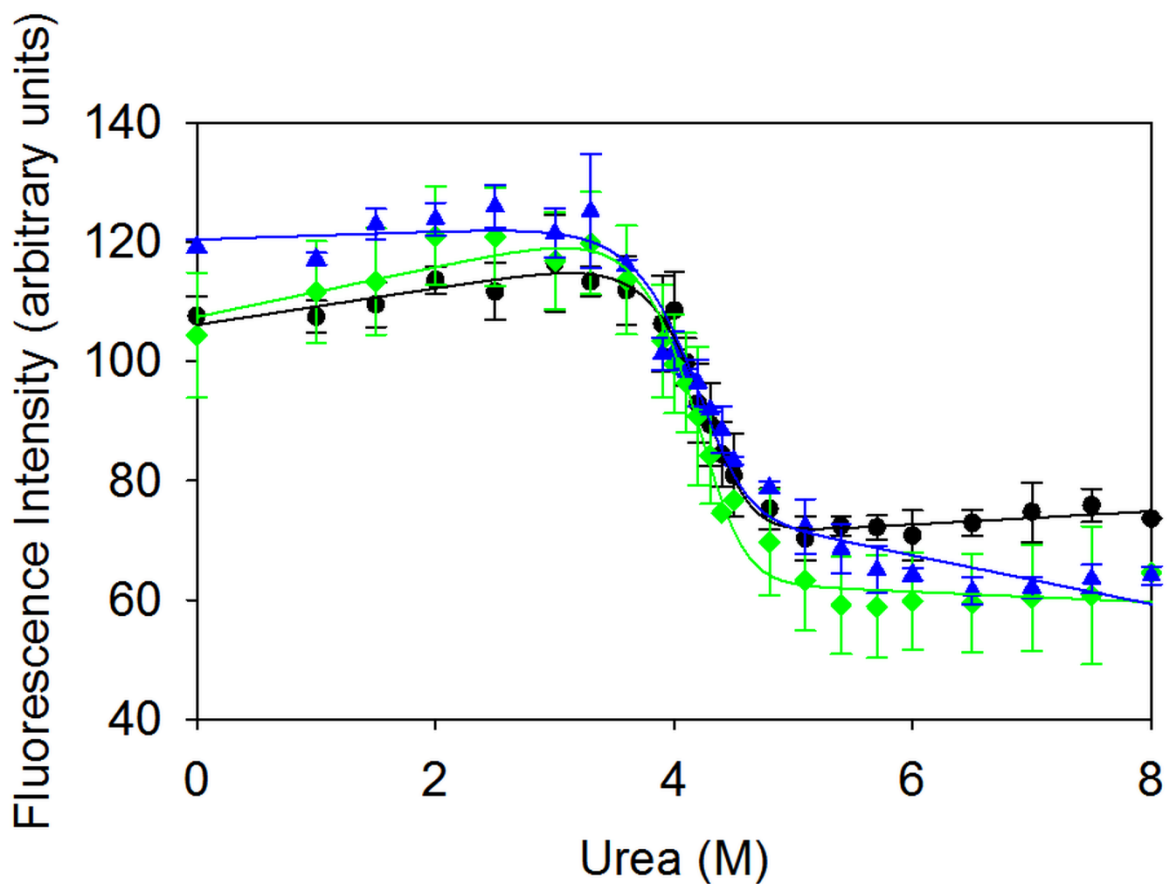
Figure S4: Urea-induced equilibrium unfolding of wild-type and mutant GSTA3-3 enzymes monitored by fluorescence spectroscopy. The unfolding of the enzyme was monitored by excitation at 280 nm with excitation measured at 330 nm. The wild-type (●), Y9F (♦) and Y9F/R15L (▲) GSTA3-3 concentration was 2 μM in 20 mM phosphate buffer, pH 7.4, containing 0.1 mM EDTA, and 0.02% (w/v) sodium azide. The points are the average of three replicates and error bars showing the standard deviation are shown.
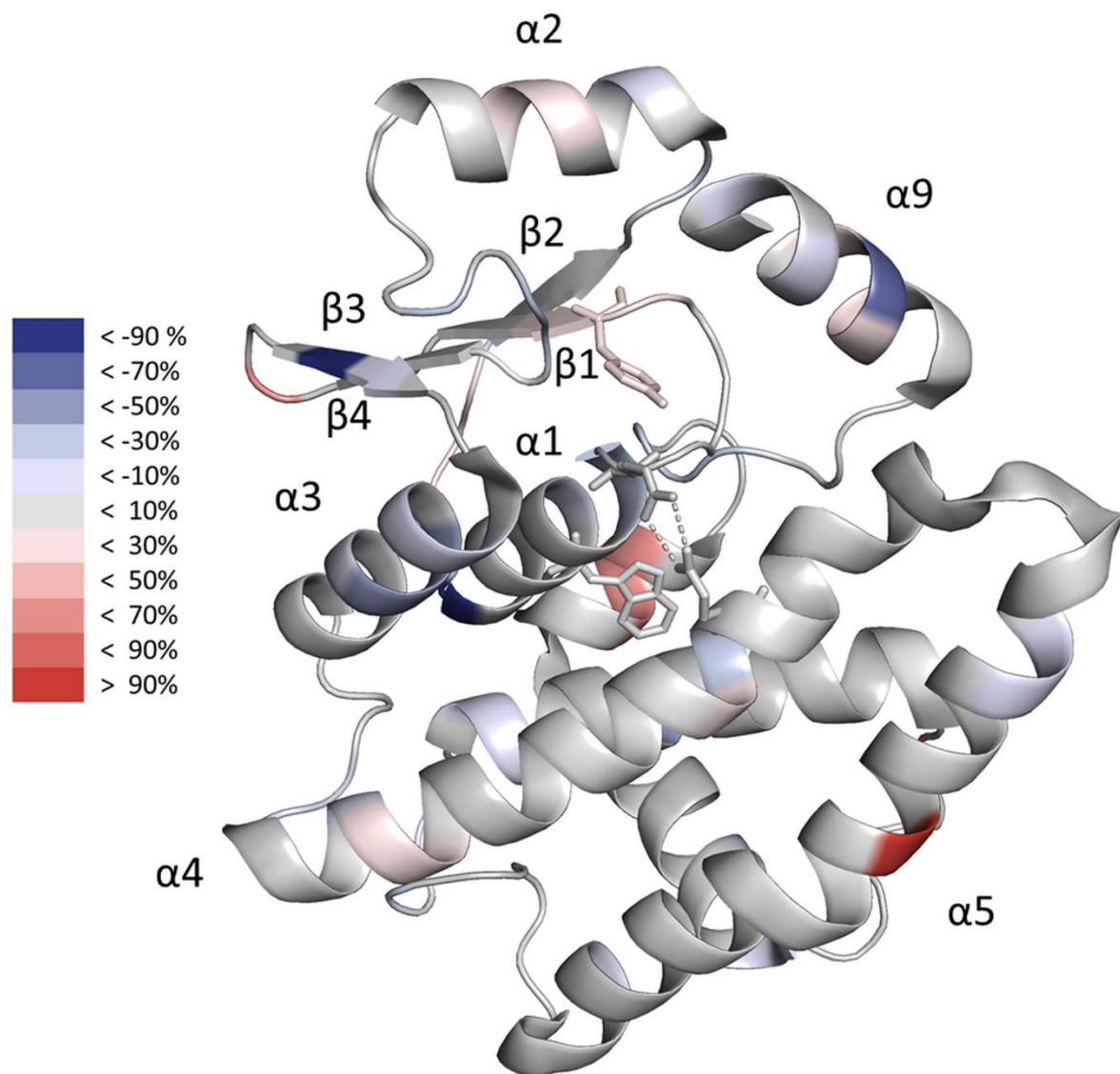
Figure S5: The Y9F/R15L double mutation has no change on the conformational flexibility of GSTA3-3 in the presence of GSH. The percentage differences in deuteration between wild-type and Y9F/R15L GSTA3-3 in the presence of GSH after 90 s are mapped onto the structure of dimeric GSTA3-3 (PDB entry 1TDI), calculated as the percentage of deuteration (Y9F/R15L) minus the percentage of deuteration (wild-type). Red coloring indicates that the level of deuterium exchange is higher for the mutant protein, while blue coloring indicates that the level of deuterium exchange is higher for the reduced protein. Helices and β-Sheets are labelled, and the positions of the Tyr9 residue, the Arg15-Glu104 salt-bridge and Trp21 are indicated.

Model	Variable	Value
Independent	Ka (M⁻¹)	6.281E4
	n	1.
	ΔH (kJ/mol)	-21.44
	Kd (M)	1.592E-5
	ΔS (J/mol·K)	18.73
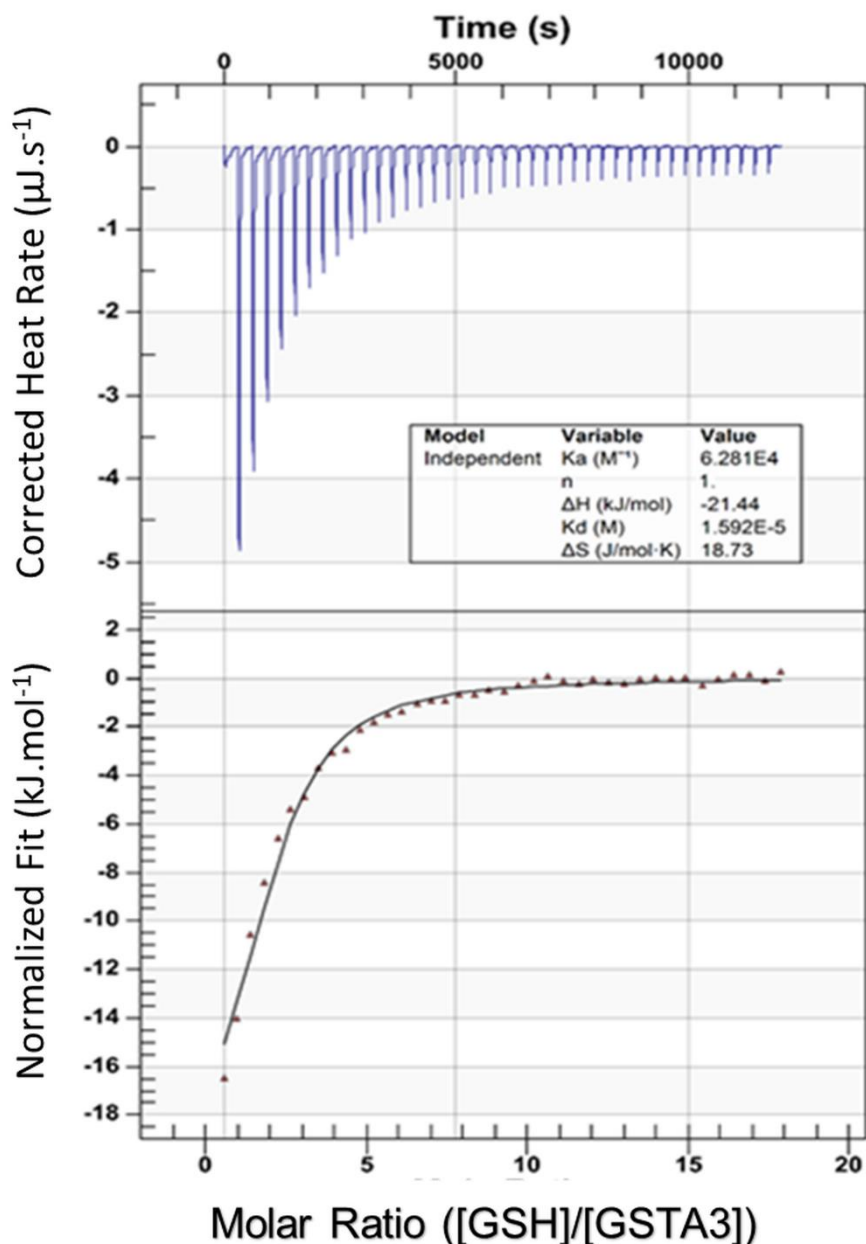
Figure S6: A representative calorimetric profile of the titration of GSTA3-3 with GSH. (A) Raw isothermal calorimetric titration curve of GSH binding to wild-type GSTA3-3 at 20 °C in 20 mM sodium phosphate buffer, pH 6.5, containing 0.1 M NaCl, 1 mM EDTA, and 0.02% (w/v) sodium azide. Protein concentration was 0.05 mM monomer and the GSH stock concentration was 2 mM. (B) Binding isotherm of integrated data in (A) corrected for heats of dilution. The solid line through the data represents the best fit obtained using NanoAnalyze software.
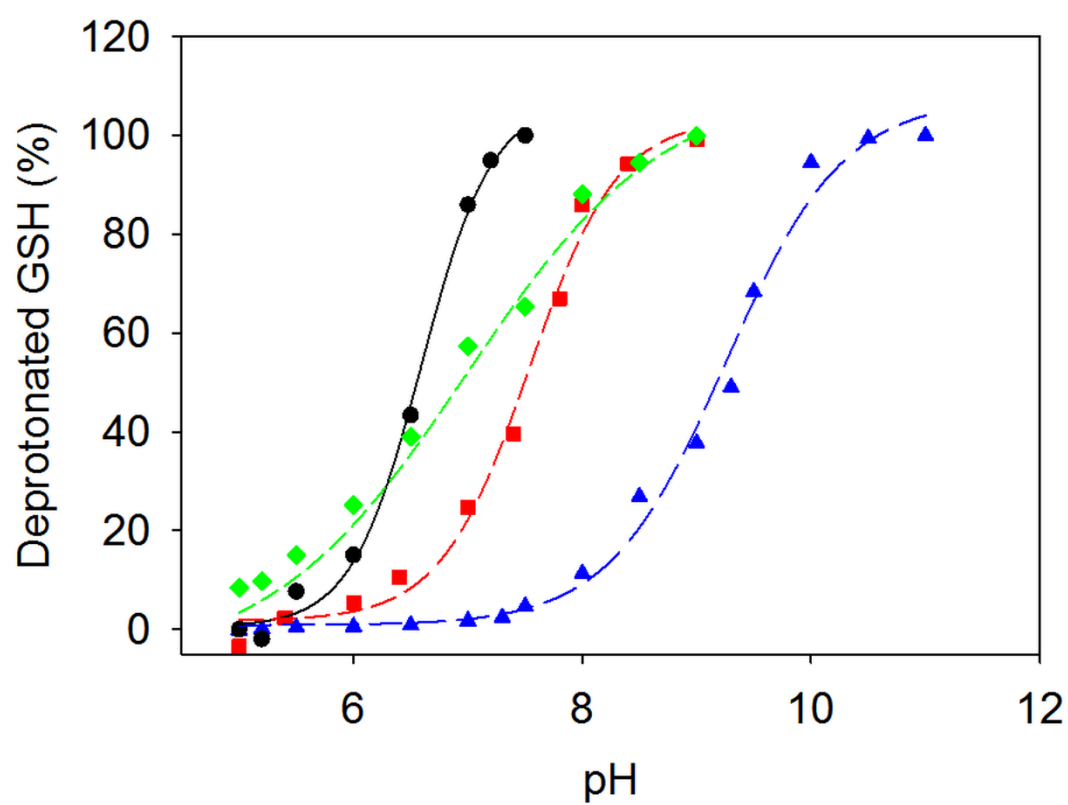
Figure S7: GSH thiolate formation expressed as a function of pH in the presence and absence of GSTA3-3 enzymes. Free GSH (▲), GSH bound to wild-type (●), Y9F (♦) and R15L (■) GSTA3-3 are shown.
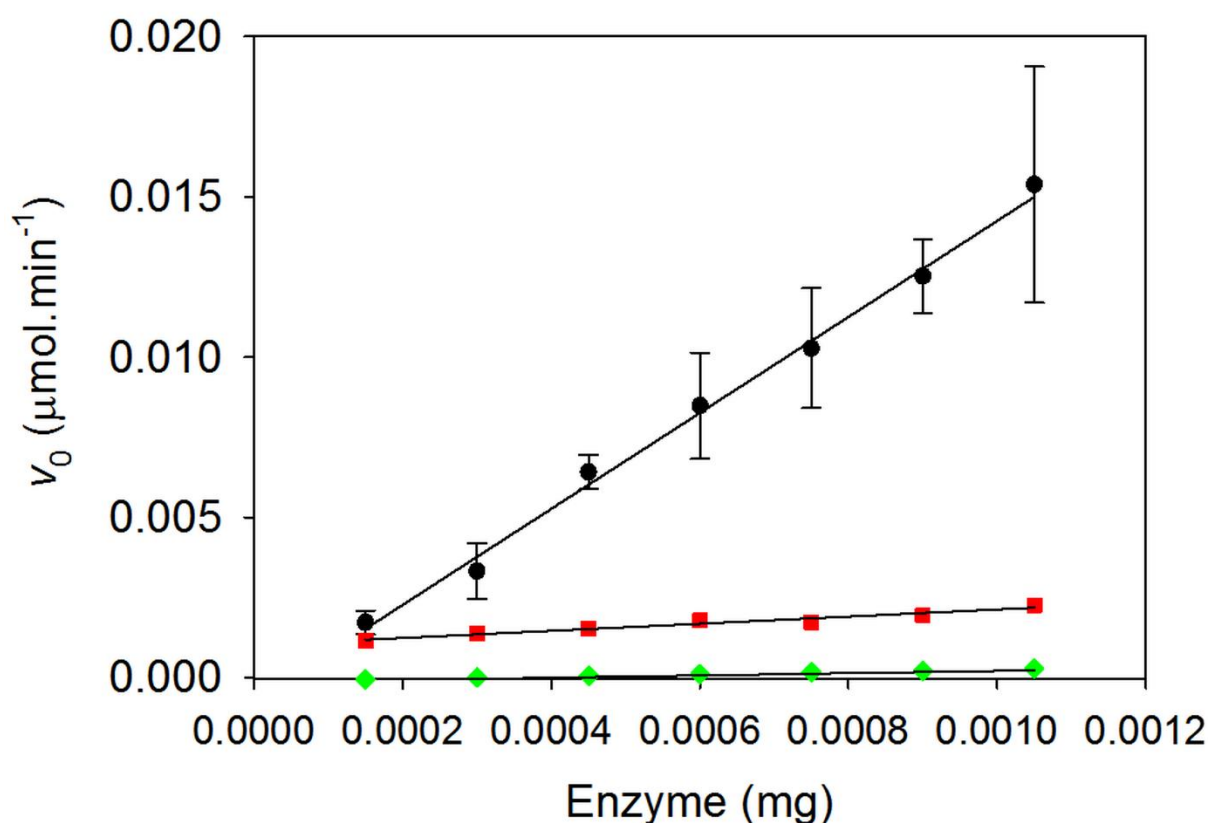
Figure S8: Specific activity of wild-type and mutant GSTA3-3 using the GSH-CDNB conjugation assay. The conjugation of CDNB to GSH by enzyme catalysis of wild-type (●), Y9F (♦) and R15L (■) GSTA3-3 was monitored by measuring the A_{340} of the formed product 1-(S-glutathionyl)-2, 4-dinitrobenzene (ε_{340} = 9600 $M^{-1}.cm^{-1}$). The reaction was performed in 0.1 M sodium phosphate buffer, pH 6.5, containing 1 mM EDTA and 0.02% (w/v) sodium azide in the presence of 1 mM GSH and 1 mM CDNB. The assay was corrected for the non-enzymatic reaction rate. The specific activity of each enzyme is the slope of the linear regression plots. The points are the average of three replicates and error bars showing the standard deviation are shown.
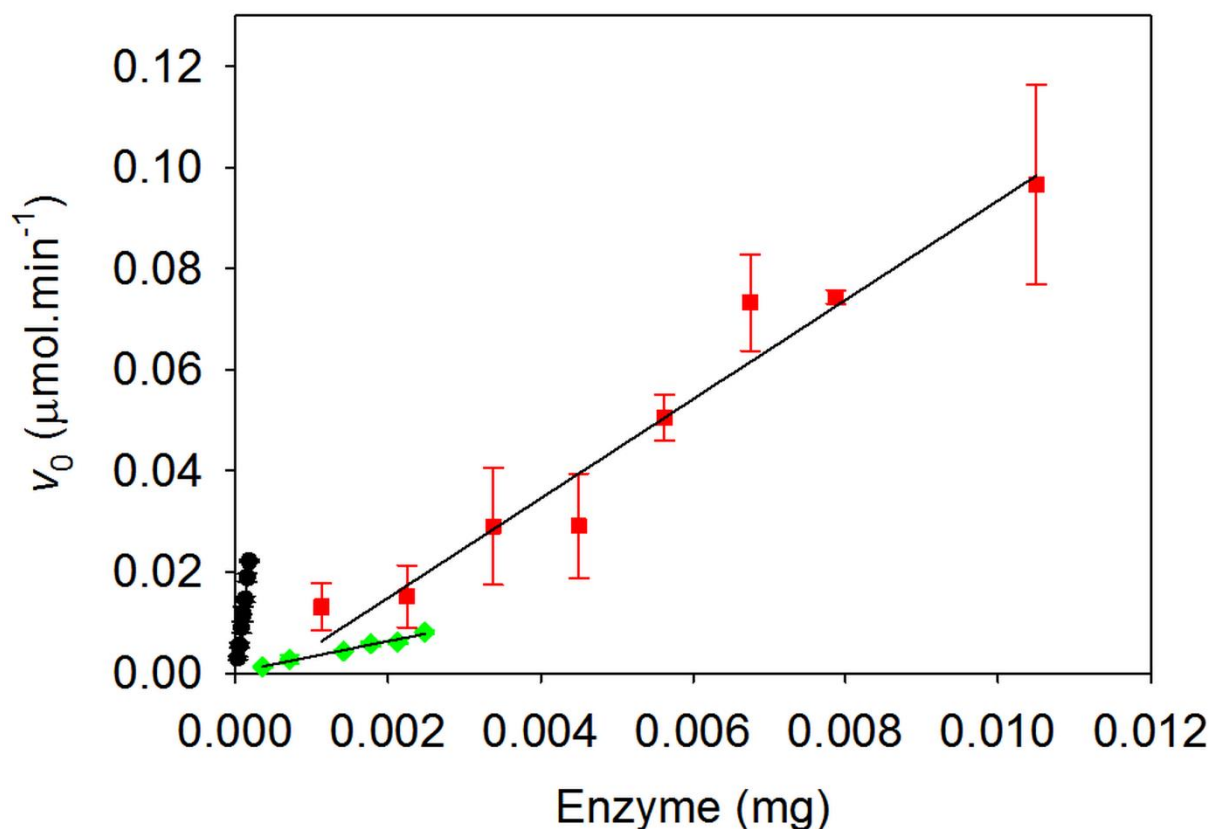
Figure S9: Specific activity of wild-type and mutant GSTA3-3 using the Δ^5-AD steroid isomerase assay. The steroid isomerization of Δ^5-AD to Δ^4-AD as catalyzed by wild-type ($\bullet$), Y9F ($\blacklozenge$) and R15L ($\blacksquare$) GSTA3-3 was monitored by measuring the A_{248} of the formed product Δ^4-AD ($\varepsilon_{248} = 16300$ $M^{-1}.cm^{-1}$). The reaction was performed in 0.1 M sodium phosphate buffer, pH 8.0, containing 1 mM EDTA and 0.02% (w/v) sodium azide in the presence of 1 mM GSH and 0.1 mM Δ^5-AD. The specific activity of each enzyme is the slope of the linear regression plots. The points are the average of three replicates and error bars showing the standard deviation are shown.
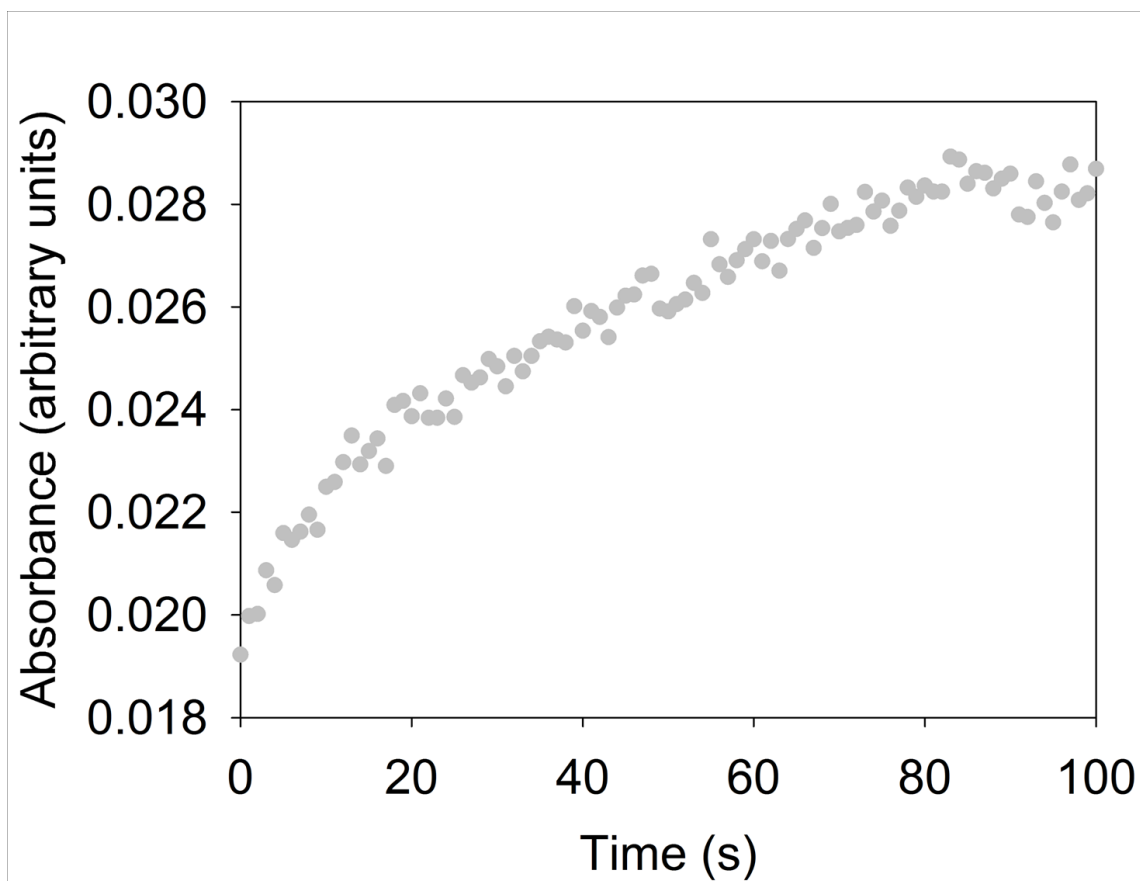
Figure S10: The reaction rate for the steroid isomerization of Δ^5-androstene-3-17-dione to Δ^4-androstene-3-17-dione, catalyzed by 1.5 nM of R15L GSTA3-3.

Chapter 5
Discussion and Conclusions

5.1. Structure, stability and conformational dynamics of GSTA3-3

The structure and stability of GSTA3-3 closely matches that of GSTA1-1, as expected for two proteins which share > 80% sequence identity (Section 3.4.; Chapter 4).[110] Additionally, neither the Y9F nor the R15L mutations, singly or together, seem to affect the structure, stability or conformational dynamics of the protein (Section 3.4.; Chapter 4).[110] The data indicates, therefore that the Arg15-Glu104 salt-bridge is neither important to structure, stability nor the conformational dynamics of the protein. It is likely that, similar to the case of GSTA1-1, the R15L mutation would create a cavity that is filled with water molecules that satisfy the hydrogen bonding requirements of Glu104.[44] Since the Arg15-Glu104 salt-bridge is unique to the Alpha class of GSTs, it is not surprising that the salt-bridge is not critical to protein stability.

However, though there were no changes in the unfolding pathways for the Y9F and Y9F/R15L (and by implication R15l) mutants as monitored by far-UV CD and fluorescence spectroscopy (Ex$_{280}$) there were significant differences in the calculated stability and m-value for the Y9F/R15L mutant when monitoring unfolding via excitation of Trp21 (Ex$_{295}$) (Section 3.4.). In particular, the lower m-value could indicate the possibility of intermediates along the unfolding path becoming more significantly populated. Monitoring unfolding via Trp21 fluorescence, itself part of an important domain-domain lock-and-key motif near the active site, is particularly more sensitive to changes near the active site than the other techniques. Indicating that while global unfolding has remained unchanged, the local stability in the region around Trp21 (and the active-site) is affected by the Y9F/R15L mutation. It is likely that the loss of the interaction between the hydroxyl group of Tyr9 and the backbone of Arg15, which can also be maintained between Tyr9 and Leu15[44] is responsible for the change in the Y9F/R15L double mutant.

Based on the slight increase in conformational dynamics at the active site of Y9F/R15L GSTA3-3 it may be that the salt-bridge does help to maintain a specific conformation that promotes catalytic efficiency, but this would need to be investigated through mutation of Glu104.

5.2. Binding and activation of GSH

Lowering the pK_a of GSH is the principal means by which the GSTA3-3 enzyme catalyses both its conjugation and steroid isomerisation reactions. Previous studies have consistently reported that GSTA3-3 reduced the pK_a of GSH further than GSTA1-1 (Chapter 4 - Table 4).[110] This may have accounted for some of the differences in the catalytic efficiency of the enzymes. The findings of this study, however, show closely matching values between GSTA1-1 and GSTA3-3, discounting this possibility. This work does show that Arg15 lowers the pK_a of GSH further than Tyr9, similar to its role in GSTA1-1.

There is, however, a clear and significant difference between the binding affinities of the Alpha class GSTs for GSH (Chapter 4 - Table 3).[110] GSTA3-3 has a ten-fold greater affinity for GSH as compared to GSTA1-1. Since the reaction rates of both the conjugation and steroid isomerisation reactions are not close to the diffusion controlled limit, an enhanced affinity for GSH could account for some of the differences in catalytic efficiencies between the enzymes. The greater affinity for GSH is likely as a result of the larger than typical active site of GSTA3-3 (Chapter 4).[110]

5.3. Catalytic activity of GSTA3-3

The data is clear that the Y9F and R15L mutations singly or combined have a deleterious effect on the enzymes catalytic activity (Chapter 4 - Table 5).[110] Since neither mutation significantly alters the structure, stability or conformational dynamics of the enzyme, however, the mutations affect the catalytic activity of the enzyme they must do so solely through the way they interact with the substrates.

Both the Y9F and R15L mutations result in comparable decreases in the catalytic activity of the steroid isomerisation reaction of GSTA3-3. This is despite the fact that evidence shows that

the Arg15 residue is more important for lowering the pK_a of GSH (Chapter 4 - Table 4)[110], the crux by which the enzyme catalyses the reaction. This argues that Tyr9 may play an additional role in the enzyme other than simply lowering the pK_a of GSH. This finding is in strong agreement with Scheme 1 (stepwise; Figure 7) which argues that Tyr9 also acts as a proton shuttle.

5.4. Role of Arg15

The R15L mutation despite breaking the Arg15-Glu104 salt-bridge did not significantly alter the structure, stability or conformational dynamics of GSTA3-3 (chapter 4)[110]. This indicates that the highly conserved Arg15 residue (in the Alpha class) is an important catalytic residue based on how it interacts with substrates. Arg15 has long been suspected to be an important catalytic residue, specifically in regard to lowering the pK_a of GSH, inferred from the role it plays GSTA1-1. Indeed, this is the case with the Arg15 residue in GSTA3-3 lowering the pK_a of GSH further than even Tyr9 which is considered the primary catalytic residue of Alpha class GSTs.

The R15L mutation has been investigated in GSTA3-3 for the first time. This study, however, has shown evidence that the R15L GSTA3-3 enzyme shows a rapid decline in its reaction rate as compared to either wild-type or Y9F GSTA3-3 (Chapter 4 - Figure 5).[110] This decline in the reaction rate is probably due to an increased susceptibility of R15L to product inhibition. Alternatively, it could be because there is a greater energy barrier to release the product. Multiple substrates of GST have shown product release to be their rate limiting step.[111] Previous experiments have indicated that the GSTA3-3 enzyme has an approximately equal affinity for the substrate Δ^5-AD and the product Δ^4-AD[11] and any change to this delicate balance could, therefore, have significant effects on catalytic activity. Computational studies have predicted that Arg15 is the most important residue in the GSTA3-3 active site for stabilising the initial binding of the reactants GSH and Δ^5-AD at the active site,[80] lending credence to this idea.

There is indeed a growing amount of evidence that suggests Arg15 is part of an electron-sharing network conserved in all GSTs (there is evidence of the network in Alpha, Delta, Mu, Omega, Pi, Sigma, Tau and Theta GSTs).[111,112] Although the residues which make up this electron-sharing network are not conserved in the primary sequences of GSTs the presence of the

network can be mapped to the same region in all GSTs. This further supports the idea that Arg15 is not important for structural or stability reasons but is instead integral because of the charge of its side group. Indeed, experiments have previously determined that the charge of Arg15 is more catalytically significant than its bulk.[111] The conservation of this electron-sharing network which nevertheless demonstrates plasticity in its make-up may be indicative of the robust nature of GSTs against point mutations which may nonetheless lead to novel functions. After all, the Arg15 residue is specific to Alpha class GSTs and integral to its proper function.

5.5. The dienolate intermediate

The possible existence of a stable dienolate intermediate has long been a matter of speculation and controversy. Recently, Daka *et al.,* (2014)[85] and Calvaresi *et al.,* (2012), have published similar energy diagrams for their proposed reaction mechanisms of GSTA3-3 steroid isomerisation reaction (Figure 21).[80,85] Both papers have argued, based on their energy diagrams, that the reaction mechanism of GSTA3-3 consist of two phases: first the C4 of Δ^5-AD is deprotonated by the GSH thiolate sulfur and subsequently the hydroxyl proton of Tyr9 is transferred to C6 creating the Δ^4-AD product. Both groups argue that the first step is rate limiting and that the second step proceeds so quickly that the reaction proceeds via an enforced-concerted mechanism. In the energy diagrams of both studies it can be seen that there is no true energy well which would normally correspond to a true intermediate (Figure 8C and 21). Even so, Daka *et al.* (2014)[85] reported to have detected a stable intermediate using absorbance spectroscopy, a finding that argues against a concerted mechanism. In light of the inability of this study to detect an intermediate, the argument for a concerted mechanism,[80,85] and the absence of any dienolate intermediate on the reactions computed potential surface,[80] it is clear that further investigation is needed to clarify whether a stabilised dienolate intermediate, as opposed to just a transition state, can truly be detected.

The existence or absence of the dienolate intermediate has important ramifications both for solving the reaction mechanism and for drug discovery. It should be noted that ketosteroid isomerase (KSI) (EC 5.3.3.1), a close analogue enzyme that catalyses the same reaction, does stabilise the dienolate intermediate during its reaction mechanism and possesses a catalytic efficiency three orders of magnitude greater than GSTA3-3.[8,69] Indeed, KSI possesses a reaction rate that closely approaches the diffusion-controlled limit. If GSTA3-3 stabilises the
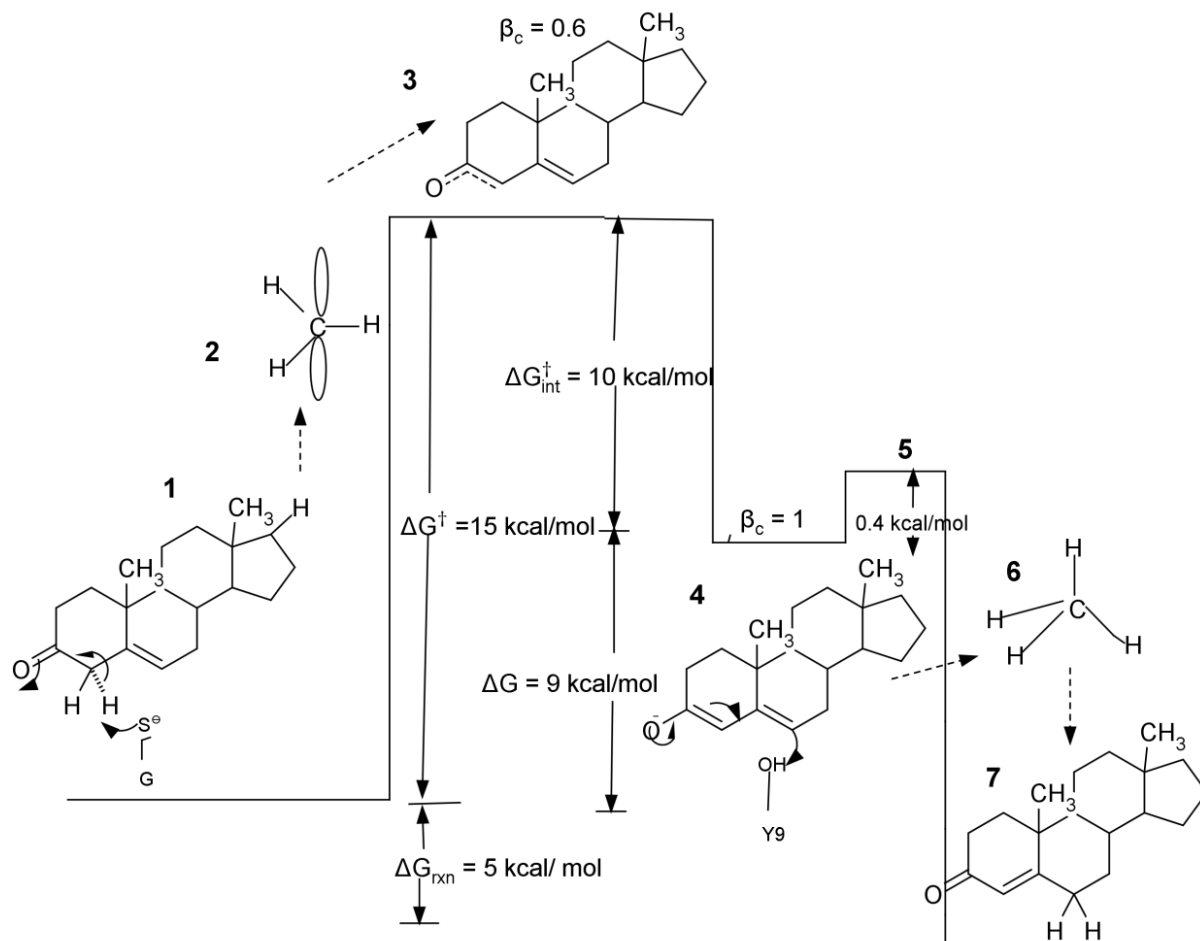
Figure 21: The reaction pathway for the isomerisation of Δ⁵–AD by hGSTA3-3 as proposed by Daka *et al.* (2014).[85] Δ^5–AD (1) is deprotonated by GS⁻ creating a charge imbalance that gives rise to a transition state (3). The transition state is stabilised by changes in orbital hybridisation and slight structural rearrangements to form the dienolate intermediate (4). Lastly, the intermediate is protonated at C6 by Tyr9 as it passes through a second transition state (5) and gives rise to the product Δ^4–AD (7). Notice the poorly defined energy well for the intermediate (4), the energy barrier between the intermediate and the second transition state (5) is only 0.4 kcal.mol⁻¹. In the computationally predicted energy diagram this energy barrier is even lower and only 0.1 kcal.mol⁻¹.[80] Such poorly defined energy wells are indicative of enforced concerted mechanisms (Compare Figure 8C)

dienolate intermediate during the reaction, why do the two enzymes have such vastly different reaction rates. Indeed, when the residues that stabilise the intermediate in KSI are mutated, the specific activity of KSI drops to closely match that of GSTA3-3.[113,114]

KSI possesses a clear oxyanion hole at its active site that stabilises the negative charge of O3 (Figure 9) with no comparable structure in the active site of GSTA3-3. How the GSTA3-3 enzyme could stabilise the dienolate intermediate is not clear. Of the many possibilities proposed, the only hypothesis, yet to be disproven, argues that the GSH cofactor plays a double role: the thiolate anion of GSH (GS$^-$) acts as a Bronsted base catalyst to deprotonate C4, while the main chain amide of the glycine residue of GSH forms a hydrogen bond stabilising the negative charge that forms on O3.[70] This view is supported by kinetic studies which show that the k_{cat} decreases 30-fold and the K_M for Δ^5-AD increases from 45 to 310 μM.[53,71] Such a change in K_M, however, has been calculated to contribute to binding energy only 1 kcal.mol^{-1}, indicating that the contribution of the GSH-glycine main chain hydrogen bond with the O3 atom contributes very little to the kinetic process.[85]

The nature and existence of the dienolate intermediate, therefore, remains contentious. The seemingly conflicting account of an enforced concerted mechanism, that may have a detectable intermediate, requires further consideration. Hypothetically, it is possible for a reaction to proceed by both a concerted and stepwise mechanism which coexist simultaneously.[84] Two kinds of circumstances have been proposed under which this could happen. In the first, a stepwise and enforced concerted mechanism could coexist when the individual steps of the reaction are separated in space and one step occurs by the diffusion controlled reaction of an intermediate. The reaction under these circumstances could occur by two separate pathways, in which the first step occurs either in the absence (stepwise) or presence (concerted) of the final reactant or catalysts. This is unlikely to be the case in regard to the GSTA3-3 catalysed reaction as the intermediate is formed already bound to the final reactant/catalysts (the enzyme itself). In the second circumstance, the different requirement for the concerted and stepwise mechanism can facilitate their coexistence if the barriers for the two mechanisms are not very different, i.e. the reaction will proceed through an intermediate if it can. Under these circumstances the stepwise mechanism would normally be too unfavourable for this pathway to make a significant contribution to the observed reaction rate.[115]

The manner in how the intermediate was detected also requires examination. The ideal wavelengths for the detection of the diene or dienolate intermediate are 238 and 256 nm, respectively.[87,88] Both wavelengths are within 10 nm or less of the ideal wavelength to detect the product (248 nm). Further, the wavelength for the diene intermediate is also only 1 nm away from the ideal wavelength to detect the deprotonation of GSH to the thiolate anion GS$^-$ (239 nm).[49] Since the catalytic mechanism predicts that during each reaction GSH will become deprotonated to GS$^-$ and then will be reprotonated during the formation of product, it can be assumed that both the formation of GS$^-$ and product will interfere with the measured absorbance at 238 and 256 nm. Additionally, the turnover number (k_{cat}) of the GSTA3-3 isomerisation reaction has been calculated at 75[85] and 230[111] s^{-1} at the extreme ends meaning that a molecule of product is formed at each active site of GSTA3-3 every 4.5-13 ms. The detection limit of traditional absorbance spectroscopy techniques is a few milliseconds. The intermediate in question could easily exist for a period of time lower than this detection limit because it is not the rate limiting step of the reaction;[70,80,85] especially in the case of an enforced concerted mechanism. The contradictory findings of a stable intermediate alongside a proposed concerted mechanism is clearly unsatisfactory, and further examination is needed solve the matter definitively.

5.6. Conclusion / Mechanistic implications

Y9F and R15L GSTA3-3 have comparable specific activities in respect to the steroid isomerisation reaction, despite the fact that the R15L mutation results in a higher pK_a for bound GSH. This is a strong indication that Tyr9 plays a role beyond that of just maintaining the pK_a of GSH. This matches the expectations of mechanism Scheme 1 (stepwise; Figure 7) for the steroid isomerisation reaction in which Tyr9 also acts as a proton shuttle. Additionally, this study found no evidence of a dienolate intermediate during the steroid isomerisation reaction, nor any compelling theories as to how such an intermediate could be stabilised by GSTA3-3. All the experimental evidence in this study agrees with the reaction scheme proposed by the computational model of Calveresi *et al*. (2012)[80], whereby the reaction proceeds through a concerted single step mechanism. The thiolate anion of GSH (GS$^-$) abstracts the C4 proton almost simultaneously to the C6 being protonated by the Tyr9 hydroxyl group. Tyr9 is then protonated by GSH in turn which resets the enzyme to its original starting conformation and the reaction may proceed again with fresh substrate. This is, in fact, the same model proposed

by Daka *et al*. (2014)[85] who detected the intermediate. Given that concerted mechanisms (even enforced concerted mechanisms) should not have detectable intermediates the inability of this study to detect the intermediate is perhaps unsurprising. All the findings of this study are, therefore, in strong agreement with the idea that the Scheme 1 (stepwise) reaction mechanism is correct and that the two steps in the reaction proceed via an enforced concerted mechanism.

Finally, for the first time in GSTA3-3, the Arg15 residue has been shown to be crucial to the steroid reaction mechanism. It not only acts to lower the pK_a of GSH (as expected) but also seems to play a crucial role in aiding the enzyme in selecting the reactant (Δ^5-AD) over the product (Δ^4-AD). In the R15L GSTA3-3 variant, the enzyme suffers from a rapidly declining reaction rate likely due to greater susceptibility to product inhibition.

GSTA3-3 has attracted significant interest and research as a potential therapeutic drug target in the treatment of diseases characterized by excessive steroid hormone production such as polycystic ovary syndrome, Cushing's syndrome, congenital adrenal hyperplasia and some cancers of the sex organs. Rational drug design would be greatly aided by a thorough understanding of the reaction mechanism of GSTA3-3. Though the existence or lack thereof of an intermediate during the GSTA3-3 catalysed steroid isomerisation reaction must remain contentious for now, hopefully this research has contributed to a more thorough understanding of the reaction mechanism.

Chapter 6
References

[1]   Ohvo-Rekila, H., Ramstedt, B., Leppimaki, P., and Slotte, J. P. (2002) Cholesterol interactions with phospholipids in membranes, *Prog Lipid Res 41*, 66-97.

[2]   Bennett, N. C., Gardiner, R. A., Hooper, J. D., Johnson, D. W., and Gobe, G. C. (2010) Molecular cell biology of androgen receptor signalling, *Int J Biochem Cell Biol 42*, 813-827.

[3]   Albery, W. J., and Knowles, J. R. (1976) Evolution of enzyme function and the development of catalytic efficiency, *Biochemistry 15*, 5631-5640.

[4]   Berg, J. M., Tymoczko, J. L., and Stryer, L. (2002) *Biochemistry, Fifth Edition*. New York: W. H. Freeman.

[5]   Moss, G. P. (1989) IUPAC-IUB Joint Commission on Biochemical Nomenclature (JCBN). The nomenclature of steroids. Recommendations 1989, *Eur. J. Biochem. 186*, 429-458.

[6]   Buhaescu, I., and Izzedine, H. (2007) Mevalonate pathway: a review of clinical and therapeutical implications, *Clin. Biochem. 40*, 575-584.

[7]   Wood, E. J. (1997), Biochemistry. A case-oriented approach. Sixth edition: By R Montgomery, T W Conway, A A Spector and D Chappell. pp. 587–618. Mosby, St Louis MO.

[8]   Pollack, R. M. (2004) Enzymatic mechanisms for catalysis of enolization: ketosteroid isomerase, *Bioorg. Chem. 32*, 341-353.

[9]   Wang, S. F., Kawahara, F. S., and Talalay, P. (1963) The mechanism of the delta5-3-ketosteroid isomerase reaction: absorption and fluorescence spectra of enzyme-steroid complexes, *J. Biol. Chem. 238*, 576-585.

[10]   Benson, A. M., Talalay, P., Keen, J. H., and Jakoby, W. B. (1977) Relationship between the soluble glutathione-dependent delta 5-3-ketosteroid isomerase and the glutathione S-transferases of the liver, *Proc Natl Acad Sci U S A 74*, 158-162.

[11]   Johansson, A. S., and Mannervik, B. (2001) Human glutathione transferase A3-3, a highly efficient catalyst of double-bond isomerization in the biosynthetic pathway of steroid hormones, *J. Biol. Chem. 276*, 33061-33065.

[12]   Raffalli-Mathieu, F., Orre, C., Stridsberg, M., Hansson Edalat, M., and Mannervik, B. (2008) Targeting human glutathione transferase A3-3 attenuates progesterone production in human steroidogenic cells, *Biochem. J. 414*, 103-109.

[13]   Hayes, J. D., Flanagan, J. U., and Jowsey, I. R. (2005) Glutathione transferases, *Annu. Rev. Pharmacol. Toxicol. 45*, 51-88.

[14]   Sheehan, D., Meade, G., Foley, V. M., and Dowd, C. A. (2001) Structure, function and evolution of glutathione transferases: implications for classification of non-mammalian members of an ancient enzyme superfamily, *Biochem. J. 360*, 1-16.

[15]   Murzin, A. G., Brenner, S. E., Hubbard, T., and Chothia, C. (1995) SCOP: a structural classification of proteins database for the investigation of sequences and structures, *J. Mol. Biol. 247*, 536-540.

[16]   Mannervik, B., and Danielson, U. H. (1988) Glutathione transferases--structure and catalytic activity, CRC *Crit. Rev. Biochem. Mol. Bol. 23*, 283-337.

[17]   Copley, S. D., and Dhillon, J. K. (2002) Lateral gene transfer and parallel evolution in the history of glutathione biosynthesis genes, *Genome Biology 3*, research0025.0021-research0025.0016.

[18]   Mannervik, B. (1985) The isoenzymes of glutathione transferase, *Adv Enzymol Relat Areas Mol Biol 57*, 357-417.

[19]   Ji, X., von Rosenvinge, E. C., Johnson, W. W., Tomarev, S. I., Piatigorsky, J., Armstrong, R. N., and Gilliland, G. L. (1995) Three-dimensional structure, catalytic properties, and evolution of a sigma class glutathione transferase from squid, a progenitor of the lens S-crystallins of cephalopods, *Biochemistry 34*, 5317-5328.

[20]   Meyer, D. J., Coles, B., Pemble, S. E., Gilmore, K. S., Fraser, G. M., and Ketterer, B. (1991) Theta, a new class of glutathione transferases purified from rat and man, *Biochem. J. 274 (Pt 2)*, 409-414.

[21]   Pemble, S. E., Wardle, A. F., and Taylor, J. B. (1996) Glutathione S-transferase class Kappa: characterization by the cloning of rat mitochondrial GST and identification of a human homologue, *Biochem. J. 319 (Pt 3)*, 749-754.

[22]   Board, P. G., Baker, R. T., Chelvanayagam, G., and Jermiin, L. S. (1997) Zeta, a novel class of glutathione transferases in a range of species from plants to humans, *Biochem. J. 328 (Pt 3)*, 929-935.

[23]   Rossjohn, J., Polekhina, G., Feil, S. C., Allocati, N., Masulli, M., Di Illio, C., and Parker, M. W. (1998) A mixed disulfide bond in bacterial glutathione transferase: functional and evolutionary implications, *Structure 6*, 721-734.

[24]   Board, P. G., Coggan, M., Chelvanayagam, G., Easteal, S., Jermiin, L. S., Schulte, G. K., Danley, D. E., Hoth, L. R., Griffor, M. C., Kamath, A. V., Rosner, M. H., Chrunyk, B. A., Perregaux, D. E., Gabel, C. A., Geoghegan, K. F., and Pandit, J. (2000) Identification, characterization, and crystal structure of the Omega class glutathione transferases, *J. Biol. Chem. 275*, 24798-24806.

[25]   Oakley, A. J., Harnnoi, T., Udomsinprasert, R., Jirajaroenrat, K., Ketterman, A. J., and Wilce, M. C. (2001) The crystal structures of glutathione S-transferases isozymes 1-3 and 1-4 from Anopheles dirus species B, *Protein Sci. 10*, 2176-2185.

[26]   Dixon, D. P., Lapthorn, A., and Edwards, R. (2002) Plant glutathione transferases, *Genome Biology 3*, reviews3004.3001-reviews3004.3010.

[27]   Harwaldt, P., Rahlfs, S., and Becker, K. (2002) Glutathione S-transferase of the malarial parasite Plasmodium falciparum: characterization of a potential drug target, *Biol. Chem. 383*, 821-830.

[28]   Walker, J., Crowley, P., Moreman, A. D., and Barrett, J. (1993) Biochemical properties of cloned glutathione S-transferases from Schistosoma mansoni and Schistosoma japonicum, *Mol. Biochem. Parasitol. 61*, 255-264.

[29]   Mannervik, B., Board, P. G., Hayes, J. D., Listowsky, I., and Pearson, W. R. (2005) Nomenclature for mammalian soluble glutathione transferases, *Methods Enzymol. 401*, 1-8.

[30]   Atkinson, H. J., and Babbitt, P. C. (2009) Glutathione transferases are structural and functional outliers in the thioredoxin fold, *Biochemistry 48*, 11108-11116.

[31]   Dirr, H., Reinemer, P., and Huber, R. (1994) X-ray crystal structures of cytosolic glutathione S-transferases. Implications for protein architecture, substrate recognition and catalytic function, *Eur. J. Biochem. 220*, 645-661.

[32]   Wilce, M. C., and Parker, M. W. (1994) Structure and function of glutathione S-transferases, *Biochim. Biophys. Acta 1205*, 1-18.

[33]   Erhardt, J., and Dirr, H. (1995) Native dimer stabilizes the subunit tertiary structure of porcine class pi glutathione S-transferase, *Eur. J. Biochem. 230*, 614-620.

[34]   Meng, E. C., Pettersen, E. F., Couch, G. S., Huang, C. C., and Ferrin, T. E. (2006) Tools for integrated sequence-structure analysis with UCSF Chimera, *BMC Bioinformatics 7*, 339.

[35]   Delano, W. L. (2002) The PyMOL Molecular Graphics System.

[36]   Allardyce, C. S., McDonagh, P. D., Lian, L. Y., Wolf, C. R., and Roberts, G. C. (1999) The role of tyrosine-9 and the C-terminal helix in the catalytic mechanism of Alpha-class glutathione S-transferases, *Biochem. J. 343 Pt 3*, 525-531.

[37]   Ladner, J. E., Parsons, J. F., Rife, C. L., Gilliland, G. L., and Armstrong, R. N. (2004) Parallel evolutionary pathways for glutathione transferases: structure and mechanism of the mitochondrial class kappa enzyme rGSTK1-1, *Biochemistry 43*, 352-361.

[38]   Armstrong, R. N. (1997) Structure, catalytic mechanism, and evolution of the glutathione transferases, *Chem. Res. Toxicol. 10*, 2-18.

[39]   Le Trong, I., Stenkamp, R. E., Ibarra, C., Atkins, W. M., and Adman, E. T. (2002) 1.3-A resolution structure of human glutathione S-transferase with S-hexyl glutathione bound reveals possible extended ligandin binding site, *Proteins 48*, 618-627.

[40]   Gu, Y., Guo, J., Pal, A., Pan, S. S., Zimniak, P., Singh, S. V., and Ji, X. (2004) Crystal structure of human glutathione S-transferase A3-3 and mechanistic implications for its high steroid isomerase activity, *Biochemistry 43*, 15673-15679.

[41]   Fabrini, R., De Luca, A., Stella, L., Mei, G., Orioni, B., Ciccone, S., Federici, G., Lo Bello, M., and Ricci, G. (2009) Monomer-dimer equilibrium in glutathione transferases: a critical re-examination, *Biochemistry 48*, 10473-10482.

[42]   Balchin, D., Fanucchi, S., Achilonu, I., Adamson, R. J., Burke, J., Fernandes, M., Gildenhuys, S., and Dirr, H. W. (2010) Stability of the domain interface contributes towards the catalytic function at the H-site of class alpha glutathione transferase A1-1, *Biochim. Biophys. Acta 1804*, 2228-2233.

[43]   Danielson, U. H., and Mannervik, B. (1985) Kinetic independence of the subunits of cytosolic glutathione transferase from the rat, *Biochem. J. 231*, 263-267.

[44]   Gildenhuys, S., Dobreva, M., Kinsley, N., Sayed, Y., Burke, J., Pelly, S., Gordon, G. P., Sayed, M., Sewell, T., and Dirr, H. W. (2010) Arginine 15 stabilizes an S(N)Ar reaction transition state and the binding of anionic ligands at the active site of human glutathione transferase A1-1, *Biophys. Chem. 146*, 118-125.

[45]   Bjornestedt, R., Stenberg, G., Widersten, M., Board, P. G., Sinning, I., Jones, T. A., and Mannervik, B. (1995) Functional significance of arginine 15 in the active site of human class alpha glutathione transferase A1-1, *J. Mol. Biol. 247*, 765-773.

[46]   Sinning, I., Kleywegt, G. J., Cowan, S. W., Reinemer, P., Dirr, H. W., Huber, R., Gilliland, G. L., Armstrong, R. N., Ji, X., Board, P. G., and et al. (1993) Structure determination and refinement of human alpha class glutathione transferase A1-1, and a comparison with the Mu and Pi class enzymes, *J. Mol. Biol. 232*, 192-212.

[47]   Liang, F. Q., Alssadi, R., Morehead, P., Awasthi, Y. C., and Godley, B. F. (2005) Enhanced expression of glutathione-S-transferase A1-1 protects against oxidative stress in human retinal pigment epithelial cells, *Exp Eye Res 80*, 113-119.

[48]   Boyland, E., and Chasseaud, L. F. (1969) The role of glutathione and glutathione S-transferases in mercapturic acid biosynthesis, *Adv Enzymol Relat Areas Mol Biol 32*, 173-219.

[49]   Graminski, G. F., Kubo, Y., and Armstrong, R. N. (1989) Spectroscopic and kinetic evidence for the thiolate anion of glutathione at the active site of glutathione S-transferase, *Biochemistry 28*, 3562-3568.

[50]   Armstrong, R. N. (1991) Glutathione S-transferases: reaction mechanism, structure, and function, *Chem. Res. Toxicol. 4*, 131-140.

[51]   Widersten, M., Bjornestedt, R., and Mannervik, B. (1996) Involvement of the carboxyl groups of glutathione in the catalytic mechanism of human glutathione transferase A1-1, *Biochemistry 35*, 7731-7742.

[52]   Arvanites, C. A., and Boerth, W. D. (2001) Modeling of the mechanism of nucleophilic aromatic substitution of fungicide chlorothalonil by glutathione, *Molecular modeling annual 7*, 245-256.

[53]   Pettersson, P. L., and Mannervik, B. (2001) The role of glutathione in the isomerization of delta 5-androstene-3,17-dione catalyzed by human glutathione transferase A1-1, *J. Biol. Chem. 276*, 11698-11704.

[54]   Wang, R. W., Newton, D. J., Huskey, S. E., McKeever, B. M., Pickett, C. B., and Lu, A. Y. (1992) Site-directed mutagenesis of glutathione S-transferase YaYa. Important roles of tyrosine 9 and aspartic acid 101 in catalysis, *J. Biol. Chem. 267*, 19866-19871.

[55]   Babbitt, P. C., and Gerlt, J. A. (1997) Understanding enzyme superfamilies. Chemistry As the fundamental determinant in the evolution of new catalytic activities, *J. Biol. Chem. 272*, 30591-30594.

[56]   Mannervik, B., and Guthenberg, C. (1981) Glutathione transferase (human placenta), *Methods Enzymol. 77*, 231-235.

[57]   Listowsky, I., Abramovitz, M., Homma, H., and Niitsu, Y. (1988) Intracellular binding and transport of hormones and xenobiotics by glutathione-S-transferases, *Drug Metab. Rev. 19*, 305-318.

[58]   Danger, D. P., Baldwin, W. S., and LeBlanc, G. A. (1992) Photoaffinity labelling of steroid-hormone-binding glutathione S-transferases with [3H]methyltrienolone. Inhibition of steroid-binding activity by the anticarcinogen indole-3-carbinol, *Biochem. J. 288*, 361-367.

[59]   Adler, V., Yin, Z., Fuchs, S. Y., Benezra, M., Rosario, L., Tew, K. D., Pincus, M. R., Sardana, M., Henderson, C. J., Wolf, C. R., Davis, R. J., and Ronai, Z. (1999) Regulation of JNK signaling by GSTp, *The EMBO Journal 18*, 1321-1334.

[60]   Cho, S. G., Lee, Y. H., Park, H. S., Ryoo, K., Kang, K. W., Park, J., Eom, S. J., Kim, M. J., Chang, T. S., Choi, S. Y., Shim, J., Kim, Y., Dong, M. S., Lee, M. J., Kim, S. G., Ichijo, H., and Choi, E. J. (2001) Glutathione S-transferase mu modulates the stress-activated signals by suppressing apoptosis signal-regulating kinase 1, *J. Biol. Chem. 276*, 12749-12755.

[61]   Khersonsky, O., and Tawfik, D. S. (2010) Enzyme promiscuity: a mechanistic and evolutionary perspective, *Annu. Rev. Biochem. 79*, 471-505.

[62]   Oakley, A. J. (2005) Glutathione transferases: new functions, *Curr. Opin. Struct. Biol. 15*, 716-723.

[63]   Todd, A. E., Orengo, C. A., and Thornton, J. M. (2002) Plasticity of enzyme active sites, *Trends Biochem. Sci. 27*, 419-426.

[64]   Yoshikuni, Y., Ferrin, T. E., and Keasling, J. D. (2006) Designed divergent evolution of enzyme function, *Nature 440*, 1078-1082.

[65]   Honaker, M. T., Acchione, M., Sumida, J. P., and Atkins, W. M. (2011) Ensemble perspective for catalytic promiscuity: calorimetric analysis of the active site conformational landscape of a detoxification enzyme, *J. Biol. Chem. 286*, 42770-42776.

[66]   Scott, C., Jackson, C. J., Coppin, C. W., Mourant, R. G., Hilton, M. E., Sutherland, T. D., Russell, R. J., and Oakeshott, J. G. (2009) Catalytic Improvement and Evolution of Atrazine Chlorohydrolase, *Appl. Environ. Microbiol. 75*, 2184-2191.

[67]   Vasu, K., Nagamalleswari, E., and Nagaraja, V. (2012) Promiscuous restriction is a cellular defense strategy that confers fitness advantage to bacteria, *PNAS. 109*, E1287-E1293.

[68]   Hubatsch, I., Ridderström, M., and Mannervik, B. (1998) Human glutathione transferase A4-4: an alpha class enzyme with high catalytic efficiency in the conjugation of 4-hydroxynonenal and other genotoxic products of lipid peroxidation, *Biochem. J. 330*, 175-179.

[69]   Hawkinson, D. C., Eames, T. C. M., and Pollack, R. M. (1991) Energetics of 3-oxo-.DELTA.5-steroid isomerase: source of the catalytic power of the enzyme, *Biochemistry 30*, 10849-10858.

[70]   Dourado, D. F. A. R., Fernandes, P. A., Mannervik, B., and Ramos, M. J. (2014) Isomerization of Δ5-Androstene-3,17-dione into Δ4-Androstene-3,17-dione Catalyzed by Human

Glutathione Transferase A3-3: A Computational Study Identifies a Dual Role for Glutathione, *J. Phys. Chem. A. 118*, 5790-5800.

[71]   Johansson, A. S., and Mannervik, B. (2002) Active-site residues governing high steroid isomerase activity in human glutathione transferase A3-3, *J. Biol. Chem. 277*, 16648-16654.

[72]   Tars, K., Olin, B., and Mannervik, B. (2010) Structural basis for featuring of steroid isomerase activity in alpha class glutathione transferases, *J. Mol. Biol. 397*, 332-340.

[73]   Pettersson, P. L., Johansson, A. S., and Mannervik, B. (2002) Transmutation of human glutathione transferase A2-2 with peroxidase activity into an efficient steroid isomerase, *J. Biol. Chem. 277*, 30019-30022.

[74]   Hou, L., Honaker, M. T., Shireman, L. M., Balogh, L. M., Roberts, A. G., Ng, K. C., Nath, A., and Atkins, W. M. (2007) Functional promiscuity correlates with conformational heterogeneity in A-class glutathione S-transferases, *J. Biol. Chem. 282*, 23264-23274.

[75]   Redinbo, M. R. (2004) Promiscuity: what protects us, perplexes us, *Drug Discov. Today 9*, 431-432.

[76]   Ekroos, M., and Sjogren, T. (2006) Structural basis for ligand promiscuity in cytochrome P450 3A4, *Proc Natl Acad Sci U S A 103*, 13682-13687.

[77]   Lairson, L. L., Watts, A. G., Wakarchuk, W. W., and Withers, S. G. (2006) Using substrate engineering to harness enzymatic promiscuity and expand biological catalysis, *Nat. Chem. Biol. 2*, 724-728.

[78]   O'Loughlin, T. L., Patrick, W. M., and Matsumura, I. (2006) Natural history as a predictor of protein evolvability, *Protein Eng. Des. Sel. 19*, 439-442.

[79]   Khersonsky, O., Roodveldt, C., and Tawfik, D. S. (2006) Enzyme promiscuity: evolutionary and mechanistic aspects, *Curr. Opin. Chem. Biol. 10*, 498-508.

[80]   Calvaresi, M., Stenta, M., Garavelli, M., Altoé, P., and Bottoni, A. (2012) Computational Evidence for the Catalytic Mechanism of Human Glutathione S-Transferase A3-3: A QM/MM Investigation, *ACS Catalysis 2*, 280-286.

[81]   Gerlt, J. A., and Gassman, P. G. (1993) An explanation for rapid enzyme-catalyzed proton abstraction from carbon acids: importance of late transition states in concerted mechanisms, *J. Am. Chem. Soc. 115*, 11552-11568.

[82]   McNaught, A. D., and Wilkinson, A. *IUPAC. Compendium of Chemical Terminology, 2nd ed. (the "Gold Book")*, WileyBlackwell; 2nd Revised edition edition.

[83]   Williams, A. (1994) The diagnosis of concerted organic mechanisms, *Chemical Society Reviews 23*, 93-100.

[84]   Jencks, W. P. (1981) Ingold Lecture. How does a reaction choose its mechanism?, *Chemical Society Reviews 10*, 345-375.

[85]   Daka, J. L., Achilonu, I., and Dirr, H. W. (2014) The isomerization of Delta5-androstene-3,17-dione by the human glutathione transferase A3-3 proceeds via a conjugated heteroannular diene intermediate, *J. Biol. Chem. 289*, 32243-32252.

[86]   Jencks, W. P. (1980) When is an intermediate not an intermediate? Enforced mechanisms of general acid-base, catalyzed, carbocation, carbanion, and ligand exchange reaction, *Accounts of Chemical Research 13*, 161-169.

[87]   Pollack, R. M., Zeng, B., Mack, J. P. G., and Eldin, S. (1989) Determination of the microscopic rate constants for the base catalyzed conjugation of 5-androstene-3,17-dione, *J. Am. Chem. Soc. 111*, 6419-6423.

[88]   Zeng, B., and Pollack, R. M. (1991) Microscopic rate constants for the acetate ion catalyzed isomerization of 5-androstene-3,17-dione to 4-androstene-3,17-dione: a model for steroid isomerase, *J. Am. Chem. Soc. 113*, 3838-3842.

[89]   Adman, E. T., Le Trong, I., Stenkamp, R. E., Nieslanik, B. S., Dietze, E. C., Tai, G., Ibarra, C., and Atkins, W. M. (2001) Localization of the C-terminus of rat glutathione S-transferase A1-1: crystal structure of mutants W21F and W21F/F220Y, *Proteins 42*, 192-200.

[90]   Papworth, C., Bauer, J., Braman, J., and Wright, D. (1996) Site-directed mutagenesis in one day with >80% efficiency. , *Strategies*, 3-4.

[91]   Chung, C. T., Niemela, S. L., and Miller, R. H. (1989) One-step preparation of competent Escherichia coli: transformation and storage of bacterial cells in the same solution, *PNAS. 86*, 2172-2175.

[92]   Ish-Horowicz, D., and Burke, J. F. (1981) Rapid and efficient cosmid cloning, *Nucleic Acids Res. 9*, 2989-2998.

[93]   Birnboim, H. C., and Doly, J. (1979) A rapid alkaline extraction procedure for screening recombinant plasmid DNA, *Nucleic Acids Res. 7*, 1513-1523.

[94]   Studier, F. W., and Moffatt, B. A. (1986) Use of bacteriophage T7 RNA polymerase to direct selective high-level expression of cloned genes, *J. Mol. Biol. 189*, 113-130.

[95] Perito, B., Allocati, N., Casalone, E., Masulli, M., Dragani, B., Polsinelli, M., Aceto, A., and Di Ilio, C. (1996) Molecular cloning and overexpression of a glutathione transferase gene from Proteus mirabilis, *Biochem. J. 318*, 157-162.

[96] Laemmli, U. K. (1970) Cleavage of structural proteins during the assembly of the head of bacteriophage T4, *Nature 227*, 680-685.

[97] Maurer, H. R. (1971) Basic principles of polyacrylamide gel electrophoresis and some recent advances of the technique, *Ann Biol Clin (Paris) 29*, 205-210.

[98] Perkins, S. J. (1986) Protein volumes and hydration effects. The calculations of partial specific volumes, neutron scattering matchpoints and 280-nm absorption coefficients for proteins and glycoproteins from amino acid sequences, *Eur. J. Biochem. 157*, 169-180.

[99] Ellman, G. L. (1959) Tissue sulfhydryl groups, *Arch Biochem Biophys 82*, 70-77.

[100] Riddles, P. W., Blakeley, R. L., and Zerner, B. (1983) Reassessment of Ellman's reagent, *Methods Enzymol. 91*, 49-60.

[101] Bradford, M. M. (1976) A rapid and sensitive method for the quantitation of microgram quantities of protein utilizing the principle of protein-dye binding, *Anal. Biochem. 72*, 248-254.

[102] Wallace, L. A., and Dirr, H. W. (1999) Folding and assembly of dimeric human glutathione transferase A1-1, *Biochemistry 38*, 16686-16694.

[103] Woody, R. W. (1995) Circular dichroism, *Methods Enzymol. 246*, 34-71.

[104] Wallace, L. A., Sluis-Cremer, N., and Dirr, H. W. (1998) Equilibrium and kinetic unfolding properties of dimeric human glutathione transferase A1-1, *Biochemistry 37*, 5320-5328.

[105] Pace, C. N. (1986) Determination and analysis of urea and guanidine hydrochloride denaturation curves, *Methods Enzymol. 131*, 266-280.

[106] Shirley, B. A. (1995) Urea and guanidine hydrochloride denaturation curves, *Merhods. Mol. Biol. (Clifton, N.J.) 40*, 177-190.

[107] Myers, J. K., Pace, C. N., and Scholtz, J. M. (1995) Denaturant m values and heat capacity changes: relation to changes in accessible surface areas of protein unfolding, *Protein Science : A Publication of the Protein Society 4*, 2138-2148.

[108] Pace, C. N. (1975) The stability of globular proteins, *CRC Crit. Rev. Biochem. 3*, 1-43.

[109]   Freire, E., Murphy, K. P., Sanchez-Ruiz, J. M., Galisteo, M. L., and Privalov, P. L. (1992) The molecular basis of cooperativity in protein folding. Thermodynamic dissection of interdomain interactions in phosphoglycerate kinase, *Biochemistry 31*, 250-256.

[110]   Robertson, G. J., Stoychev, S. H., Sayed, Y., Achilonu, I., and Dirr, H. W. (2017) The effects of mutating Tyr9 and Arg15 on the structure, stability, conformational dynamics and mechanism of GSTA3-3, *Biophys. Chem. 224*, 40-48.

[111]   Dourado, D. F., Fernandes, P. A., Mannervik, B., and Ramos, M. J. (2010) Glutathione transferase A1-1: catalytic importance of arginine 15, *J Phys Chem B 114*, 1690-1697.

[112]   Winayanuwattikun, P., and Ketterman, A. J. (2005) An Electron-sharing Network Involved in the Catalytic Mechanism Is Functionally Conserved in Different Glutathione Transferase Classes, *J. Biol. Chem. 280*, 31776-31782.

[113]   Wu, Z. R., Ebrahimian, S., Zawrotny, M. E., Thornburg, L. D., Perez-Alvarado, G. C., Brothers, P., Pollack, R. M., and Summers, M. F. (1997) Solution structure of 3-oxo-delta5-steroid isomerase, *Science 276*, 415-418.

[114]   Kuliopulos, A., Mildvan, A. S., Shortle, D., and Talalay, P. (1989) Kinetic and ultraviolet spectroscopic studies of active-site mutants of delta 5-3-ketosteroid isomerase, *Biochemistry 28*, 149-159.

[115]   Palmer, J. L., and Jencks, W. P. (1980) Nonenforced concerted general-acid catalysis of the dehydration step in formaldehyde thiosemicarbazone formation, *J. Am. Chem. Soc. 102*, 6466-6472.